



**Michigan
Technological
University**

Michigan Technological University
Digital Commons @ Michigan Tech

Dissertations, Master's Theses and Master's Reports

2018

A BAYESIAN NETWORK APPROACH TO BATTERY AGING IN ELECTRIC VEHICLE TRANSPORTATION AND GRID INTEGRATION

Mehdi Jafari

Michigan Technological University, mjafari@mtu.edu

Copyright 2018 Mehdi Jafari

Recommended Citation

Jafari, Mehdi, "A BAYESIAN NETWORK APPROACH TO BATTERY AGING IN ELECTRIC VEHICLE TRANSPORTATION AND GRID INTEGRATION", Open Access Dissertation, Michigan Technological University, 2018.

<https://digitalcommons.mtu.edu/etdr/588>

Follow this and additional works at: <https://digitalcommons.mtu.edu/etdr>



Part of the [Power and Energy Commons](#)

A BAYESIAN NETWORK APPROACH TO BATTERY AGING IN ELECTRIC
VEHICLE TRANSPORTATION AND GRID INTEGRATION

By

Mehdi Jafari

A DISSERTATION

Submitted in partial fulfillment of the requirements for the degree of

DOCTOR OF PHILOSOPHY

In Electrical Engineering

MICHIGAN TECHNOLOGICAL UNIVERSITY

2018

© 2018 Mehdi Jafari

This dissertation has been approved in partial fulfillment of the requirements for the Degree of DOCTOR OF PHILOSOPHY in Electrical Engineering.

Department of Electrical and Computer Engineering

Dissertation Advisor: *Dr. Lucia Gauchia*

Committee Member: *Dr. Kuilin Zhang*

Committee Member: *Dr. Laura E. Brown*

Committee Member: *Dr. Wayne W. Weaver*

Department Chair: *Dr. Daniel R. Fuhrmann*

Table of Contents

List of figures.....	vi
List of tables.....	ix
Preface.....	x
Abstract.....	xi
Outline.....	1
1 Analyzing Battery Aging Models	6
1.1 Introduction	7
1.2 Material and Electrode Level Models	8
1.3 Cell Level Models	15
1.4 Module and Pack Level.....	22
1.5 Application Level	26
1.6 Conclusions	28
References.....	28
2 REV-Cycle: A MATLAB-based Tool.....	35
2.1 Introduction	36
2.2 Large Data Real-Life Driving Cycles	37
2.3 REV-Cycle Software Tool	39
2.4 Electric Vehicle Model.....	41
2.5 Results for Highway Driving Cycles.....	44
2.6 Conclusion.....	49
References.....	50
3 Simulation and Analysis of the Effect of Real-World Driving Styles.....	52
3.1 Introduction	53
3.2 Simulations and Results for Highway Driving Cycles.....	54
3.2.1 Single Cycle Simulation Results.....	55
3.2.2 Driving Style Analysis in All Cycles.....	59
3.3 Conclusion.....	71

	References.....	72
4	Deterministic Aging Evaluation: Driving and V2G Services.....	74
	4.1 Introduction	75
	4.2 Driving Data	77
	4.3 Driving Cycles Analysis.....	78
	4.4 Aging Evaluation Model	81
	4.5 Daily Case Scenarios Study	87
	4.5.1 Aging of different driving styles.....	88
	4.5.2 Aging of different recharging options.....	90
	4.5.2.1 Scenario 2: Difference of charging	90
	4.5.2.2 Scenario 3: Recharging behavior	91
	4.5.2.3 Scenario 4: Every-other-day L-2 charging	92
	4.5.3 Aging of daily utility service	92
	4.5.3.1 Scenario 5: Frequency regulations and	93
	4.5.3.2 Scenario 6: Every other day L-2 charging with	95
	4.5.3.3 Scenario 7: Morning solar energy storage	96
	4.6 Different Climates' Impact on Battery Aging.....	97
	4.7 Discussion	100
	4.8 Conclusions	103
	References.....	104
5	Probabilistic Aging Evaluation: Hierarchical Bayesian Network Model	108
	5.1 Introduction	109
	5.2 Bayesian Models and EV Battery Aging Factors.....	112
	5.3 BN Modeling Process.....	113
	5.3.1 Network Development.....	113
	5.3.2 Mathematical Expression.....	115
	5.3.3 MCMC Sampling Implementation	117
	5.4 Training Data.....	120
	5.5 Model Evaluation with Test Set	123

5.6	Case Study: BN Model Performance	124
5.6.1	EV Daily Driving and Grid Services	125
5.6.2	Effect of grid services' contributions.....	129
5.6.3	Impact of location/weather change	131
5.7	Conclusion.....	132
	References.....	133
	Conclusions.....	136
	Contributions.....	139
	Future work.....	140
A	Copyright documentation.....	141

List of figures

Fig. 1. Graphical outline	3
Fig. 1.1. Trend of the aging models analyses in the chapter.....	8
Fig. 1.2. Li-ion cell schematic	9
Fig. 1.3. Material and electrode level aging models' block diagram.....	14
Fig. 1.4. Main aging causes in negative and positive electrodes	15
Fig. 1.5. Aging factors in the cell level models	17
Fig. 1.6. Cell level aging models block diagram	22
Fig. 1.7. Electric quantity -Capacity Scatter diagram for pack capacity	25
Fig. 2.1. Data recording method	38
Fig. 2.2. Real-life Driving Cycles of 5 Vehicles along I-80.....	39
Fig. 2.3. Main window of the developed tool REV-Cycle	40
Fig. 2.4. Measured and fitted impedance at 20%, 60%, and 90% SOC	43
Fig. 2.5. Time domain electrical model of battery.....	43
Fig. 2.6. (a) Battery experimental vs. simulated voltage, (b) the error.....	44
Fig. 2.7. Velocity profile for standard cycles HW-FET and HW-US06	47
Fig. 2.8. Velocity profile for real-life driving cycles.....	48
Fig. 2.9. SOC change in studied standard cycles.....	48
Fig. 2.10. SOC change for real driving cycles.....	49
Fig. 3.1. (a) EUDC and (b) HWFET driving cycles velocity	55
Fig. 3.2. (a) Heavy and (b) Light traffic cycles velocity	56
Fig. 3.3. Battery power: (a) EUDC cycle and (b) HWFET cycle.....	57
Fig. 3.4. Power demand from the battery	58
Fig. 3.5. SOC profiles: (a) heavy traffic and (b) light traffic cycle	59

Fig. 3.6.	Maximum battery power versus acceleration*velocity	60
Fig. 3.7.	Average battery power versus average acceleration	62
Fig. 3.8.	DOD versus average acceleration	63
Fig. 3.9.	Average and maximum kWh/100miles of 240 cycles.....	64
Fig. 3.10.	The average gradient of SOC	65
Fig. 3.11.	(a) Frequency and (b) the Rayleigh probability density	67
Fig. 3.12.	(a) Frequency and (b) Rayleigh probability density	68
Fig. 3.13.	Capacity loss in different driving styles	69
Fig. 4.1.	Driving time patterns of SPMD connected vehicle dataset.....	78
Fig. 4.2.	EV battery performance and aging simulation process.....	79
Fig. 4.3.	Velocity profile and Battery power for a single driving.....	80
Fig. 4.4.	Battery SOC and voltage profile for a single driving.....	80
Fig. 4.5.	C-rates' frequencies and daily driving duration	82
Fig. 4.6.	Cycle aging estimation of 2.4 Ah 26650 LPF cell	85
Fig. 4.7.	Comparison of estimated cell capacity with experimental data	85
Fig. 4.8.	Estimated cell capacity compared to experimental data.....	86
Fig. 4.9.	Driving cycles' DOD and capacity loss trend	87
Fig. 4.10.	Daily battery power and SOC for scenario 1.....	89
Fig. 4.11.	All drivers' overnight charging time trend.....	90
Fig. 4.12.	Battery capacity for all drivers, comparison of driving styles.....	90
Fig. 4.13.	Different charging facilities effect on the cell's capacity fade.....	91
Fig. 4.14.	Battery capacity comparison for uncontrolled and controlled charging	92
Fig. 4.15.	Daily and every other day charging effect on the battery capacity	93
Fig. 4.16.	Daily battery power and SOC for scenario 5.....	94

Fig. 4.17.	Comparison of frequency regulation and peak shaving	95
Fig. 4.18.	Cell capacity for Scenario 6	96
Fig. 4.19.	PV panels generated current for storage in the EV battery	97
Fig. 4.20.	Effect of morning solar energy storage and evening peak shaving.....	97
Fig. 4.21.	Capacity fade for active vs. passive thermal management systems	99
Fig. 4.22.	Capacity fade in different climates.....	99
Fig. 4.23.	Normal distribution of temperature data	99
Fig. 5.1.	Graphical view of the developed BN	115
Fig. 5.2.	Sample autocorrelation for acceleration data	120
Fig. 5.3.	Capacity fade data for three different test conditions.....	120
Fig. 5.4.	(a) Chain of samples for a capacity fade data point and (b) Histogram	121
Fig. 5.5.	Training set: (a) Capacity fade percentage gamma PDFs and	122
Fig. 5.6.	Model parameters' PDF	123
Fig. 5.7.	Test set: (a) capacity fade estimation distributions and.....	124
Fig. 5.8.	Directly affected parts of BN network in driving data	125
Fig. 5.9.	(a) Velocity kernel and (b) acceleration PDFs	126
Fig. 5.10.	PDFs of (a) EV power train efficiencies, (b) Auxiliary	127
Fig. 5.11.	(a) Beta PDFs of SOC and (b) gamma PDFs of Ah for all drivers	128
Fig. 5.12.	(a) Capacity fade PDFs and (b) mean of capacity fade PDFs	129
Fig. 5.13.	Contribution Coefficients PDFs in different frequency of grid services.....	130
Fig. 5.14.	(a) Total Ah and (b) capacity fade PDFs.....	131
Fig. 5.15.	(a) Temperature and (b) capacity fade distributions.....	132

List of tables

Table 2-1. Simulation parameters	44
Table 2-2. Statistical Analyses of Simulated Cycles	46
Table 3-1. Rayleigh Distribution Parameters of C_{rate} Data	69
Table 3-2. Statistical Results of All Simulated Cycles	71
Table 4-1. Simulated case scenarios	88
Table 4-2. Statistical results of simulations	102

Preface

Chapters of this dissertation contains published material. The following list provides the published material in conferences and journals.

M. Jafari, L. E. Brown, L. Gauchia, “Comprehensive Bayesian Network Model for EV Battery Capacity Fade,” In preparation.

M. Jafari, L. Gauchia, “Analyzing Li-ion Battery Aging Models: It Is a Matter of Scalability,” In preparation.

M. Jafari, A. Gauchia, S. Zhao, K. Zhang, L. Gauchia, “Electric Vehicle Battery Cycle Aging Evaluation in Real-World Daily Driving and Vehicle-to-Grid Services,” *IEEE Trans. Transportation Electrification*, 2017.

M. Jafari, A. Gauchia; K. Zhang, L. Gauchia, “Simulation and Analysis of the Effect of Real-World Driving Styles in an EV Battery Performance and Ageing,” *IEEE Trans. Transportation Electrification*, 2015.

A. Gauchia, M. Jafari, K. Zhang, L. Gauchia, “REV-cycle: A MATLAB-based tool for large-data analysis of real-life driving cycles for electric vehicles,” in *Transportation Electrification Conference and Expo (ITEC), IEEE*, 2015.

Mehdi Jafari had the main contribution on modeling and simulation, and writing the material for all of these publications.

Abstract

Nowadays, batteries in electric vehicles (EVs) are facing a variety of tasks in their connection to the power grid in addition to the main task, driving. All of these tasks play a very significant role in the battery aging, but they are highly variable due to the change in the driver behavior, grid connection availability and weather conditions. The effect of these external factors in the battery degradation have been studied in literature by mostly deterministic and some stochastic approaches, but limited to specific cases.

In this dissertation, first, a large-scale deterministic approach is implemented to evaluate the effect of variations in the EV battery daily tasks. To do so, a software tool named REV-Cycle is developed to simulate the EV powertrain and studied the effect of driving behavior, recharging facilities and timings, grid services and temperature/weather change effects, one by one. However, there are two main problems observed in the deterministic aging evaluation: First, the battery capacity fade factors such as temperature, cycling current, state of charge (SOC) ... are dependent to the external variables such as location, vehicle owner's behavior and availability of the grid connection. Therefore, it is not possible to accurately evaluate the battery degradation with a deterministic model, while its inputs are stochastic. Second, the battery aging factors' dependency is hierarchical and it is not easy to follow and implement this hierarchy with deterministic models.

Therefore, using a hierarchical probabilistic framework is proposed that can better represent the problem and realized that the Bayesian statistics with Markov Chain Monte Carlo (MCMC) can provide the problem solving structure needed for this purpose. A comprehensive hierarchical probabilistic model of the battery capacity fade is proposed

using Hierarchical Bayesian Networks (HBN). The model considers all uncertainties of the process including vehicle acceleration and velocity, grid connection for charging and utility services, temperatures and all unseen intermediate variables such as battery power, auxiliary power, efficiencies, etc. and estimates the capacity fade as a probability distribution. Metropolis-Hastings MCMC algorithm is applied to generate the posterior distributions. This modeling approach shows promising result in different case studies and provides more informative evaluation of the battery capacity fade.

Outline

The battery health and life cycle, similar to a living being, is heavily dependent to the events happening in its life. The usage profile and behavior pattern can significantly affect the battery health condition. The battery aging phenomena happens deep inside the battery cell, in the material level; however, its signs can be noticed in the macro-scale as the capacity fade and power fade. The capacity fade of the battery decreases the battery durability in a cycle of charge/discharge and its power fade limits its performance in providing higher current in specific cycles. Therefore, precise battery degradation evaluation and state of health estimation is important to first, have an accurate judgement about expectation from the battery performance in its specific application, and second, improve the battery health profile in order to enhance its lifespan, like a living being.

There are different approaches on the research about battery degradation, which can be mainly classified into two groups: offline laboratory/simulation-based researches and online application-based studies. The first group focuses on the experimental studies in the lab, trying to model the battery behavior in different cycling conditions with mathematical expressions. Results of these studies are important to add knowledge about the battery's behavior, realistic evaluation of its performance for specific applications and improve the design/production process. Although this method of study illustrates the general trend of the battery behavior, it has limitations on being exactly applicable to all the battery technologies and even different applications of a same battery technology, as each battery has its own usage condition.

The second group, on the other hand, studies the battery in its working environment, uses very limited information from the battery manufacturer and mostly relies on the measurements while the battery is delivering energy to its specific customer. This method

provides estimations about the battery health condition to improve the battery performance while working with a better control on the battery management systems (BMS). Note that these studies are not completely separate and there is a gray area between these methods.

My research lies down in the first group of mentioned studies, i.e. the offline simulation-based aging evaluation. My goal in this research was to study the battery capacity fade in electric vehicle application and find the most realistic evaluation of the EV battery capacity fade considering all its external effectual factors and their changes in different conditions of either usage or weather. Reviewing the literature in this subject, we realized some shortcomings. Some studies perform extensive aging tests on the battery cells in constant charge/discharge currents in different temperatures, while an EV current profile is very fluctuating. Others that use dynamic current profiles for test rely on the standard drive cycles which are significantly different from the real driving cycles. Studies that consider driving data eliminate the effect of temperature change. Most of them ignore the effect of different charging facilities and/or different utility services. Presented mathematical models in these studies suffer from similar limitations.

All of these problems are because of the multiple effecting factors on the battery aging which cannot be applied in one set of tests/simulations due to the time limitations. Even if a scenario is defined to perform the testing considering most of the factor, there are numerous scenarios that can be defined and it is impossible to study the battery degradation in all of them. Most of these factor are stochastic as they depend on the driver behavior or weather condition. In this research, the dependency of the battery capacity fade to its probabilistic external factors is modeled in a hierarchical approach to cover the mentioned shortcomings. This work has been carried out in different phases shown in the graphical outline of Fig. 1.

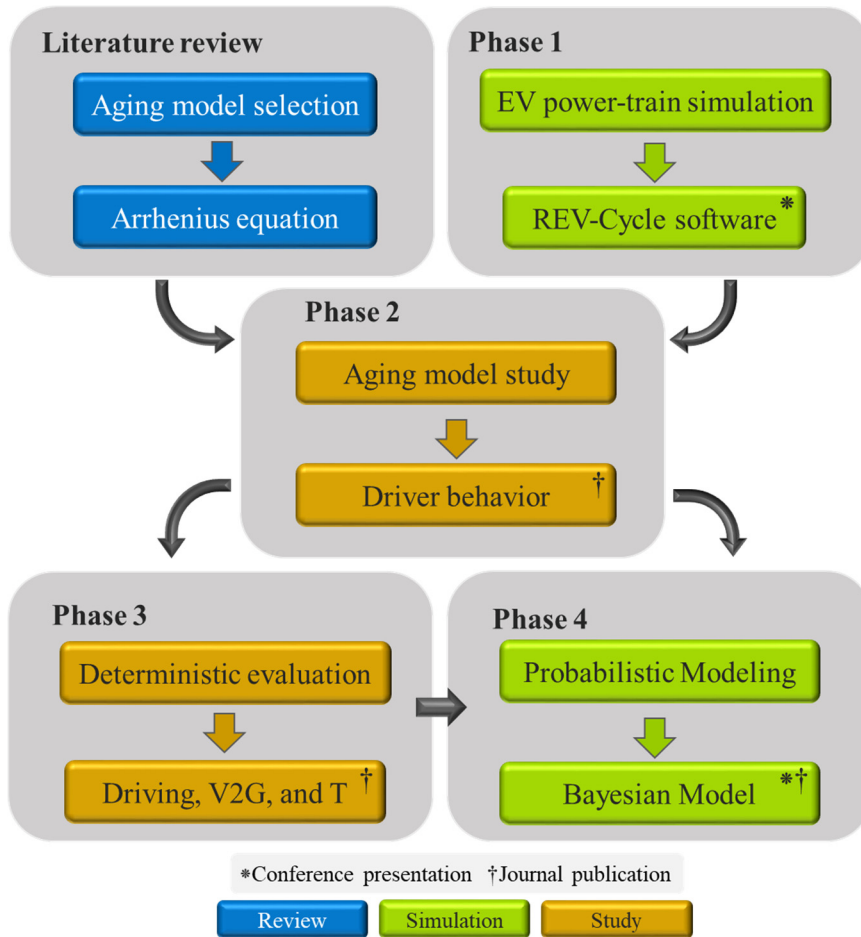


Fig. 1. Graphical outline

The literature review of the battery aging studies helped to decide about the aging model that could be used for the evaluation of the EV battery capacity fade. Outcome of this part was selecting the Arrhenius equation as the backbone of the capacity fade mathematical model. However, to be able to simulate the battery performance in an EV, it was necessary to simulate the EV power-train which is done in Phase 1. In this phase, a simulation tool in MATLAB named REV-Cycle (Real Electric Vehicle Cycle Analyzer) is developed to be able to test an EV battery performance in real driving data. The battery electrical equivalent model (ECM) in this tool was obtained experimentally on a commercial EV battery. By this simulation tool, the performance of the EV battery in

standard driving cycles and recorded real-world driving data are compared. Combining the aging model obtained from literature review and REV-Cycle form from Phase 1, in Phase 2, the effect of different driving behaviors on the battery capacity fade for more than 200 drivers is studied. The driving style in this part was classified to aggressive, mild and gentle based on their average acceleration. The battery energy consumption, power demand and the capacity fade were studied for groups of drivers. The capacity fade evaluated considering the effect of the battery current rate and ampere-hour.

The battery aging model simulated in Phase 2 is used in Phase 3 to evaluate the EV battery capacity fade in different daily driving, recharging, and vehicle to grid (V2G) scenarios. Note that the model itself was deterministic and therefore, the outputs of this phase are deterministic. In this phase, for the driving part, recorded data from 50 driver are used, for the recharging, standard L1 and L2 charger and for the utility services, either recorded data or the real data from online resources are employed. Daily scenarios are defined considering different combination and sequences of these events. Also, the effect of different climates/thermal management systems are studied. Although the results of this part reveals interesting facts about the battery capacity fade in different tasks, they cannot reflect the uncertainties of the battery aging external factor and their hierarchy, due to the deterministic definition of each scenario. For instance, driving distance is fixed to 29 miles per day or the contribution of each charging facility is fixed in the daily charging events.

Therefore, using the variables (as aging factors), sensitivity of the capacity fade to these variables, and the data from Phase 3, in Phase 4, a hierarchical probabilistic solution for the battery capacity fade estimation is proposed. Considering that the Bayesian model is a strong method of probabilistic modeling, a Hierarchical Bayesian Network model for the EV battery capacity fade is generated. A Bayesian Network including all uncertainties of the measurements and process models is developed and Markov Chain Monte Carlo

method is used to solve this probabilistic problem. The developed model considers effects of temperature change, driving behavior change, charging facilities difference, utility services possibility plus all uncertainties in the measurements, sampling and modeling through probability distributions and presents more informative results about the EV battery's capacity fade. The process that how the model is developed, trained and tested with a set of experimental data and used for the EV different case studies are presented. Results indicate that Bayesian approach is a very successful tool in estimating the unseen hidden variables of the battery capacity fade and it is a strong tool with high accuracy in case of limited observation. Also, it is observed that the probabilistic presentation of the battery aging conveys more useful information about the battery health condition and therefore result are more realistic and reliable.

Chapter 1

Analyzing Battery Aging Models¹

Abstract

In this chapter, the battery aging models are reviewed and analyzed. In the literature, the battery aging studies and proposed models are highly dependent to the requirements of different disciplines and researches. Chemical and material scientists are more interested in what happens inside the cell, while from the engineering view, the cell's performance in a module, pack or in a specific application is more important. Therefore, the proposed battery aging models can be classified based on the research's view "scale". This chapter explores the different battery aging scales from the material level to electrode, cell, module, pack and application level and presents the different mathematical models proposed for each level in the literature. Purpose of this chapter is to build the fundamental knowledge about the battery aging, which will be useful in the next chapters.

¹ The material contained in this chapter is in preparation for submission to a journal.

1.1 Introduction

As batteries are found in increasingly more devices, from portable to transportation and grid, battery aging remains as a challenging factor for manufacturers and users. Batteries, and in particular Li-ion, show high energy density, but limited lifetime [1]. Up to this point, batteries were mainly used for single tasks, but this scenario is moving towards multiple tasks. An example is an electric vehicle driving, recharging and providing grid services. As each task has a different priority, aging cost or benefit, all these factors need to be considered when scheduling the tasks during the life of the battery.

It can become even more relevant when batteries are repurposed for second life. For example, in transportation, due to the high power and energy demands, the battery end of life is reached when the capacity degrades to an 80% of the original capacity. Therefore, there is still available capacity that can be repurposed as a second life in less demanding applications [2]. In this second life, the battery starts from a degraded point due to its first life and will increase in degradation. Therefore, modeling and identifying the causes of degradation is highly relevant. However, approaches are spread out at different scales due to the dichotomy of aging taking place at the material level, but decision making and control taking place at the system level [3].

Available reports about the battery aging studies have mostly focused on the material-level aging mechanisms and methods and estimation methods without analyzing the mathematical aging models used for these purposes. While these are necessary, it may not be sufficient for all researchers or engineers, as depending on their perspective, they would first need to identify in which scale they need to gain the aging modeling information, and second, how to model/simulate the battery aging in that specific scale. The objective of this chapter is to analyze the current approaches to the battery aging

modeling in each scale, identifying how each model scales up and its applicability to different purposes (real-time control, battery repurposing selection, etc.). This review will help the readers to identify the main aging factors and variables in each scale, mathematical aging models and their strength and weaknesses to be able to simulate the models for their own purpose. Fig. 1.1 provides the graphical illustration of this chapter's trend.

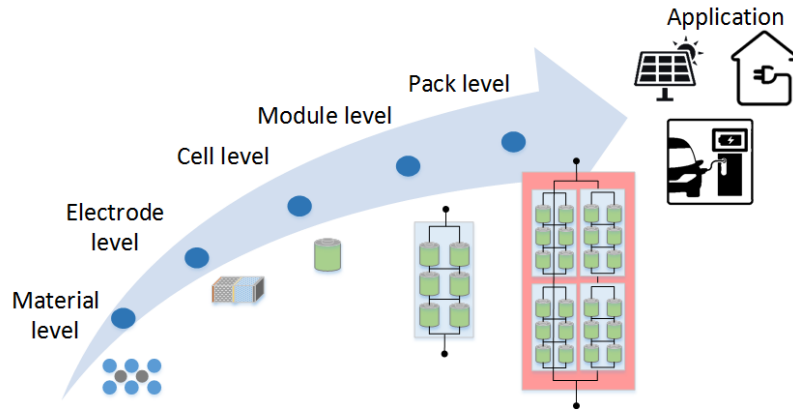


Fig. 1.1. Trend of the aging models analyses in the chapter

1.2 Material and Electrode Level Models

Before discussing the aging phenomenon inside the battery cell, a brief overview on the Li-ion battery cell performance will be helpful. A Li-ion battery cell has three main parts; negative electrode, electrolyte and positive electrode (Fig. 1.2).

During discharge, Li ions de-intercalate from the negative electrode, passing through the electrolyte, intercalate in the positive electrode. At the same time, electrons travel in same direction through the external circuit. The opposite reactions happen during the charge. To quantify this phenomenon, the Single Particle (SP) model presented in [4]–[7] is used widely in aging study literature. Based on SP, the governing equations of Li-ion battery cell include the conservation of charge and species in solid and electrolyte phases as follows [6]:

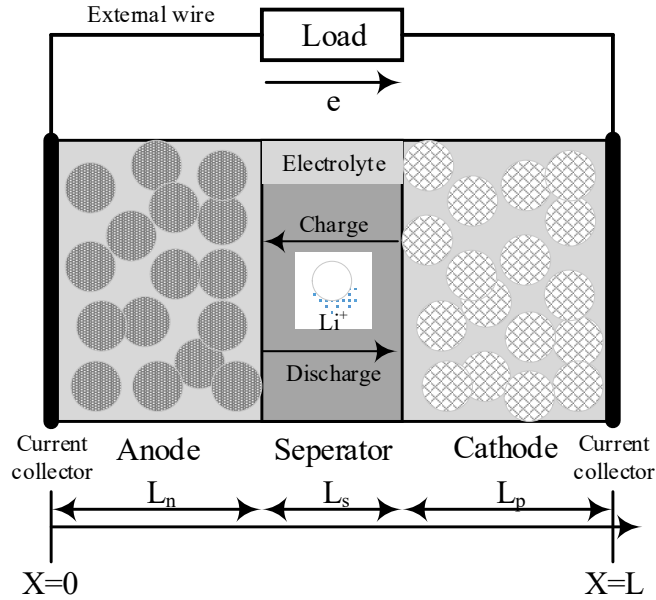


Fig. 1.2. Li-ion cell schematic

Conservation of charge in solid phase:

$$\frac{\partial}{\partial x} \left(\sigma^{eff} \frac{\partial}{\partial x} \phi_s \right) = j^{Li} \quad (1-1)$$

$$\text{Boundary Conditions: } -\sigma_-^{eff} \frac{\partial}{\partial x} \phi_s |_{x=0} = \sigma_+^{eff} \frac{\partial}{\partial x} \phi_s |_{x=L} = \frac{I}{A}$$

Conservation of charge in electrolyte phase:

$$\frac{\partial}{\partial x} \left(\kappa^{eff} \frac{\partial}{\partial x} \phi_e \right) + \frac{\partial}{\partial x} \left(\kappa_D^{eff} \frac{\partial}{\partial x} \ln c_e \right) = -j^{Li} \quad (1-2)$$

$$\text{Boundary Conditions: } \frac{\partial}{\partial x} \phi_s |_{x=L_-} = \frac{\partial}{\partial x} \phi_s |_{x=L_+ + L_{sep}} = 0$$

$$\frac{\partial}{\partial x} \phi_e |_{x=0} = \frac{\partial}{\partial x} \phi_e |_{x=L} = 0$$

Conservation of species in solid phase:

$$\frac{\partial c_s}{\partial t} = \frac{D_s}{r^2} \frac{\partial}{\partial r} \left(r^2 \frac{\partial c_s}{\partial r} \right) \quad (1-3)$$

$$\text{Boundary Conditions: } \frac{\partial}{\partial r} c_s |_{r=0} = 0, \quad D_s \frac{\partial}{\partial r} c_s |_{r=R_s} = \frac{j^{Li}}{a_s F}$$

Conservation of species in electrolyte phase:

$$\frac{\partial(\varepsilon_e c_e)}{\partial t} = \frac{\partial}{\partial x} \left(D_e^{eff} \frac{\partial}{\partial x} c_e \right) + \frac{1-t_+^0}{F} j^{Li} \quad (1-4)$$

$$\text{Boundary Condition: } \frac{\partial}{\partial x} c_e |_{x=0} = \frac{\partial}{\partial x} c_e |_{x=L} = 0$$

where, the solid and electrolyte potentials ϕ_s and ϕ_e and the lithium concentrations in the solid and electrolyte phases c_s and c_e are the variable of these equations. The electronic conductivity σ^{eff} , ionic conductivity κ^{eff} and the electrolyte diffusion coefficient D_e^{eff} are corrected by Bruggeman factor [4]. The solid and electrolyte phase volume fractions are defined by ε_s and ε_e , respectively. Detailed discussion about these equations can be found in [8]. The Li-ion current density j^{Li} can be calculated using Butler-Volmer equation as follow:

$$j^{Li} = a_s i_0 \left[\exp \left(\frac{\alpha_s F}{RT} \eta - \frac{R_{SEI}}{a_s} j^{Li} \right) - \exp \left(\frac{\alpha_c F}{RT} \eta - \frac{R_{SEI}}{a_s} j^{Li} \right) \right]. \quad (1-5)$$

Here, i_0 is the exchange current density, F , R and T are the Faraday's constant, the gas constant and the temperature, respectively. α_s and α_c are the negative and positive electrodes transfer coefficients. The local surface over-potential, η can be calculated by:

$$\eta = \phi_s - \phi_e - U \quad (1-6)$$

where U is the open circuit potential and is a function of state of charge (SOC) and can be defined empirically [9], [10]. The equation (1-5) can be written for both the positive and negative electrodes separately [11]. Solving the Eqs. (1-1)-(1-4) defines the performance of the battery cell. These equations are the base for the material and electrode level aging studies.

Inside a Li-ion battery cell, aging starts in the electrodes/electrolyte interface. The degradation in the positive and negative electrodes follow different mechanisms [12]. Negative electrode is commonly carbon-based and is made of graphite, titanate or silicon [13]. The major source of aging in the negative electrode is the formation of a resistive layer between the electrode and electrolyte surface due to the side reactions named solid electrolyte interface (SEI) [14]. The SEI is normally formed during first cycling of the battery and protects the electrode from corrosion and the electrolyte from reduction [15], [16]. However, in the long term, SEI's thickness and shape continues to grow and penetrates the porous structure of the negative electrode leading to (i) loss of effective surface of the electrode (ii) increased resistance against Li ions penetration and (iii) loss of cycleable lithium [17]–[19]. Note that the electrolyte materials define the SEI shape and properties [20].

Studies show that the high temperatures enhance the aging associated with SEI formation [21]–[23] and low temperatures lead to Li plating due to the lower rate of lithium diffusion which reduces the cycleable lithium [24]. Another aging factor in the negative electrode can be the mechanical or electrical contact loss between the anode active materials and parts due to the cycling [25]. Most of the aging models in the material and electrode level focus on the aging in the negative electrode/electrolyte interface as they believe that side reactions and as a result SEI formation are more likely in the negative electrode due to its potential [26], [27]. Chiu et al. [28] have defined a time-variant parameter $c_{irr}^N(t)$ to present the loss of Li concentration in the negative electrode at N^{th} cycling. After each cycle, they update the Li concentration in the negative electrode (solid phase) c_s as follow:

$$c_s^{N+1} = c_s^N - c_{irr}^N(t = \tau_N) \quad (1-7)$$

where τ_N is the total discharge time of the cell at the N^{th} cycle. To calculate the $c_{irr}^N(t)$ general Arrhenius equation is used (1-8) and its parameters A_d and E_a are calculated from experiments performed by [29].

$$\frac{dc_{irr}^N(t)}{dt} = A_d \exp\left[\frac{-E_a}{RT(t)}\right]. \quad (1-8)$$

Safari et al. [30] have considered the side reactions kinetic equation as the index for SEI formation rate as follow:

$$i_s = -Fk_{f,s}c_{EC} \exp\left(-\frac{\beta_s F}{RT}(\Phi_1 - R_{SEI}i_t)\right). \quad (1-9)$$

And the growth rate of the SEI by [31]:

$$\frac{\partial \delta}{\partial t} = -\frac{i_s M_{SEI}}{2F \rho_{SEI}} \quad (1-10)$$

where, δ is the SEI thickness. $k_{f,s}$ and c_{EC} refer to rate constant of side reactions and solvent concentration in the SEI film, respectively. β_s is the charge transfer coefficient for the side reactions and R_{SEI} and i_t are the SEI resistance and electrode total current, respectively. M_{SEI} stands for the SEI molecular weight and ρ_{SEI} is its density.

In [11], [32], Prada et al. have improved the previous model by adding the thermal behavior of the battery and also calculating both the capacity fade and power fade from the side reactions current density. The capacity fade is quantified by the percentage loss of the lithium available charge Q_s in the negative electrode as follow:

$$\frac{dQ_s}{dt} = S_n i_s \quad (1-11)$$

where S_n is the negative electrode' active surface. To find the power fade, the rate of rise of the SEI resistance is calculated from (1-12).

$$\frac{dR_{SEI}}{dt} = -\frac{1}{\kappa_{SEI}S_n} \frac{i_s M_{SEI}}{2F\rho_{SEI}} \quad (1-12)$$

The increase in SEI film resistance decreases the electrode porosity and effective diffusion coefficient which leads to increase in the ohmic resistance and power fade. Note that the total SEI film resistance is the sum of the initial resistance and its increase due to the SEI formation as follow [33]:

$$R_{film} = R_{ini} + \frac{\delta_{SEI}}{\kappa_{SEI}}. \quad (1-13)$$

Randall et al. [34] suggest that the model in [33] has a bulk computation burden for the BMS and control purposes. Therefore, they have presented an incremental model for SEI resistance and capacity fade calculations with simplifying assumptions as quasi-equilibrium state for cell and neglecting local electrolyte and electrode surface concentration variations, uniform intercalation and side reactions current density in anode surface and equal anode and cathode charge transfer coefficients. These simplifications account for less than 1% error, based on the results.

Also, Tanim et al. [35] have developed another reduced order non-linear physic-based SP model and combined it with the aging calculations of Eqs. (1-11) and (1-12) which simplifies and reduces the model computations. Graphical illustration of the discussed battery performance and aging models is presented in Fig. 1.3. The current and temperature are the input variables for the models. Open circuit voltage (OCV) as a function of SOC comes from the experiments and electro-chemical properties are defined for every battery chemistry and materials. Output of these models are the battery voltage, capacity and power losses. In each iteration of simulation, Li current density is used to calculate the side reactions and as a result the aging variables. Then, the SEI resistance and Li concentration in negative electrode are updated for the next simulation step.

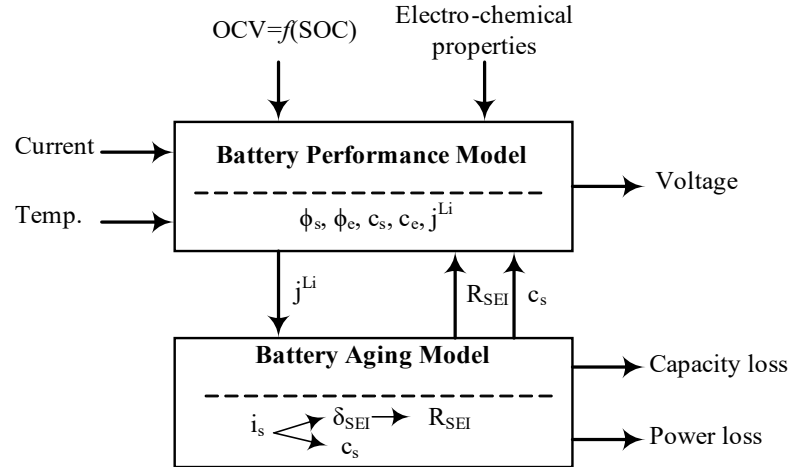


Fig. 1.3. Material and electrode level aging models' block diagram

Aging in the positive electrode happens slightly different than the negative electrode. The SEI formation in the positive electrode is dependent on the material used in the electrode but it cannot be detected easily [36]. Experiments show that the impedance rise due to the cycling in the negative electrode is higher than the positive electrode [37] which indicates that the main SEI formation takes place on the negative electrode surface. Although the first stage of aging in the Li-ion cell is the SEI formation and cycleable Li loss in the negative electrode, the second stage in the battery cell aging is the loss of active materials in the positive electrode, which causes the cathode to be more intercalated at the end of each discharge [23].

The cathode active material loss can be result of structural disordering, phase transitions and metal dissolution [38]. The positive electrode aging is not limited to the active materials loss; it also can be caused by the inactive components degradation as binder decomposition, corrosion of the current collector and oxidation of the conductive agents [39]. Literature in the positive electrode aging mainly focus on the experimentally oriented studies and do not present mathematical modeling of aging in the cathode. Fig. 1.4 summarizes the aging causes in the positive and negative electrodes.

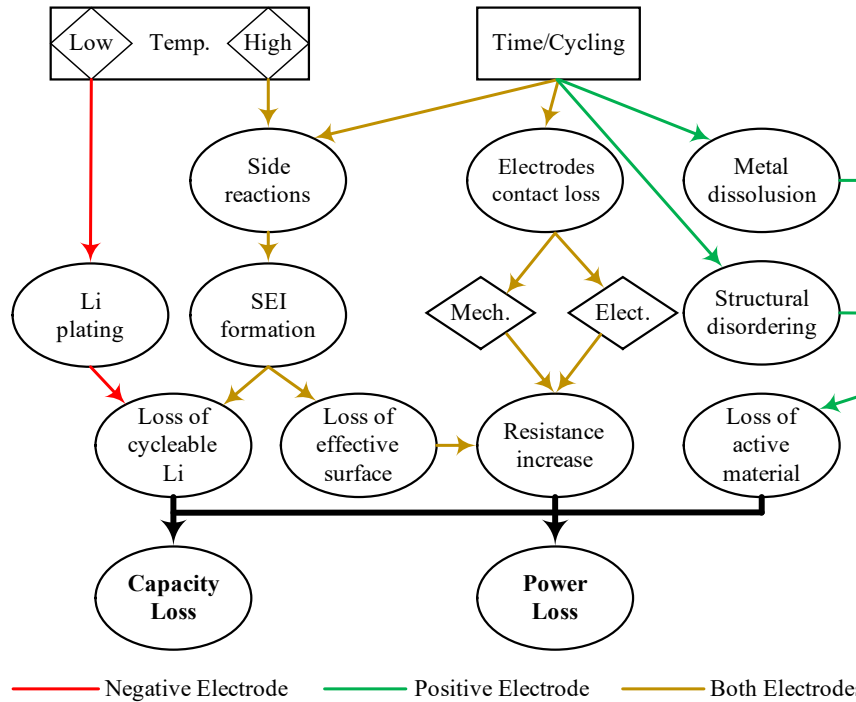


Fig. 1.4. Main aging causes in negative and positive electrodes

In summary, the material and electrode level capacity and power fade models can be simulated by: first, calculating the side reactions current, second, obtaining the SEI film thickness, then SEI resistance growth for power fade analysis and third, calculating the cycleable lithium loss for the capacity fade analysis. These models have high accuracy due to their detailed inside-the-cell dynamic equations without requiring bulk experimental measurements, but they have complicated differential equations to be solved in each iteration and therefore, high computational load.

1.3 Cell Level Models

Aging models in the material and electrode level include the governing electro-chemical differential equations to simulate both the real time performance and aging of the battery, as observed in the previous section. These equations are solved simultaneously and after each iteration, the parameters related to the aging such as cycleable lithium loss and

SEI resistance are updated. However, in the cell level aging models, the battery cell is considered as an electrical equivalent circuit with time-variant elements. Scaling up from the material level to the cell level is changing the view from the electro-chemical reactions inside the cell to the electrically measurable variable as voltage, impedance, ampere-hour (Ah) on the cell terminals.

The battery aging phenomenon happens in both the storage and cycling modes. The aging associated with the storage period, “calendar aging” is dependent to the storage temperature, SOC of the battery and time (1-14) [40]. As the SOC of the battery and its terminal voltage are directly related, some literature have translated the battery SOC to its storage voltage [41], [42]. For the aging caused by the battery utilization, “cycle aging”, the effectual factors are ambient temperature, SOC, depth of discharge (DOD), charge/discharge current and number of cycles (1-15) [43]–[45].

$$Q_{cal.} = f(T, SOC, t) \quad (1-14)$$

$$Q_{cyc.} = g(T, SOC, DOD, I_{ch/dch}, N) \quad (1-15)$$

$Q_{cal.}$ and $Q_{cyc.}$ refer to the percentage calendar and cycle capacity fade. The calculation from the mentioned aging factors to the capacity and power losses is shown in Fig. 1.5.

Studies on the cell level aging modeling are empirically-oriented and present fitted mathematical models which follow the data derived from extensive experimental work. Due to the large amount of time and work needed for the battery aging tests, these tests are performed under accelerated aging condition with elevated temperatures. Note that the higher temperature has significant effect on the battery aging acceleration [45]. So, Bloom et al [46] tested 0.9Ah 18650 cells in temperatures above 40°C to investigate the calendar and cycle life of the battery. They used general Arrhenius equation to fit the experimental data (1-16).

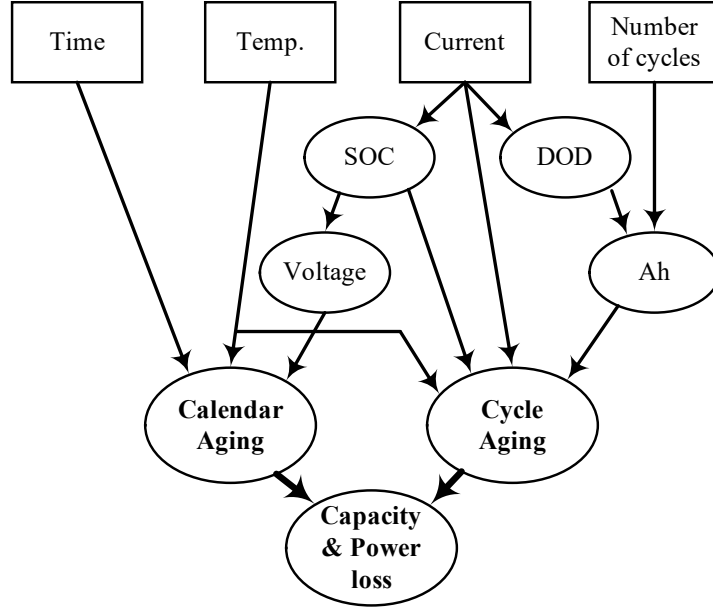


Fig. 1.5. Aging factors in the cell level models

$$Q = B \exp\left(\frac{-E_a}{RT}\right) t^z \quad (1-16)$$

where, B is pre-exponential factor, E_a is the activation energy in J , R is universal gas constant, T is the temperature and t is time. z is the power factor. Numerical values of these parameters for different test conditions are presented in [46]. Their model explains the battery capacity fade and power fade in both the calendar and cycle aging with power law of time. Although the time is a reasonable variable in the calendar aging evaluation, the capacity fade due to the cycling is more dependent to the Ampere-hour (Ah) throughput. In addition, in constant current charge and discharge cycles, the Ah throughput is directly related to the time. Therefore, authors in [47] altered the time to Ah in Arrhenius equation to be able to study the effect of different C-rates on the battery aging (1-17). Based on their model, the pre-exponential factor and activation energy are a function of C-rate and the power factor is a constant value.

$$Q_{cyc.} = B \exp\left(\frac{-31700+370.3 \times C_{rate}}{RT}\right) Ah^{0.55} \quad (1-17)$$

Ah in this equation can be calculated as:

$$Ah = N.DOD.C \quad (1-18)$$

where, C is the rated capacity of the battery cell and N is the number of cycles. Numerical data for B provided in [47] adopted to fit an exponential function of C-rate as follow [48]:

$$\ln B = 1.226 \exp(-0.2797 \text{ C-rate}) + 9.263. \quad (1-19)$$

This model includes the effect of temperature, DOD, C-rate and number of cycles, however it is not considering the impact of SOC. Authors in [49] present a similar model relating the pre-exponential factor B to the SOC of the battery during cycling (1-20).

$$Q_{cyc.} = (\alpha \text{ SOC} + \beta) \exp\left(\frac{-E_a + \eta \times \text{C-rate}}{RT}\right) Ah^z \quad (1-20)$$

Values for α , β , η and z can be found in [49]. These models are helpful to evaluate the battery health condition. However, they are valid only in identical repetitive conditions. Han et al [50] have employed accumulated damage theory and modeled the battery degradation in each cycle which can be different from the previous cycling conditions. They have presented a discrete capacity fade model (1-21)-(1-23) calculating the capacity loss associated with each cycle and adding it to the capacity loss of previous cycles.

$$Q_{cyc.(1)} = B \exp\left(\frac{-E_a}{RT}\right) \cdot N, \quad N = 1 \quad (1-21)$$

$$Q_{cyc.(N+1)} = Q_{cyc.(N)} + k_1 \exp\left(\frac{k_2}{T}\right) \cdot Q_{cyc.(N)}^{k_3} \quad (1-22)$$

$$k_1 = zB^{\frac{1}{z}}, k_2 = -\frac{E_a}{zR}, k_3 = \frac{z-1}{z} \quad (1-23)$$

This model provides the parameters resulted from tests and it is a practical model that should be calibrated to avoid accumulated error due to the difference in the test and real world conditions.

Another practical model that can be used for real world battery degradation simulations is presented by Lam et al. [51] considering the effect of SOC, DOD, temperature and Ah throughput. Authors referred to [52] to calculate the average SOC, SOC_{avg} and its standard deviation, SOC_{dev} from the SOC profile of the battery after a cycling as (1-24) and (1-25).

$$SOC_{ave} = \frac{1}{Ah} \int_{Ah} SOC(Ah) dAh \quad (1-24)$$

$$SOC_{dev} = \sqrt{\frac{3}{Ah} \int_{Ah} (SOC(Ah) - SOC_{avg})^2 dAh} \quad (1-25)$$

Following Millner's work [49], the capacity fade is calculated by the multiplication of exponentials of SOC_{ave} and SOC_{dev} . However, Lam's experimental results fitting shows an empirical function. By including the temperature effect, the capacity fade model is concluded as follow:

$$Q_{cyc.} = \sum_i^N \left(\left(\frac{k_1 SOC_{dev,i} \exp(k_2 SOC_{avg,i})}{k_3 \exp(k_4 SOC_{dev,i})} + \right) \exp\left(-\frac{E_a}{R} \left(\frac{1}{T_i} - \frac{1}{T_{ref}}\right)\right) \right) \cdot Ah_i \quad (1-26)$$

where, k_1 to k_4 are calculated from the experimental results' fitting. Although the temperature dependency in most of the aging models is indicated by the Arrhenius law, Omar et al [53] claim that the Li-ion cells characteristic is not completely exponential and therefore they suggest polynomial function for the temperature factor simulation in the battery model (1-27) based on the test results.

$$CL(T) = k_1 T^3 + k_2 T^2 + k_3 T + k_4 \quad (1-27)$$

where CL is the cycle number before end of life (EOL) of the battery. Similarly, they use the experimental data to fit exponential functions to include the discharge current I_d , DOD and charge current I_{ch} .

$$CL(I_d) = k_5 \exp(k_6 I_d) + k_7 \exp(k_8 I_d) \quad (1-28)$$

$$CL(DOD) = k_9 \exp(k_{10} DOD) + k_{11} \exp(k_{12} DOD) \quad (1-29)$$

$$CL(I_{ch}) = k_{13} \exp(k_{14} I_{ch}) + k_{15} \exp(k_{16} I_{ch}) \quad (1-30)$$

k_1 to k_{16} are concluded from the fittings and can be found in [50]. Considering these equations as core part of the model, authors evaluate the effect of each factor in each cycling and calculate the maximum number of cycling in different conditions.

Not all the aging models focus on the cycle aging, some studies explore the calendar aging specifically. Ecker et al [41] suggest that the calendar aging is square root of time and is affected by the temperature and voltage which can be calculated by experimental data fitting method used by [54], [55] for super capacitor aging calculations. However, the calendar aging does not always change by the square root of the time. Different tests show that it may have linear dependency to time or even combination of both [44]. Considering both perspectives, battery calendar aging can be fitted to (1-31).

$$Q_{cal.} = k_1 t + k_2 \sqrt{t} \quad (1-31)$$

Where, k_1 and k_2 can represent the effect of the temperature and the SOC/voltage by an exponential function, polynomial function or combination of both. Marongui et al [42] consider the square root dependency of capacity fade to the time ($k_1 = 0$) and define an exponential fitting function for k_2 as follow:

$$k_2 = \alpha \exp\left(-\frac{\beta}{T}\right) \cdot \exp(\lambda V) \quad (1-32)$$

where, V stands for the storage voltage.

To present a more comprehensive study, [40] considers both the calendar and cycle degradation in the capacity fade modeling. For the calendar life, it studies the storage

voltage, V , and temperature effect and for the cycle life, it tests the effect of DOD and the average voltage, V_{avg} . By testing the battery cells in both the storage and cycling modes and combining their aging effectual factor, the aging model is presented as follow:

$$Q = Q_{cal.} + Q_{cyc.} = \alpha t^{0.75} + \beta Ah^{0.5} \quad (1-33)$$

where:

$$\alpha = (k_1 V + k_2) \exp\left(\frac{k_3}{T}\right) \quad (1-34)$$

$$\beta = k_4 (V_{avg} + k_5)^2 + k_6 DOD + k_7 \quad (1-35)$$

And k_1 to k_7 are calculated from fitting results. In [56], an energy based aging model considering calendar and cycle aging is presented. A new term as “state of energy (SOE)” is defined which is very similar to the SOC. Total capacity fade in this model is sum of calendar and cycle agings as:

$$Q = Q_{cal.} + Q_{cyc.} \quad (1-36)$$

where the calendar life is affected by the SOE and the temperature as follow:

$$Q_{cal.} = Q_{cal.0} \exp\left(\frac{SOE - SOE_0}{k_1}\right) \cdot \exp\left(\frac{T - T_0}{k_2}\right) \sqrt{t}. \quad (1-37)$$

$Q_{cal.0}$ is the nominal capacity fade in the condition with SOE_0 and T_0 . k_1 and k_2 are fitting parameters. For the cycle aging, different cycles' accumulated capacity fade is considered. For each cycle, a polynomial function of change of SOE as (1-38) calculates the capacity fade.

$$Q_{cyc.} = \sum_i^N (k_3 \Delta SOE_i^3 + k_4 \Delta SOE_i^2 + k_5 \Delta SOE_i) \quad (1-38)$$

Again, k_3 to k_5 are fitting parameters from experiments.

As indicated in Fig. 1.6 and similar to the material and electrode level models, the current and temperature are the input variables in the cell level models. OCV and circuit elements (R, L and C) are obtained from the experiments as functions of SOC and temperature. SOC from the performance model is used besides the current and temperature to calculate the aging and update the capacity.

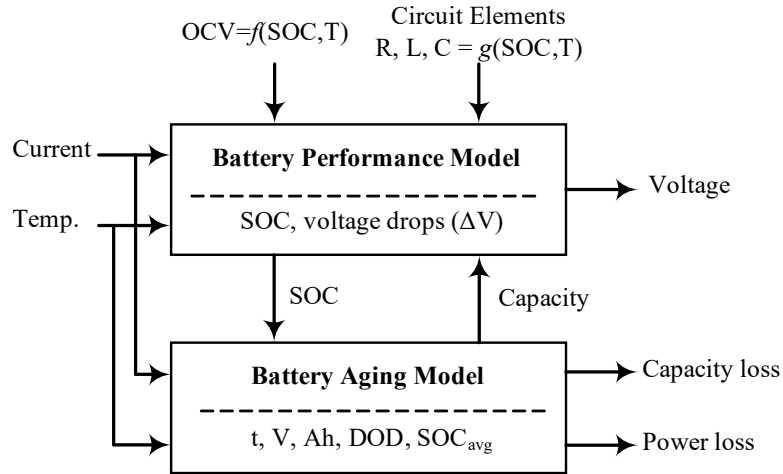


Fig. 1.6. Cell level aging models block diagram

As observed, cell level aging models rely on the experimental results and therefore, they are valid only for the specific battery technology and defined test conditions. Although these models are easy to simulate and reduce the computational load, they are less accurate compared to the material level models. One way to improve the accuracy of these models is to recalibrate the model parameters for any specific condition.

1.4 Module and Pack Level

A single Li-ion battery cell has limited power and capacity. Thus, for the high power and energy applications, the cells are connected in series or parallel configurations to form battery modules and pack with increased voltage, current and stored energy capability. However, internal differences among the cells of a module or a pack is unavoidable. The

source of this difference can be either the difference in the cells' production process, or different working conditions such as temperature and loading [57]. Among 20,000 fresh cells, measured initial capacity has a normal distribution with 1.3% deviation. Direct current internal resistance result for these cells has the same distribution with 5.8% deviation [58].

This phenomenon leads to inhomogeneous aging in the connected cells of a module or pack. For instance, two parallel-connected cells with 20% difference in the internal resistance experience 40% higher peak currents [59] compared to the case that two cell work dependently. These increased current peaks cause extra heat production in the cell. Also, the location of the cell inside the module and pack affects its heat dissipation and changes the cell temperature [60]. Therefore, boosted current and temperature causes expedited aging in these cells, refereeing to the aging models of previous section. Based on Gonoana et al., 20% difference in internal resistance of a pair of parallel cells can reduce the cycle life of both cells by 40 % [61]. In the series connected cells, the expediting aging factor is temperature, as the currents in series cells are equal.

Considering this discussion, aging models developed for the cell level are not sufficient to predict the aging behavior of a module or a pack. Pack simulation from cell model is valid only if the cell-to-cell variations are considered [62]. First step in solving the problem is to calculate/estimate the amount of imbalance between the cells to have quantitative understanding of the different working conditions for the cells. "State of Balance" is a concept presented by Wang et al. [57] to estimate the cells imbalance for dynamic equalization adjustment. One major imbalance factor is temperature which causes mismatch on the cell resistance leading to unbalanced currents and different aging behavior. During the discharge of a module with parallel cells, cell with higher temperature has higher current extraction until 75% DOD. After that, current falls until 90 % DOD and

then rises again to the end of discharge. This result shows significant impact of temperature in cells' performance, reported in [63]. Authors indicate linear relationship between the capacity fade difference and temperature difference between cells. Also, Le Bel et al. [64] explored the parallel connected cells aging by an electro-thermal model to include the current imbalance effect for better understanding of the aging difference in single cell and pack. Incremental capacity analysis (ICA) is reported to be a suitable tool for study of the difference in cell and pack capacity fade due to difference in the internal resistance, temperature too [65], [66].

Next step is to bridge the gap between cell aging models and module/pack aging calculations. In a battery pack with parallel and series cells, the basic approach is to neglect the current imbalance in the parallel cells and consider them as a bigger cell due to the passive balance control, then, calculate the aging for the series cells considering their working condition by updating the cell aging model using the SOC and SOH information from the pack. At this point, deciding about the pack capacity fade from cells' aging information can follow several methods [67]–[69]. The simplest method is to select the most aged cell as the representative of whole pack and calculate the pack capacity fade as follow [70], [71]:

$$Q_p = \max Q_{c,i} \quad i = 1:M \quad (1-39)$$

where, $Q_{c,i}$ is each cell's capacity fade and M is the number of cells. Disadvantage of this method is that it overestimates the pack capacity fade. Taking the average of cells capacity fade for the pack aging estimation is another approach that underestimates the total capacity fade. Therefore, authors in [58], [69] suggest to use probabilistic aging estimation, which finds the probability distribution of cells capacity and presents the whole pack capacity by a probability distribution function. However, the results show that although the estimation error is improved, this method still underestimates the pack aging, slightly.

Another method presented in [67], [68] defines chargeable and dischargeable electric quantities (CEQ and DEQ) for each cell to relate the pack capacity to individual cells capacity. Based on their definition, the pack capacity is the sum of minimum CEQ and minimum DEQ among the pack's cells as follow:

$$C_p = \min(SOC \cdot C) + \min((1 - SOC) \cdot C) \quad (40)$$

where, SOC and C are the all cells' SOC and capacity vectors. The graphical illustration of the process to calculate the pack capacity from cells' capacities is indicated in Fig. 1.7 which is named "Electric quantity -Capacity Scatter Diagram" (ECSD). In this method, for a specific SOC, the cell with minimum chargeable electric quantity to 100% SOC and the cell with minimum dischargeable electric quantity to 0% SOC are distinguished. These quantities are the charge and discharge capability of the whole cell before reaching to the voltage limits of full charge and full discharge. Therefore, total capacity of the pack is the sum of these quantities. As noticed, the pack capacity in this method is not necessarily defined by the cells with minimum capacity.

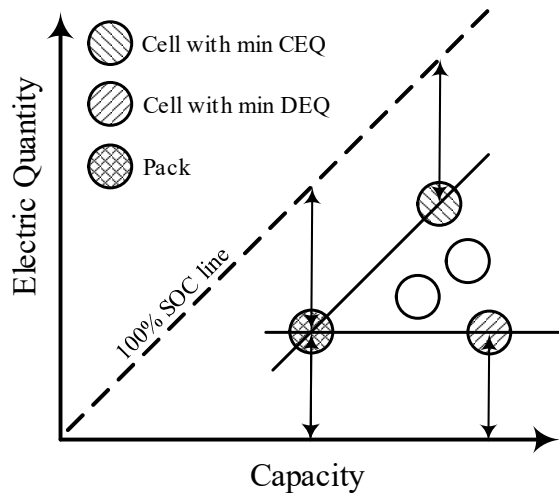


Fig. 1.7. Electric quantity -Capacity Scatter diagram for pack capacity estimation from its cells capacity [67]

1.5 Application Level

All the aging models presented in the cell level and the methods discussed to use those models and expand them to the module and pack level aging are concluded in the test condition that the battery is separated from its application and it is possible to test the battery as many time as required for the study. However, in a real-world battery life it is not easy to stop the battery's task, separate it from the defined application and test it frequently. Therefore, in the application level other methods are used to simplify the aging estimation with minimum measurement and test requirements. Note that, studies in this level do not present aging models for the simulation purposes and they focus on the estimation methods to be implemented in BMS in real life battery applications.

The main objective in these methods is to prevent stopping the battery task and they can be categorized in two principle groups: experimentally oriented and adoptive methods [72]. The experimental methods measure and store the aging related variables and calculate the aging in each state of life of the battery using simplified aging model and knowledge from the history of the battery performance. Resistance measurement in different current signals [73], joule effect which is the generated heat by the internal resistance [74] and Ah throughput counting [75], [76] are some of these approaches. Remmlinger et al. [77] proposed a resistance estimation method using a specific current signal detection while the battery is working and measuring the voltage for resistance calculation. Ah throughput counting method using the aging model presented in [43] is another study presented in [78]. As the working condition of a battery such as loading and temperature change during its life, total Ah counting rises the aging estimation error. Therefore, Marano et al. [79] suggested to use effective Ah counting which defines weighting coefficients for each Ah considering the different working conditions. Although these methods have low

computational burden and are easy to implement in the BMS, they require large data storing capacity and also, they have less accuracy due to the accumulated error during time.

Adoptive methods calculate the parameters sensitive to the aging such as resistance and estimate the life of the battery from those calculations. These methods eliminate the need for bulk measurements and simulations of the battery performance. For this purpose, they use different algorithms such as Kalman filter [80] and its improved versions, observers [81], fuzzy logic [82], artificial neural networks [83] and least squares [84]. All these methods can target specific aging related parameter in the battery. For example, Gholizadeh et al. [85] have used sliding mode type observer (SMO) and Remmlinger et al. [86] employed linear parameter-varying (LPV) model on series resistance measurements. They have used general measurements which are available in the BMS. In [87], Kalman filter is applied for aging estimation by cell capacitance from Randles' equivalent circuit model and it is shown that the aging of the battery has linear relationship with that capacitive property. Adoptive methods have higher accuracy compared to the experimental methods, however they have high computational load and are not easy to implement.

Along with the experimental and adoptive methods that focus on the measurement of an aging related parameter and/or development of a computational method using several measured parameters, another approach is to reduce the measurements and computations by sampling small group of cells [88]. In this method, a new circuit topology of the battery pack is needed which separates it into two test and main groups. The circuit configuration is in a way that while the main group is working, the test group cells can be separated by relays and measurements can be performed without disturbing the function of the battery. This method simplifies and reduces the computational burden with the cost of slightly lowering the accuracy.

1.6 Conclusions

This chapter reviewed the battery aging models and classified them in different scales. The material and electrode level models focus on the electrochemical equation of the inside the cell materials. Although these models are more detailed, but they have complicated analyses and high amount of calculation burden. Cell level models are derived from the experimental data and they are useful in simulation. However, they cannot be used for the cases very different from the test conditions. Module, pack and application level studies do not present mathematical model, instead they use cell level models and adapt them for the higher scales. Considering the gained knowledge about the aging models, the suitable choice for our research is a mathematical model from the cell level studies (Eq. (1-17)) and update it for EV application. To do so, we need a tool that simulates the EV and its battery performance. Therefore, the first step is to develop the EV power-train model, which is presented in the next chapter.

References

- [1] A. Yoshino, "The birth of the lithium-ion battery," *Angewandte Chemie - International Edition*, vol. 51, no. 24, pp. 5798–5800, 2012.
- [2] L. C. Casals, B. A. García, F. Aguesse, and A. Iturrondobeitia, "Second life of electric vehicle batteries: relation between materials degradation and environmental impact," *International Journal of Life Cycle Assessment*, 2015.
- [3] B. Pilvelait, C. Rentel, G. L. Plett, M. Marcel, and D. Carmen, "An Advanced Battery Management System for Lithium Ion Batteries," *Ndia Gr. Veh. Syst. Eng. Technol. Symp.*, pp. 1–7, 2011.
- [4] W. B. Gu and C. Y. Wang, "Thermal-Electrochemical Modeling of Battery Systems," *J. Electrochem. Soc.*, vol. 147, no. 8, p. 2910, 2000.
- [5] J. Fuller, Thomas F. Doyle, Marc. Newman, "Simulation and Optimization of the Dual Lithium Ion Insertion Cell," *J. Electrochem. Soc.*, vol. 141, no. 1, p. 1, 1994.
- [6] M. Doyle, T. F. Fuller, and J. Newman, "Modeling of Galvanostatic Charge and Discharge of the Lithium Polymer Insertion Cell," *J. Electrochem. Soc.*, vol. 140, no. 6, pp. 1526–1533, 1993.

- [7] M. Doyle, J. Newman, and J. Reimers, "A quick method of measuring the capacity versus discharge rate for a dual lithium-ion insertion cell undergoing cycling," *J. Power Sources*, vol. 52, no. 2, pp. 211–216, 1994.
- [8] S. Atlung, K. West, and T. Jacobsen, "I %," pp. 1311–1321, 1979.
- [9] W. Fang, O. J. Kwon, and C. Y. Wang, "Electrochemical-thermal modeling of automotive Li-ion batteries and experimental validation using a three-electrode cell," *Int. J. Energy Res.*, vol. 34, no. 2, pp. 107–115, 2010.
- [10] P. Ramadass, B. Haran, R. White, and B. N. Popov, "Mathematical modeling of the capacity fade of Li-ion cells," *J. Power Sources*, vol. 123, no. 2, pp. 230–240, 2003.
- [11] E. Prada, D. Di Domenico, Y. Creff, J. Bernard, V. Sauvant-Moynot, and F. Huet, "Simplified Electrochemical and Thermal Model of LiFePO₄-Graphite Li-Ion Batteries for Fast Charge Applications," *J. Electrochem. Soc.*, vol. 159, no. 9, pp. A1508–A1519, 2012.
- [12] F. Joho, P. Novák, and M. E. Spahr, "Safety Aspects of Graphite Negative Electrode Materials for Lithium-Ion Batteries," *J. Electrochem. Soc.*, vol. 149, no. 8, pp. A1020–A1024, 2002.
- [13] Y. P. Wu, E. Rahm, and R. Holze, "Carbon anode materials for lithium ion batteries," *J. Power Sources*, vol. 114, no. 2, pp. 228–236, 2003.
- [14] P. Arora, "Capacity Fade Mechanisms and Side Reactions in Lithium-Ion Batteries," *J. Electrochem. Soc.*, vol. 145, no. 10, p. 3647, 1998.
- [15] R. Imhof, "In Situ Investigation of the Electrochemical Reduction of Carbonate Electrolyte Solutions at Graphite Electrodes," *J. Electrochem. Soc.*, vol. 145, no. 4, p. 1081, 1998.
- [16] H. Buqa, A. Würsig, J. Vetter, M. E. Spahr, F. Krumeich, and P. Novák, "SEI film formation on highly crystalline graphitic materials in lithium-ion batteries," in *Journal of Power Sources*, 2006, vol. 153, no. 2, pp. 385–390.
- [17] K. Amine *et al.*, "Factors responsible for impedance rise in high power lithium ion batteries," in *Journal of Power Sources*, 2001, vol. 97–98, pp. 684–687.
- [18] J. Y. Song, H. H. Lee, Y. Y. Wang, and C. C. Wan, "Two- and three-electrode impedance spectroscopy of lithium-ion batteries," *J. Power Sources*, vol. 111, no. 2, pp. 255–267, 2002.
- [19] M. Broussely, S. Herreyre, P. Biensan, P. Kasztejna, K. Nechev, and R. J. Staniewicz, "Aging mechanism in Li ion cells and calendar life predictions," in *Journal of Power Sources*, 2001, vol. 97–98, pp. 13–21.
- [20] G. E. Blomgren, "Electrolytes for advanced batteries," *J. Power Sources*, vol. 81–82, pp. 112–118, 1999.
- [21] M. Koltypin, D. Aurbach, L. Nazar, and B. Ellis, "More on the performance of LiFePO₄ electrodes - The effect of synthesis route, solution composition, aging, and temperature," *J. Power Sources*, vol. 174,

- no. 2, pp. 1241–1250, 2007.
- [22] O. Erdinc, B. Vural, and M. Uzunoglu, “A dynamic lithium-ion battery model considering the effects of temperature and capacity fading,” in *2009 International Conference on Clean Electrical Power, ICCEP 2009*, 2009, pp. 383–386.
- [23] Q. Zhang and R. E. White, “Capacity fade analysis of a lithium ion cell,” *J. Power Sources*, vol. 179, no. 2, pp. 793–798, 2008.
- [24] S. S. Zhang, K. Xu, and T. R. Jow, “The low temperature performance of Li-ion batteries,” *J. Power Sources*, vol. 115, no. 1, pp. 137–140, 2003.
- [25] Y. Wang, X. Guo, S. Greenbaum, J. Liu, and K. Amine, “Solid Electrolyte Interphase Formation on Lithium-Ion Electrodes: A [^{sup 7}]Li Nuclear Magnetic Resonance Study,” *Electrochem. Solid-State Lett.*, vol. 4, no. 6, p. A68, 2001.
- [26] D. Aurbach, B. Markovsky, A. Rodkin, M. Cojocaru, E. Levi, and H. J. Kim, “An analysis of rechargeable lithium-ion batteries after prolonged cycling,” *Electrochim. Acta*, vol. 47, no. 12, pp. 1899–1911, 2002.
- [27] M. Broussely *et al.*, “Main aging mechanisms in Li ion batteries,” in *Journal of Power Sources*, 2005, vol. 146, no. 1–2, pp. 90–96.
- [28] K.-C. Chiu, C.-H. Lin, S.-F. Yeh, Y.-H. Lin, C.-S. Huang, and K.-C. Chen, “Cycle life analysis of series connected lithium-ion batteries with temperature difference,” *J. Power Sources*, vol. 263, pp. 75–84, 2014.
- [29] J. Wang *et al.*, “Cycle-life model for graphite-LiFePO₄ cells,” *J. Power Sources*, vol. 196, no. 8, pp. 3942–3948, 2011.
- [30] M. Safari, M. Morcrette, a. Teyssoit, and C. Delacourt, “Multimodal Physics-Based Aging Model for Life Prediction of Li-Ion Batteries,” *J. Electrochem. Soc.*, vol. 156, no. 3, p. A145, 2009.
- [31] G. Ning, R. E. White, and B. N. Popov, “A generalized cycle life model of rechargeable Li-ion batteries,” *Electrochim. Acta*, vol. 51, no. 10, pp. 2012–2022, 2006.
- [32] M. Petit, E. Prada, and V. Sauvant-Moynot, “Development of an empirical aging model for Li-ion batteries and application to assess the impact of Vehicle-to-Grid strategies on battery lifetime,” *Appl. Energy*, vol. 172, pp. 398–407, 2016.
- [33] P. Ramadass, B. Haran, P. M. Gomadam, R. White, and B. N. Popov, “Development of First Principles Capacity Fade Model for Li-Ion Cells,” *J. Electrochem. Soc.*, vol. 151, no. 2, p. A196, 2004.
- [34] A. V. Randall, R. D. Perkins, X. Zhang, and G. L. Plett, “Controls oriented reduced order modeling of solid-electrolyte interphase layer growth,” *J. Power Sources*, vol. 209, pp. 282–288, 2012.
- [35] T. R. Tanim and C. D. Rahn, “Aging formula for lithium ion batteries with solid electrolyte interphase

- layer growth,” *J. Power Sources*, vol. 294, pp. 239–247, 2015.
- [36] M. Kerlau, M. Marcinek, V. Srinivasan, and R. M. Kostecki, “Reprint of ‘Studies of local degradation phenomena in composite cathodes for lithium-ion batteries,’” *Electrochim. Acta*, vol. 53, no. 3 SPEC. ISS., pp. 1386–1393, 2007.
- [37] K. Amine, J. Liu, and I. Belharouak, “High-temperature storage and cycling of C-LiFePO₄/graphite Li-ion cells,” *Electrochem. commun.*, vol. 7, no. 7, pp. 669–673, 2005.
- [38] M. Wohlfahrt-Mehrens, C. Vogler, and J. Garche, “Aging mechanisms of lithium cathode materials,” in *Journal of Power Sources*, 2004, vol. 127, no. 1–2, pp. 58–64.
- [39] J. Vetter *et al.*, “Ageing mechanisms in lithium-ion batteries,” *J. Power Sources*, vol. 147, no. 1–2, pp. 269–281, 2005.
- [40] J. Schmalstieg, S. Käbitz, M. Ecker, and D. U. Sauer, “A holistic aging model for Li(NiMnCo)O₂ based 18650 lithium-ion batteries,” *J. Power Sources*, vol. 257, pp. 325–334, 2014.
- [41] M. Ecker *et al.*, “Development of a lifetime prediction model for lithium-ion batteries based on extended accelerated aging test data,” *J. Power Sources*, vol. 215, pp. 248–257, 2012.
- [42] A. Marongiu, M. Roscher, and D. U. Sauer, “Influence of the vehicle-to-grid strategy on the aging behavior of lithium battery electric vehicles,” *Appl. Energy*, vol. 137, pp. 899–912, 2015.
- [43] Y. Zhang, C. Y. Wang, and X. Tang, “Cycling degradation of an automotive LiFePO₄ lithium-ion battery,” *J. Power Sources*, vol. 196, no. 3, pp. 1513–1520, 2011.
- [44] W. Waag, S. Käbitz, and D. U. Sauer, “Experimental investigation of the lithium-ion battery impedance characteristic at various conditions and aging states and its influence on the application,” *Appl. Energy*, vol. 102, pp. 885–897, 2013.
- [45] H. Song *et al.*, “Capacity fade of LiFePO₄/graphite cell at elevated temperature,” *J. Solid State Electrochem.*, vol. 17, no. 3, pp. 599–605, 2013.
- [46] I. Bloom *et al.*, “An accelerated calendar and cycle life study of Li-ion cells,” *J. Power Sources*, vol. 101, no. 2, pp. 238–247, 2001.
- [47] J. Wang *et al.*, “Cycle-life model for graphite-LiFePO₄ cells,” *J. Power Sources*, vol. 196, no. 8, pp. 3942–3948, 2011.
- [48] J. Shen, S. Dusmez, and a Khaligh, “Optimization of Sizing and Battery Cycle Life in Battery/UC Hybrid Energy Storage System for Electric Vehicle Applications,” *Ind. Informatics, IEEE Trans.*, vol. PP, no. 99, p. 1, 2014.
- [49] G. Suri and S. Onori, “A control-oriented cycle-life model for hybrid electric vehicle lithium-ion batteries,” *Energy*, vol. 96, pp. 644–653, 2016.
- [50] X. Han, M. Ouyang, L. Lu, and J. Li, “A comparative study of commercial lithium ion battery cycle life

- in electric vehicle: Capacity loss estimation,” *J. Power Sources*, vol. 268, pp. 658–669, 2014.
- [51] L. Lam and P. Bauer, “Practical capacity fading model for Li-ion battery cells in electric vehicles,” *IEEE Trans. Power Electron.*, vol. 28, no. 12, pp. 5910–5918, 2013.
- [52] A. Millner, “Modeling lithium ion battery degradation in electric vehicles,” *2010 IEEE Conf. Innov. Technol. an Effic. Reliab. Electr. Supply, CITRES 2010*, pp. 349–356, 2010.
- [53] N. Omar *et al.*, “Lithium iron phosphate based battery - Assessment of the aging parameters and development of cycle life model,” *Appl. Energy*, vol. 113, pp. 1575–1585, 2014.
- [54] O. Bohlen, J. Kowal, and Dirk Uwe Sauer, “Ageing behaviour of electrochemical double layer capacitors. Part II. Lifetime simulation model for dynamic applications,” *J. Power Sources*, vol. 173, no. 1, pp. 626–632, 2007.
- [55] O. Bohlen, J. Kowal, and D. U. Sauer, “Ageing behaviour of electrochemical double layer capacitors. Part I. Experimental study and ageing model,” *J. Power Sources*, vol. 172, no. 1, pp. 468–475, 2007.
- [56] C. Guenther, B. Schott, W. Hennings, P. Waldowski, and M. A. Danzer, “Model-based investigation of electric vehicle battery aging by means of vehicle-to-grid scenario simulations,” *J. Power Sources*, vol. 239, pp. 604–610, 2013.
- [57] S. Wang, L. Shang, Z. Li, H. Deng, and J. Li, “Online dynamic equalization adjustment of high-power lithium-ion battery packs based on the state of balance estimation,” *Appl. Energy*, vol. 166, pp. 44–58, 2016.
- [58] S. Paul, C. Diegelmann, H. Kabza, and W. Tillmetz, “Analysis of ageing inhomogeneities in lithium-ion battery systems,” *J. Power Sources*, vol. 239, pp. 642–650, 2013.
- [59] X. Gong, R. Xiong, and C. C. Mi, “Study of the Characteristics of Battery Packs in Electric Vehicles with Parallel-Connected Lithium-Ion Battery Cells,” *IEEE Trans. Ind. Appl.*, vol. 51, no. 2, pp. 1872–1879, 2015.
- [60] T. Bruen and J. Marco, “Modelling and experimental evaluation of parallel connected lithium ion cells for an electric vehicle battery system,” *J. Power Sources*, vol. 310, pp. 91–101, 2016.
- [61] R. Gogoana, M. B. Pinson, M. Z. Bazant, and S. E. Sarma, “Internal resistance matching for parallel-connected lithium-ion cells and impacts on battery pack cycle life,” *J. Power Sources*, vol. 252, pp. 8–13, 2014.
- [62] M. Dubarry, N. Vuillaume, and B. Y. Liaw, “From single cell model to battery pack simulation for Li-ion batteries,” *J. Power Sources*, vol. 186, no. 2, pp. 500–507, 2009.
- [63] N. Yang, X. Zhang, B. Shang, and G. Li, “Unbalanced discharging and aging due to temperature differences among the cells in a lithium-ion battery pack with parallel combination,” *J. Power Sources*, vol. 306, pp. 733–741, 2016.

- [64] F. Lebel, S. Wilke, B. Schweitzer, M. Roux, and J. P. F. Trov, "A Lithium-Ion Battery Electro-Thermal Model of Parallellized Cells," pp. 3–8, 2016.
- [65] C. Weng, Y. Cui, J. Sun, and H. Peng, "On-board state of health monitoring of lithium-ion batteries using incremental capacity analysis with support vector regression," *J. Power Sources*, vol. 235, pp. 36–44, 2013.
- [66] C. Weng, X. Feng, J. Sun, and H. Peng, "State-of-health monitoring of lithium-ion battery modules and packs via incremental capacity peak tracking," *Appl. Energy*, vol. 180, pp. 360–368, 2016.
- [67] Y. Zheng, M. Ouyang, L. Lu, and J. Li, "Understanding aging mechanisms in lithium-ion battery packs: From cell capacity loss to pack capacity evolution," *J. Power Sources*, vol. 278, pp. 287–295, 2015.
- [68] M. Ouyang, X. Feng, X. Han, L. Lu, Z. Li, and X. He, "A dynamic capacity degradation model and its applications considering varying load for a large format Li-ion battery," *Appl. Energy*, vol. 165, pp. 48–59, 2016.
- [69] C.-Y. Chang, P. Tulpule, G. Rizzoni, W. Zhang, and X. Du, "A probabilistic approach for prognosis of battery pack aging," *J. Power Sources*, vol. 347, pp. 57–68, 2017.
- [70] B. Scrosati, J. Garche, and W. Tillmetz, *Advances in Battery Technologies for Electric Vehicles*. 2015.
- [71] A. Cordoba-Arenas, S. Onori, G. Rizzoni, and G. Fan, "Aging propagation in advanced battery systems: Preliminary results," in *IFAC Proceedings Volumes (IFAC-PapersOnline)*, 2013, vol. 7, no. PART 1, pp. 313–318.
- [72] M. Bercibar, I. Gandiaga, I. Villarreal, N. Omar, J. Van Mierlo, and P. Van Den Bossche, "Critical review of state of health estimation methods of Li-ion batteries for real applications," *Renew. Sustain. Energy Rev.*, vol. 56, pp. 572–587, 2016.
- [73] C. Zhang, J. Liu, S. M. Sharkh, and C. Zhang, "Identification of dynamic model parameters for lithium-ion batteries used in hybrid electric vehicles," *Int. Symp. Electr. Veh.*, vol. 1, pp. 1–11, 2009.
- [74] J. D. Kozlowski, "Electrochemical cell prognostics using online impedance measurements and model-based data fusion techniques," *IEEE Aerosp. Conf. Proc.*, vol. 7, pp. 3257–3270, 2003.
- [75] K. S. Ng, C. S. Moo, Y. P. Chen, and Y. C. Hsieh, "Enhanced coulomb counting method for estimating state-of-charge and state-of-health of lithium-ion batteries," *Appl. Energy*, vol. 86, no. 9, pp. 1506–1511, 2009.
- [76] I. J. Fernández, C. F. Calvillo, A. Sánchez-Miralles, and J. Boal, "Capacity fade and aging models for electric batteries and optimal charging strategy for electric vehicles," *Energy*, vol. 60, pp. 35–43, 2013.
- [77] J. Remmlinger, M. Buchholz, M. Meiler, P. Bernreuter, and K. Dietmayer, "State-of-health monitoring of lithium-ion batteries in electric vehicles by on-board internal resistance estimation," *J. Power Sources*, vol. 196, no. 12, pp. 5357–5363, 2011.

- [78] S. Ebbesen, P. Elbert, and L. Guzzella, "Battery State-of-Health Perceptive Energy Management for Hybrid Electric Vehicles," *IEEE Trans. Veh. Technol.*, vol. 61, no. 7, pp. 2893–2900, 2012.
- [79] V. Marano, S. Onori, Y. Guezennec, G. Rizzoni, and N. Madella, "Lithium-ion batteries life estimation for plug-in hybrid electric vehicles," *Veh. Power Propuls. Conf. 2009. VPPC '09. IEEE*, pp. 536–543, 2009.
- [80] G. L. Plett, "Extended Kalman filtering for battery management systems of LiPB-based HEV battery packs - Part 2. Modeling and identification," *J. Power Sources*, vol. 134, no. 2, pp. 262–276, 2004.
- [81] I. S. Kim, "A technique for estimating the state of health of lithium batteries through a dual-sliding-mode observer," *IEEE Trans. Power Electron.*, vol. 25, no. 4, pp. 1013–1022, 2010.
- [82] H. G. Schweiger *et al.*, "Comparison of several methods for determining the internal resistance of lithium ion cells," *Sensors*, vol. 10, no. 6, pp. 5604–5625, 2010.
- [83] J. Zhang and J. Lee, "A review on prognostics and health monitoring of Li-ion battery," *J. Power Sources*, vol. 196, no. 15, pp. 6007–6014, 2011.
- [84] G. K. Prasad and C. D. Rahn, "Model based identification of aging parameters in lithium ion batteries," *J. Power Sources*, vol. 232, pp. 79–85, 2013.
- [85] M. Gholizadeh and F. R. Salmasi, "Estimation of state of charge, unknown nonlinearities, and state of health of a lithium-ion battery based on a comprehensive unobservable model," *IEEE Trans. Ind. Electron.*, vol. 61, no. 3, pp. 1335–1344, 2014.
- [86] J. Remmlinger, M. Buchholz, T. Soczka-Guth, and K. Dietmayer, "On-board state-of-health monitoring of lithium-ion batteries using linear parameter-varying models," *J. Power Sources*, vol. 239, pp. 689–695, 2013.
- [87] C. R. Gould, C. M. Bingham, D. A. Stone, and P. Bentley, "New battery model and state-of-health determination through subspace parameter estimation and state-observer techniques," *IEEE Trans. Veh. Technol.*, vol. 58, no. 8, pp. 3905–3916, 2009.
- [88] F. Camci, C. Ozkurt, O. Toker, and V. Atamuradov, "Sampling based State of Health estimation methodology for Li-ion batteries," *J. Power Sources*, vol. 278, pp. 668–674, 2015.

Chapter 2

REV-Cycle: A MATLAB-based Tool for Large-Data Analysis of Real-Life Driving Cycles for Electric Vehicles¹

Abstract

Electric vehicles are increasingly being adopted due to environmental awareness and competitive technical performance and reducing prices. Their research and development has sometimes relied on the use of standard driving cycles. However, these cycles cannot reproduce the variations of traffic flow in real world. That is why in this chapter a software tool is developed which is able to analyze real-life driving cycles for electric vehicles. To do so, a driving trajectory process tool is used to obtain large data for vehicles driving in the same stretch of highway. To show the performance of the developed tool, sample cycles are analyzed and simulated for electric vehicles automatically in the REV-Cycle (Real Electric Vehicle Cycle analyzer) software presented.

¹ The material contained in this chapter was previously published in iTEC 2015 Conference and Expo.

2.1 Introduction

The transportation sector shift towards electrified vehicles is consolidating due to policy incentives, increasingly competitive energy storage performance and cost, and growing social awareness on sustainability, among other factors [1]. The transition to electrified vehicles has heavily relied on already in-use procedures for internal combustion engine (ICE) vehicles. One of the most common tests carried out for ICE-powered vehicles is the fuel economy test [2]. This test is, for the U.S., a federal standardized test designed by the U.S. Environmental Protection Agency (EPA). The tests are carried out in a laboratory controlled environment, where the vehicle is tested under city and highway driving cycles. The carbon in the exhaust is then an indicator of the fuel burned during the test, giving as a result the vehicle fuel economy [3].

Even if the fuel economy test is extensively used for ICE-powered vehicles, it is of no use for electric vehicles when the vehicle is exclusively powered by energy storage systems and/or fuel cells. However, these cycles are regularly used to model, simulate and estimate the battery performance and state-of-charge (SOC) for electric vehicles [4]. This allows developing experimentally validated powertrain components models, battery SOC estimation algorithms [5], and vehicle energy management [6], among others. However, real driving conditions greatly differ from standardized ones, as they include sudden accelerations and braking, and traffic flow dynamics that cannot be easily standardized [7].

The electric vehicle performance greatly depends on these variable driving conditions, as well as on the battery technology, sizing, temperature, and battery ageing [8]. It is therefore necessary to be able to methodologically study the electric vehicle performance under real driving conditions, as the consumer satisfaction on its performance is key to increase the electric vehicle adoption. Available work on this area is focused on a

particular driving pattern or location [9], a single vehicle driving cycle [10], does not formally link traffic flow theory with electric vehicle simulation [11] and cannot represent accurately battery performance. Most of these challenges are due to the interdisciplinary nature of the work needed, which include deep knowledge of traffic flow theory, electric vehicle powertrain components, and battery testing and modeling.

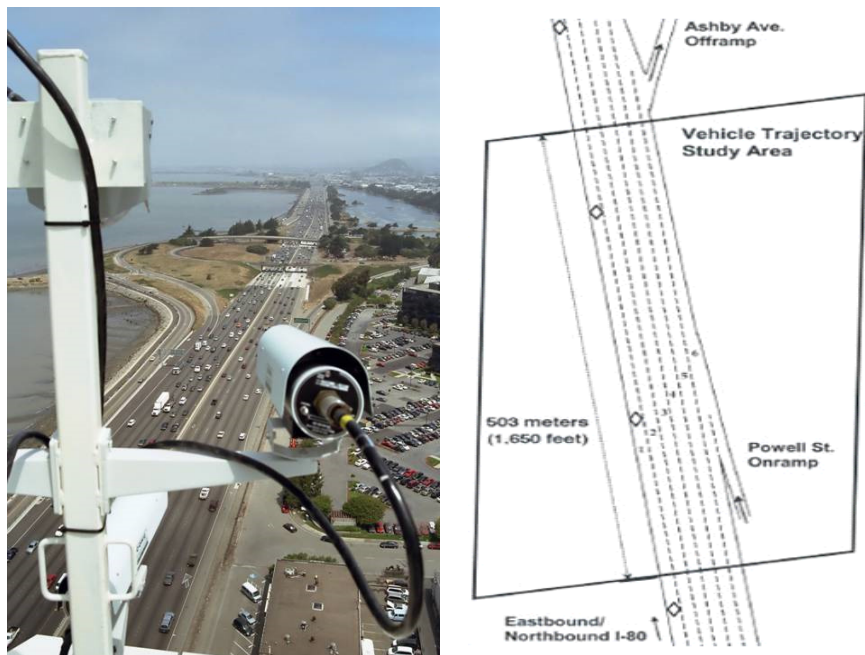
This chapter presents a software tool, REV-Cycle (Real Electric Vehicle cycle analyzer), that is able to connect results from a large-data vehicle driving trajectories under real traffic flow dynamics with an electric vehicle model in MATLAB. The cycles obtained (in the order of hundreds), can be organized through MATLAB, and fed to the electric vehicle model. The model includes an experimentally validated Li-ion based battery model. This will allow studying the effects of varying driving conditions on the vehicle requirements and its effect on the battery performance.

2.2 Large Data Real-Life Driving Cycles

The driving data are obtained in a collaboration with Dr. Zhang from the department of civil and environmental engineering at MTU. These freeway dataset collected detailed vehicle trajectory (time-distance profile) data with 0.1 second time resolution on eastbound I-80 in the San Francisco Bay area in Emeryville, CA, on April 13, 2005. The study area was approximately 500 meters (1,640 feet) in length and consisted of six freeway lanes, including a high-occupancy vehicle (HOV) lane. The grade is 0 percent throughout this section. Seven synchronized digital video cameras, mounted from the top of a 30-story building adjacent to the freeway, recorded vehicles passing through the study area.

The stretch of highway I-80 studied is depicted in Fig. 2.1(a). As it can be observed, the data was collected using a digital video camera mounted on top of the building overlooking the highway. The aerial photograph in Fig. 2.1(b) shows the extent of the I-80

study area in relation to the building from which the video cameras were mounted. The coverage area shows the number of lanes and location of the Powell Street onramp within the I-80 study area. A driving cycle processing procedure is implemented in an open source transportation data hub software tool – NeXTA [12] to process driving cycles for all the vehicles on this stretch freeway. Using this driving cycle processing procedure, the driving cycle of each individual vehicle along this stretch of freeway is saved into an individual *.csv file. Each *.csv file is a real-life driving cycle and ready for driving cycle analysis. For the sake of readability, Fig. 2.2 only shows 5 vehicle driving cycles on I-80 for 200 ms. The differences seen in these 5-vehicle driving cycles indicate that the standard driving cycles cannot represent the real-life driving situations, since vehicles drive differently in real-life even along the same stretch of freeway.



(a)

(b)

Fig. 2.1. Data recording method: (a) Digital video camera recording and (b) Aerial photograph

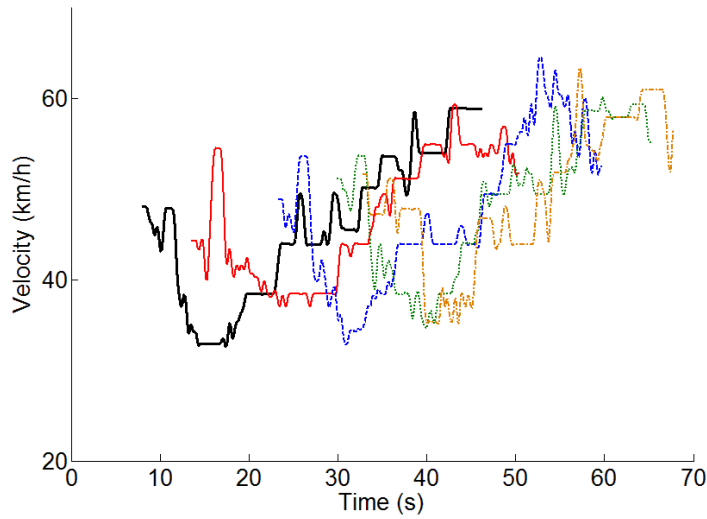


Fig. 2.2. Real-life Driving Cycles of 5 Vehicles along I-80

2.3 REV-Cycle Software Tool

A MATLAB-based software tool (REV-Cycle) has been developed in order to analyze the large data of real traffic measurements obtained in the previous Section. The proposed software is a user friendly interface that provides a tool to analyze a specific cycle [13] and also simulates an electric vehicle. Results of the simulations are stored in arrays which then are displayed to the user by means of graphs and numeric results as popup windows.

The proposed software provides, among other parameters, information of the power, traction force and energy required to overcome the real cycle. In addition, REV-Cycle simulates an electric vehicle running on that particular real cycle by means of a validated Li-ion battery model. The main window of the developed tool is depicted in Fig. 2.3.

On the left hand side, the user introduces the vehicle, control and electric machine properties and on the right hand side it analyzes the cycle and simulates, for that particular real traffic cycle, the electric vehicle behavior. It is worth noting that a browser tool to

select a *.csv file that contains speed, time, grade, etc. of the real traffic, is also part of the developed software. In addition, the software allows to run and analyze all of the *.csv files contained in the folder automatically without user intervention. This allows a large data analysis of all the vehicles driving through a particular road section in a uniform and traceable way.

The simulated electric vehicle is implemented with a driver control over the velocity as well as on the electric machine current, thus, being able to accurately follow the velocity profile described in the *.csv file. Note that these profiles are a capture of real traffic data. Therefore, considerable programming has been carried out in order to control the vehicle, as initial velocity is not zero and time frame changes depending on each particular file. The user can modify the control parameters so that the simulation follows the target velocity, therefore, being able to provide an accurate value of energy consumption, SOC, etc.

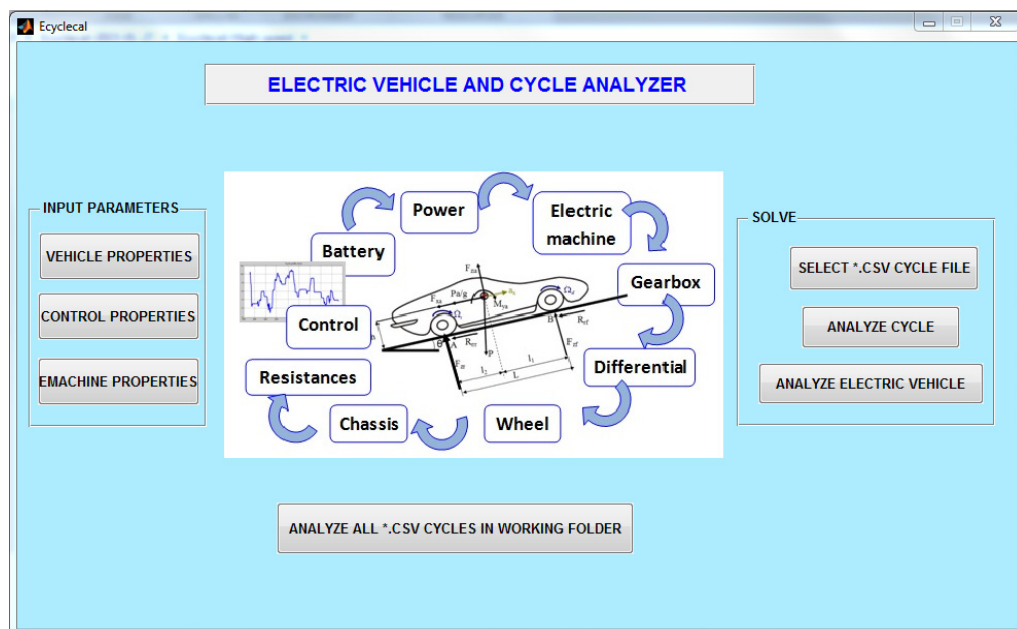


Fig. 2.3. Main window of the developed tool REV-Cycle

2.4 Electric Vehicle Model

This section deals with the model developed for the EV. There are three main parts in the model; mechanical aspects, electrical parts and control system. On the mechanical side, the vehicle longitudinal resistances are considered for the longitudinal dynamics as the sum of the aerodynamic drag, the rolling resistance and the grade.

$$F_{res.} = F_{aerod.} + F_{roll.} + F_{grad.} = 0.5\rho C_x A_f v^2 + W f_r \cos\theta + W \sin\theta \quad (2-1)$$

where, ρ is the air density (1.225 kg/m^3), C_x the aerodynamic coefficient, A_f the vehicle frontal area, W the vehicle weight, f_r the rolling coefficient and θ the road grade. The total resistive force of the vehicle is calculated by summing up the aerodynamic, the rolling and the gradient forces as follow, and included in the traction force calculation:

$$F_{veh.} - (F_{aerod.} + F_{roll.} + F_{grad.}) = m \frac{dv}{dt} \quad (2-2)$$

where, $F_{veh.}$ is the traction force and m is the vehicle mass . The transmission model includes inertia and transmission ratio for the gearbox and differential. Transmission ratio is defined as the ratio between the input speed and the output speed of the transmission acting as a speed reducer and as a torque multiplier.

On the electrical side, the electric machine is modeled considering electro-mechanical conversion and transfer function of windings. It is important to note that the parameters for modeling are entered by the user through user interface window. The voltage applied to electric machine is the output variable of the power electronic converter which is controlled by the modulation coefficient. The main focus for the EV modeled is its battery, as it is the sole energy source for the vehicle and studying its behavior during driving cycles is one of main objectives in this study.

The battery model used in developed tool REV-Cycle is an experimentally validated Li-ion battery model. To extract battery model parameters from experiment, first, frequency bandwidth of demand power from the battery in driving cycles is calculated and then frequency domain test is performed on battery in the obtained bandwidth. Note that the frequency domain tests are performed on different SOC values to obtain the relation between battery impedance parameters and SOC. Nyquist plot of test and fit results for 20%, 60% and 90% SOC are shown in Fig. 2.5. This figure indicates that the developed model is able to follow the frequency behavior of the battery impedance with high accuracy. Note that the model's accuracy is valid for all considered SOC values in test. Considering the calculated parameters, it is possible to define a time domain electrical model for the battery which is shown in Fig. 2.5. In this equivalent circuit, all resistors and capacitors are polynomial function of SOC as follows:

$$R_1 = 0.170 - 0.035 \text{ SOC} - 0.035 \text{ SOC}^2 \quad (2-3)$$

$$C_1 = 5942 - 9678.84 \text{ SOC} + 9602.76 \text{ SOC}^2 \quad (2-4)$$

$$R_2 = 0.020 - 0.015 \text{ SOC} - 0.004 \text{ SOC}^2 \quad (2-5)$$

$$C_2 = 45.79 - 36.81 \text{ SOC} + 13.67 \text{ SOC}^2. \quad (2-6)$$

Also, open circuit voltage (OCV) indicated in figure is related to SOC as follow:

$$OCV (V) = 26.05 + 0.15 \text{ SOC} + 3.51 \text{ SOC}^2. \quad (2-7)$$

Note that, the experiments are performed on a battery module and for the EV battery pack model, parallel and series combination of this model is used to reach the desired power and energy rating. To show the battery model accuracy, one of the experimental results is presented in Fig. 2.6, where the simulated and experimental battery voltages are depicted. Error was found to be below a 2.5%, depending on the cycle harshness.

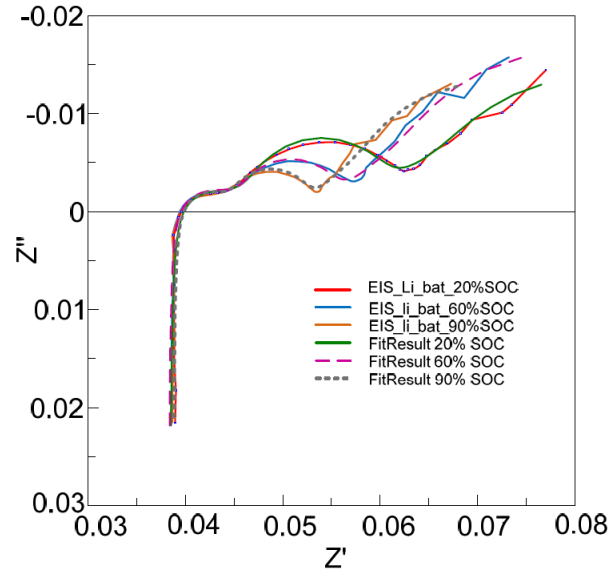


Fig. 2.4. Measured and fitted impedance at 20%, 60%, and 90% SOC

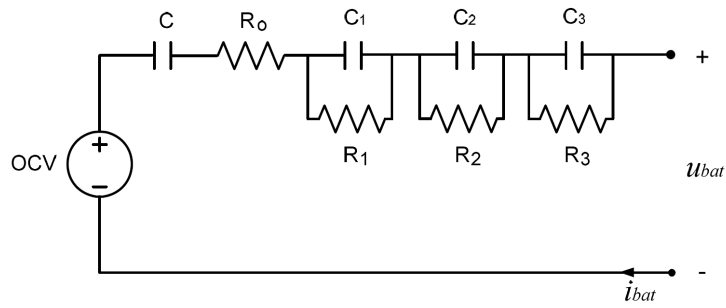
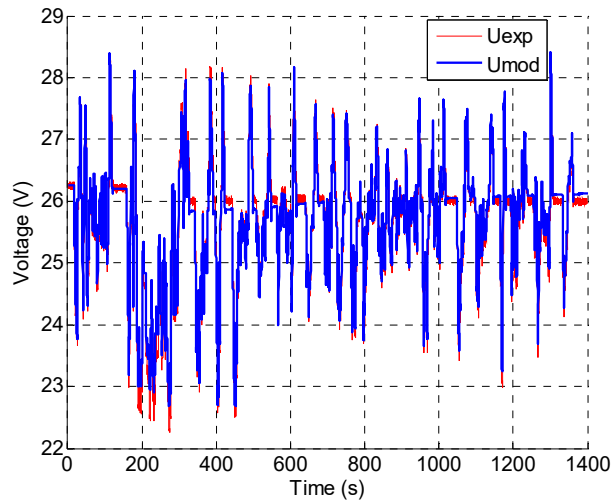
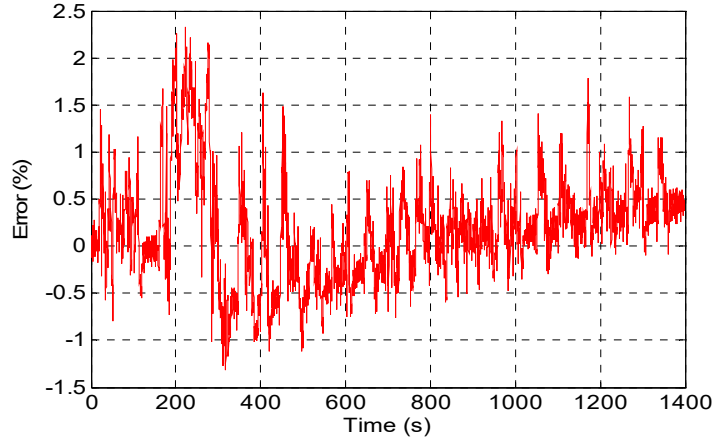


Fig. 2.5. Time domain electrical model of battery



(a)



(b)

Fig. 2.6. (a) Battery experimental vs. simulated voltage, (b) the error

Table 2-1. Simulation parameters

	Vehicle mass (kg)	1650
	Frontal area (m ²)	2.304
	Drag Coeff.	0.28
<i>Mechanical properties</i>	Rolling Coeff.	0.007
	Differential gear ratio	3.29
	Transmission ratio	1.5
	Wheel diameter (m)	0.52
	Electric machine voltage (V)	400
	Electric machine current (A)	337
<i>Electrical properties</i>	Rated speed (rpm)	2840
	Rotor inertia (kg.m ²)	0.12
	Battery capacity (kWh)	36
	Battery voltage (V)	380

The last part of the EV model is the control system which is implemented with two PI controllers on velocity and electric machine current. The PI controllers force the EV

model velocity to follow the reference velocity described in the selected driving cycle by controlling the electric machine voltage and battery current. Note that the PI coefficients for current control are calculated using the electric machine parameters, while the velocity control PI coefficients are entered by the user as a damping ratio and rise time in the “Control Properties” section of the user interface window. Main mechanical and electrical parameters of the simulations are presented in Table 2-1.

2.5 Results for Highway Driving Cycles

Simulation results for the developed REV-Cycle tool are presented for three cases: standard highway cycles (HW-FET and higher acceleration HW-US06), high velocity cycles which are the cycles recorded during light traffic hours in the I-80 highway and low velocity cycles related to heavy traffic hours in same highway as discussed before. For the sake of readability, 5 cycles are selected for each driving case. Table 2-2 presents the statistical analyses of cycles simulated in REV-Cycle tool. There are significant differences between standard cycles and real driving cycles. As shown in Table 2-2, the average acceleration of the real driving cycles for both high and low velocity cycles are much higher than standard cycles.

Even for the HW-US06 which is known as high acceleration cycle, average acceleration is about one third of real driving cycles. Because of this large difference in the acceleration profile, the maximum charge and discharge current and power for the battery in the real driving cycles are much higher compared to the standard cycles, even though the average current and power pulled out of the battery is lower in the real driving cases. This means that the EV battery is in more stressful conditions in real driving and so its aging process will be faster.

Table 2-2. Statistical Analyses of Simulated Cycles

		SOC (%)	Module Current (A)			Battery Power (kW)			Average Acc. (m/s ²)
			Max charge	Max discharge	Average	Max charge	Max discharge	Average	
Standard Cycles	HWFET	2.1245	25.62	21.41	4.99	39.18	29.82	7.11	0.1713
	HW_US06	1.9437	36.10	72.90	9.55	56.19	89.45	13.07	0.3273
Real-Life High Velocity Vehicles	#1	0.1069	54.51	136.60	5.02	88.91	143.53	5.74	0.7622
	# 2	0.1201	72.72	188.85	5.41	122.44	168.40	5.52	0.8830
	# 3	0.1287	64.43	194.69	5.79	106.93	173.66	5.47	1.150
	# 4	0.1102	61.37	198.65	5.15	101.26	172.10	5.29	0.9687
	# 5	0.1334	70.14	222.76	6.82	117.35	179.61	6.44	1.022
Real-Life Low Velocity Vehicles	#1	0.0818	35.75	95.78	1.34	56.21	121.41	1.69	0.7402
	# 2	0.0968	44.85	107.85	2.46	71.75	123.13	3.09	0.7004
	# 3	0.1336	45.50	164.87	3.06	72.9	158.7	3.56	0.9019
	# 4	0.0914	30.06	95.26	2.12	46.70	112.85	2.72	0.7053
	# 5	0.1172	41.94	112.99	2.58	66.53	127.72	3.02	0.8135

Comparing the real-life high and low velocity cycles, the average acceleration, battery current and power are lower for low velocity cycles, and obviously the consumed SOC is also lower in average. Figs. 2.7 and 2.8 presents the velocity vs. time for the studied cycles. In Fig. 2.7, the two standard cycles are shown. Average velocity and acceleration for HW-FET is lower than HW-US06, while the cycle’s duration is about twice.

Figs. 2.8(a) and 2.8(b) indicates the real-life high and low velocity cycles, respectively. Considering these figures and comparing them with standard cycles, real driving cycles are more dynamic and reflect the traffic flow in real-life highway driving.

Even during light traffic hours in highway, vehicles have very dynamic velocity profile, which is not reflected in standard cycles. It is important to note that although the standard cycles look very dynamic in figure, but zooming in and comparing in the same time scale, the difference between the standard and real-life driving cycles will be considerable as observed in the statistical analysis. Also, during heavy traffic hours, vehicles experience several stops and go, while standard highway driving cycles do not have this aspect.

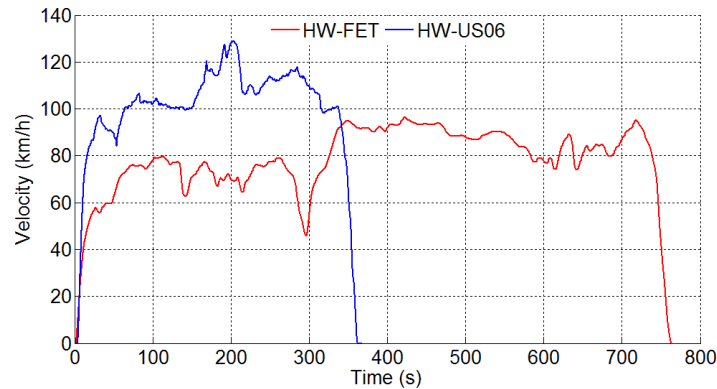


Fig. 2.7. Velocity profile for standard cycles HW-FET and HW-US06

The two main differences between the high and low velocity cycles (Figs. 2.8(a) and 2.8(b)) are the average velocity and stops that the vehicles experience in heavy traffic conditions. Both cycles have a very dynamic flow and severe changes in velocities, as shown by the high acceleration and deceleration during driving period. As a result of this high acceleration and deceleration in real driving cycles compared to standard cycles, the SOC profile in real driving cycles will be harsh and EV battery will experience severe charge and discharge conditions which affects its state of health and aging.

Figs. 2.9 and 2.10 depict the battery pack SOC variations for standard and real-life driving cycles, respectively. As expected, the SOC variation for standard cycles is higher than for real driving cycles, because of its high average velocity and cycle duration. Also, the SOC has very dynamic change in real driving cases as it is obvious from Figs. 2.10(a)

and 2.10(b), while the standard cycles are more gentle, if the same time scale is taken for the comparison. Also, SOC consumption during the low velocity cycles is lower than the high velocity cycles, on average.

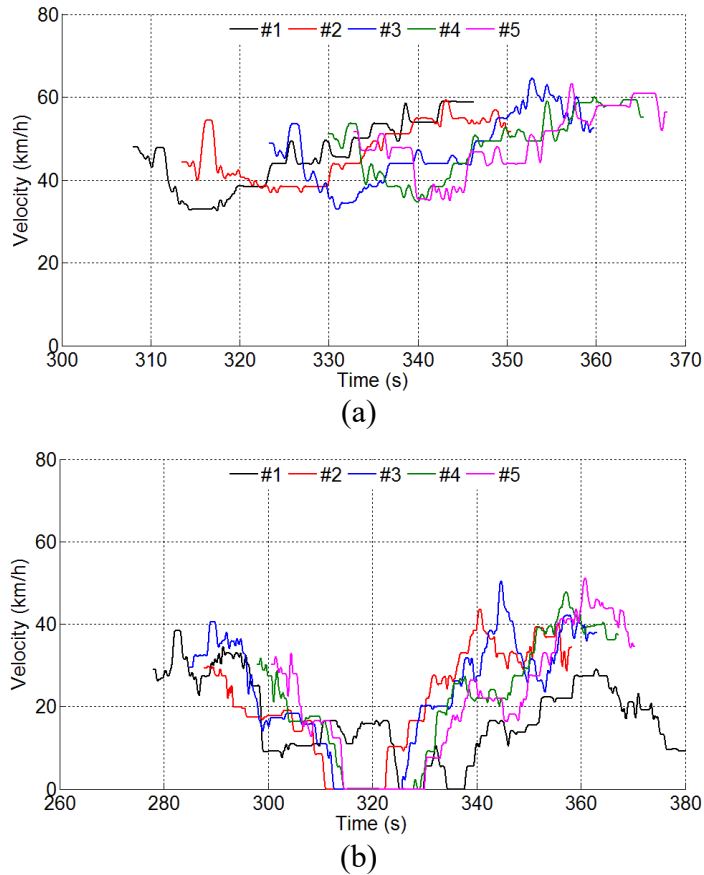


Fig. 2.8. Velocity profile for real-life driving cycles: (a) high velocity and (b) low velocity cases

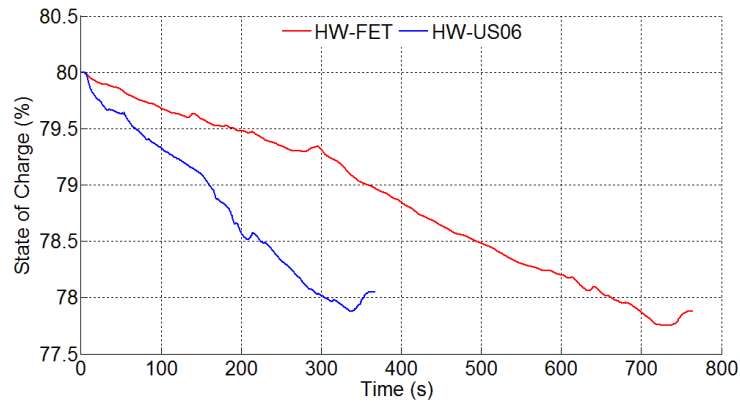
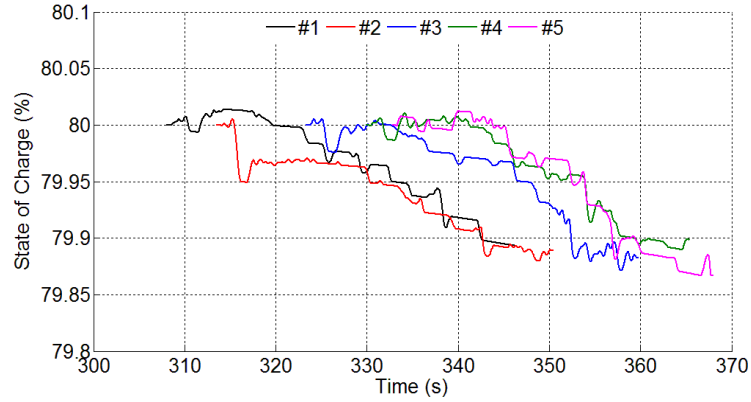
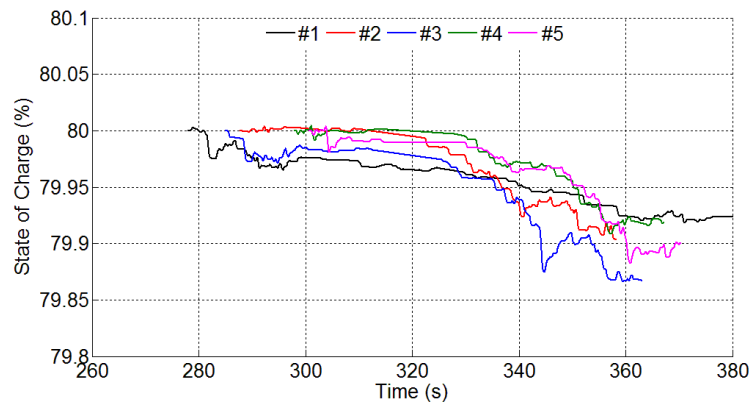


Fig. 2.9. SOC change in studied standard cycles



(a)



(b)

Fig. 2.10. SOC change for real driving cycles: (a) high velocity and (b) low velocity cases

2.6 Conclusion

In this chapter, the MATLAB-based software tool named “REV-Cycle” is presented to analyze an EV performance in real-life driving cycles. Considering the presented results, although the standard highway driving cycles are useful to perform basic vehicle tests and present an index to compare different vehicles, they do not reflect the real-life driving patterns. Therefore, besides the regular standard tests, to study an EV performance, it is essential to test the vehicles or models in real driving cycles, especially in battery health and aging researches. So, using a software tool such as REV-Cycle with the capability of

analyzing large scale data can be very useful to study real-life performance of an EV. The proposed tool has modeled an EV from the battery to the wheels and has used an experimentally validated model for the battery pack modeling. The REV-Cycle allows the user to change different parameters in the vehicle and test it in real driving conditions.

The developed tool will be used in the next chapter to study the difference of driving styles and their effect on the power and energy demand from the battery and its capacity fade.

References

- [1] A. Emadi, "Transportation 2.0", *IEEE Power and Energy Magazine*, July/August 2011
- [2] www.fueleconomy.gov/feg/how_tested.shtml
- [3] S. Plotkin, "Examining fuel economy and carbon standards for light vehicles", *Energy Policy*, vol. 37, no. 10, pp. 3843-3853, October 2009
- [4] M. Cipek, D. Pavkovic, and J. Petric, "A control-oriented simulation model of a power-split hybrid electric vehicle", *Applied Energy*, vol. 101, pp. 121-133, January 2013
- [5] C. Hu, B.D. Youn, and J. Chung, "A multiscale framework with extended Kalman filter for lithium-ion battery SOC and capacity estimation", *Applied Energy*, vol. 92, pp. 694-704, April 2012
- [6] L. Serrao, S. Onori, and G. Rizzoni, "A comparative analysis of energy management strategies for hybrid electric vehicles", *Journal of Dynamic Systems, Measurement, and Control*, vol. 133, May 2011
- [7] D. Karbowski and K. Zhang, "Evaluation of Energy Consumption of Vehicles Along a Stretch of Congested Freeway", Transportation Research Board 91st Annual Meeting, Washington, DC, January 2012, Paper #12-4736
- [8] A. Simpson, "Cost-benefit analysis of plug-in hybrid electric vehicle technology", *22nd International Battery, Hybrid and Fuel Cell Electric Vehicle Symposium and Exhibition*, Yokohama, Japan, October 23-28 2006
- [9] A. Devie, E. Vinot, S. Pelissier, and P. Venet, "Real-world battery duty profile of a neighbourhood electric vehicle", *Transportation Research Part C*, pp. 122-133, 2012
- [10] A. Barré, F. Suard, M. Gerard, M. Montaru, and D. Riu, "Statistical analysis for understanding and predicting battery degradations in real-life electric vehicle use", *Journal of Power Sources*, vol. 254, pp. 846-856, 2014

- [11] J. Wu, K. Li, Y. Jiang, Q. Lv, L. Shang, and Y. Sun, "Large-scale battery system development and user-specific driving behavior analysis for emerging electric-drive vehicles", *Energies*, vol. 4, pp. 758-779, 2011
- [12] <https://code.google.com/p/nexta/>
- [13] L. Guzzella, A. Sciarretta. *Vehicle Propulsion Systems: Introduction to Modeling and Optimization*. 2005.

Chapter 3

Simulation and Analysis of the Effect of Real-World Driving Styles in an EV Battery Performance and Aging¹

Abstract

This chapter presents the large data analysis of the real-world driving cycles and studies the effect of different driving styles on the EV battery performance and aging. For this study, the presented tool in the previous chapter (REV-Cycle) is used. Also, the real-world driving data are recorded as mentioned in Chapter 2. In this study, driving cycles are classified to three styles as aggressive, mild and gentle driving based on their average acceleration. Also, two standard driving cycles (EUDC and HWFET) are simulated by the software and the results are compared. The results show that the real driving cycles are very different from the standard cycles. On the other hand, the driving style has considerable effect on the energy consumption and the battery aging. From the aging point of view, the aggressive driving style leads to higher C_{rate} demand from the battery and it expedited the capacity fade process.

¹ The material contained in this chapter was previously published in IEEE Transactions on Transportation Electrification.

3.1 Introduction

There are different studies on the EV battery performance, aging modeling and health monitoring in the literature [1-8]. Han et al. [1-2] have tested several commercial lithium-ion batteries for the aging mechanisms and capacity fade estimation. In these studies, constant charge and discharge cycles are used to test the batteries and genetic algorithms are employed to estimate the battery aging. In [3-5], the test results are used to provide a mathematical analysis for the battery performance and aging estimation. Although these studies are useful to understand the battery behavior and develop a mathematical model to estimate its aging and capacity fade, however, they mostly have used simple constant current charge/discharge profiles or the standard driving cycles for the test and so, they suffer from the lack of real-world driving experience and performance of the battery in the EV.

A group of studies on EV batteries [6-8] have focused on the statistical analysis of the battery performance in the driving tests. In [6] and [7], the data is collected from driving an EV in a specific driving cycle and used to analyze the battery performance on the tested driving cycles by performing statistical analysis on the data. Weng et al. [8] have suggested data measurement on a set of test driving cycles to study the state of health (SOH) of the EV battery. In these cases, the results are more reliable due to the data collection method they have used, however, this method is costly and time consuming due to the real driving tests. In addition, the tested driving cycles are mostly repetition of a driving loop to model a daily driving cycle and so, they do not exactly follow the real-world driving patterns. On the previous cases, a single vehicle was tested, making difficult the extrapolation of results to a larger population of vehicles and cases.

Real-world driving conditions greatly vary from the standard driving cycles used for the regular tests, as they have sudden changes in the acceleration due to the different driving styles and traffic flow conditions. The EV's battery performance is greatly dependent to the driving conditions, the battery technology, sizing, temperature, and battery aging [9-11]. Available work on this area has not linked the real traffic flow to the EV performance testing and therefore cannot represent the battery performance completely. Most of these challenges are due to the interdisciplinary nature of the work needed, which include deep knowledge of traffic flow theory, electric vehicle powertrain components, and battery testing and modeling. Considering the discussed issues, developing an EV model based on a mathematical model validated by the experimental study and testing it by the real-world driving patterns to evaluate the battery performance will cover the gap between the different methodologies. In this chapter, a large data analysis of real-world driving cycles is presented using REV-Cycle. It connects the results from large-data vehicle driving trajectories under real traffic flow dynamics with an EV model. The EV battery performance is tested in real driving patterns and the effect of different driving styles on the battery behavior and aging is studied.

3.2 Simulations and Results for Highway Driving Cycles

The driving cycles obtained from the I-80 highway and used in the simulations can be classified in two main groups: the cycles recorded during light traffic hours of the highway which have high velocity (referred as “light traffic cycles”) and the cycles related to the heavy traffic hours of the highway with low velocity (referred as “heavy traffic cycles”). 240 cycles obtained from the highway camera recording and NeXTA software are fed into it and the output results for the presented EV model are displayed in two sections: single cycle simulation results and driving style analysis in all cycles.

3.2.1 Single Cycle Simulation Results

To show the EV model performance, EUDC and HWFET standard driving cycles and two sample driving cycles are tested through “analyze cycle” button of the main user interface window and the results are presented in Figs. 3.1 and 3.2. The EV model follows the reference velocity given by the driving cycle with a high precision. Fig. 3.1 shows the velocity profiles for the standard driving cycles. Figs. 3.2(a) and (b) shows the reference and modeled velocity profile for a heavy traffic cycle and a light traffic cycle, respectively. The main difference between standard and real driving cycles is that the real driving cycles are more dynamic because they reflect the real traffic condition and driving styles.

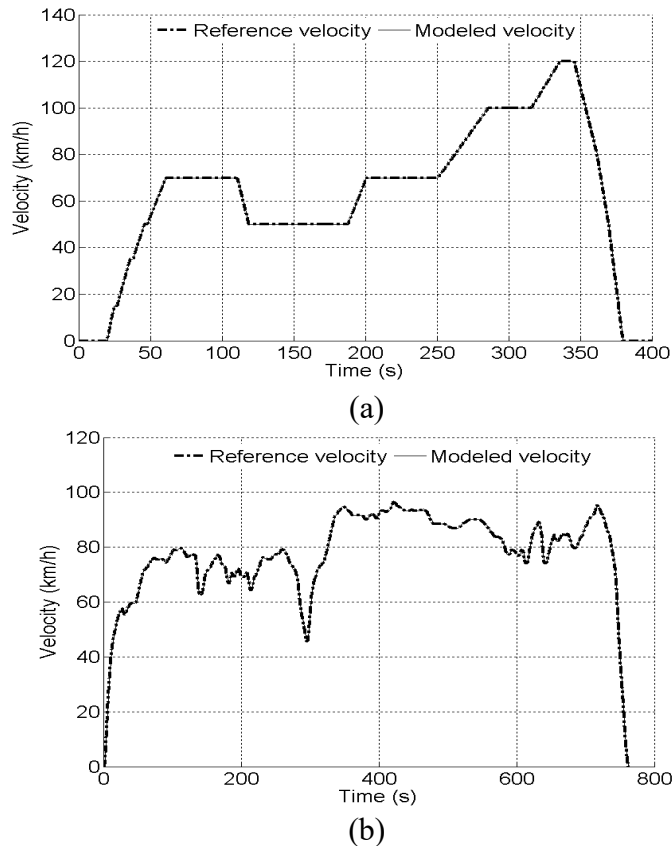
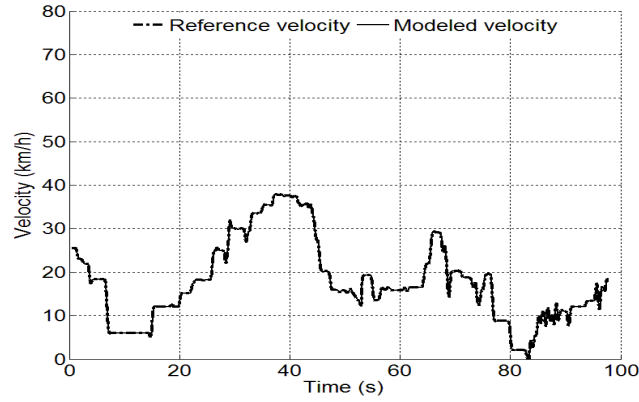


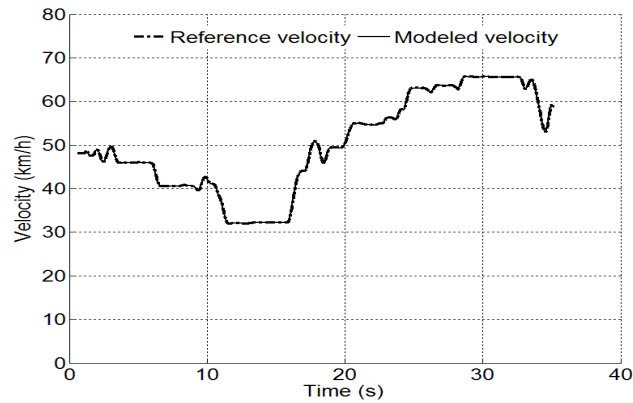
Fig. 3.1. (a) EUDC and (b) HWFET driving cycles velocity

The difference between the heavy and light traffic cycles is their velocity, as the average velocity for the light traffic cycle is about three times the heavy traffic cycle's

average velocity. Because of this difference, the vehicle in light traffic cycle travels the study area in less time and consumes more energy in this period.



(a)

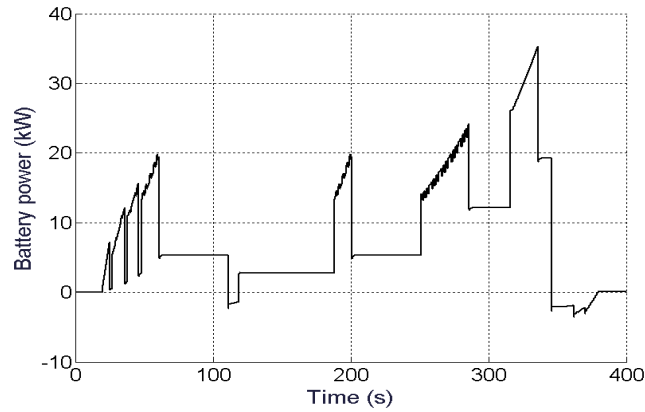


(b)

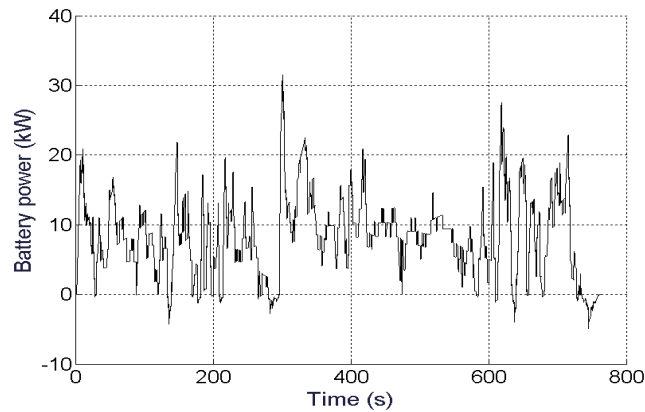
Fig. 3.2. (a) Heavy and (b) Light traffic cycles velocity

The power demanded from the battery while modeling the presented driving cycles are shown in Figs. 3.3 and 3.4. Comparing the standard and real driving cycles power demand, the standard cycles require lower power because of their low acceleration and deceleration, while in the real driving cases, power demand from the battery is very high. Also, as shown in Fig. 3.4, the battery power in the heavy traffic cycle is more dynamic than the light traffic cycle due to the traffic flow in the highway. During the heavy traffic

hours, the drivers need to accelerate and brake more frequently, and consequently require more dynamic power than during light traffic hours. The SOC for these driving cycles are shown in Fig. 3.5(a) and (b) as the energy consumption profile. As it can be observed, the depth of discharge (*DOD*) for light traffic cycle is higher, because of the higher average velocity.

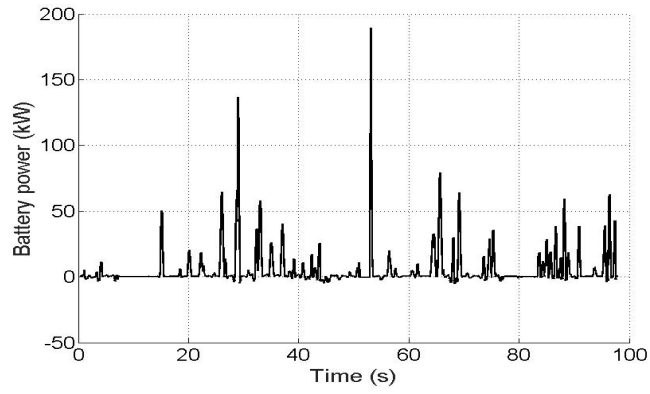


(a)

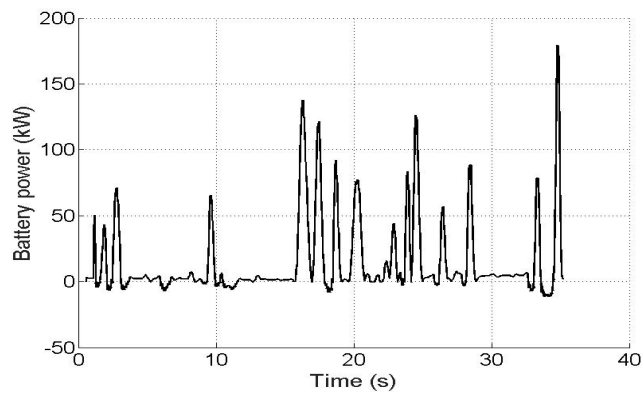


(b)

Fig. 3.3. Battery power: (a) EUDC cycle and (b) HWFET cycle

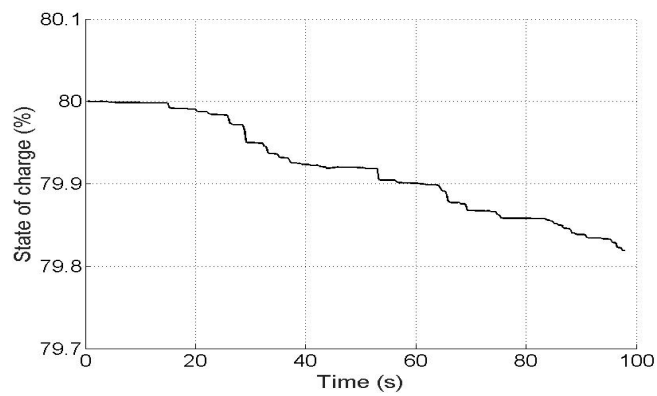


(a)

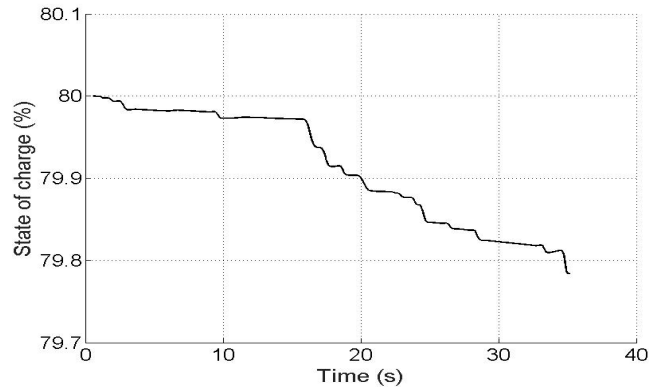


(b)

Fig. 3.4. Power demand from the battery: (a) heavy traffic cycle and (b) light traffic cycle



(a)



(b)

Fig. 3.5. SOC profiles: (a) heavy traffic and (b) light traffic cycle

3.2.2 Driving Style Analysis in All Cycles

As mentioned before, 240 driving cycles, representing large data analysis of real-world driving patterns, have been simulated and tested by means of the developed software. This part of the analysis is performed automatically by running the driving cycles one by one, simulating them and saving the pre-defined output variables such as battery voltage, current, SOC and power, electric machine voltage and current, velocity and acceleration, etc. In addition, the written code processes the data for each cycle and saves it in specific output variables.

To present the detailed output data from the simulation of all cycles and to be able to compare them, all variables are normalized. The acceleration, velocity, SOC and gradient of SOC are normalized based on the maximum value occurred in all driving cycles. The power is normalized with the rated power of the electric machine and the base value for the current is the value at which the battery is completely discharged in 1h.

Considering the fact that both the velocity and the acceleration heavily influence the demanded battery power, the maximum power demand from the battery for each driving cycle versus velocity and acceleration is depicted in Fig. 3.6. The x-axis of this plot is the

acceleration at the time of maximum power multiplied by the velocity. Information is presented as per-unit (p.u.) values to allow comparison between cycles, as relative to the rated power and the maximum acceleration and velocity obtained. Data from all driving cycles are classified into 4 groups: (1) cycles with the acceleration and velocity lower than the average values, (2) cycles with lower acceleration and higher velocity than the average values, (3) cycles with lower acceleration and higher velocity than average values and (4) cycles with higher acceleration and velocity than average values. It can be highlighted that in general, the drivers with higher acceleration demand higher maximum power from the battery, while the low acceleration driving style demands lower maximum power. Also, it can be concluded that, among tested driving cycles, the drivers with low acceleration that travel faster demand lower maximum battery power than the drivers with high acceleration which go slower, on average. Considering this figure, it is necessary to classify the different driving cycles based on their velocity and acceleration for detailed study of different driving patterns on the battery performance and aging.

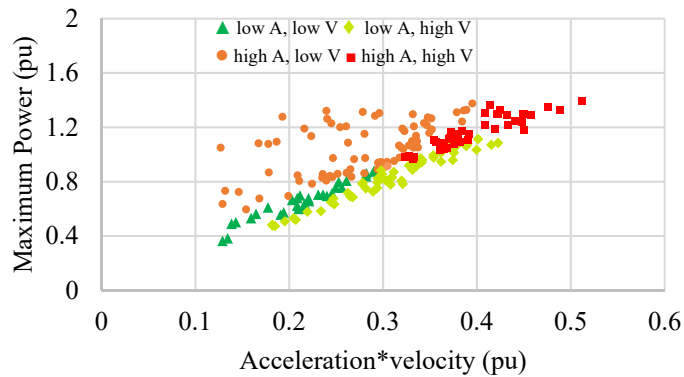


Fig. 3.6. Maximum battery power versus acceleration*velocity

It is important to note that the cycles are classified into two groups based on the velocity as the heavy traffic cycles and light traffic cycles, as mentioned before. From the acceleration point of view, the developed tool classifies the cycles into three groups of

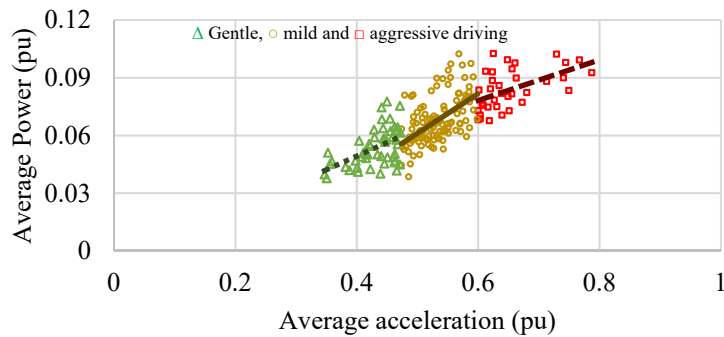
driving styles as aggressive, mild and gentle driving, based on the average acceleration each driver had while driving on the data recorded part of the highway. Since the maximum acceleration happens instantly and it does not reflect the driving style in a longer driving period, it is not a proper index to classify the driving styles. When the simulation is run for all the cycles, the user will have the following outputs:

- A structure for each saved variable (current, power, SOC, gradient of SOC, acceleration, velocity, etc.) containing the name of simulated cycles and data profile of each cycle.
- Classification of driving styles as aggressive, mild or gentle driving.
- A variable containing statistical data (average, maximum, minimum, etc.) of all saved variables for each cycle with their classification. The data of this variable are used for the basic interpretation of output variables and the plots.
- A variable indicating the frequency of C_{rate} values in the current profile of all driving cycles and the battery capacity loss associated with each driving style in all cycles.

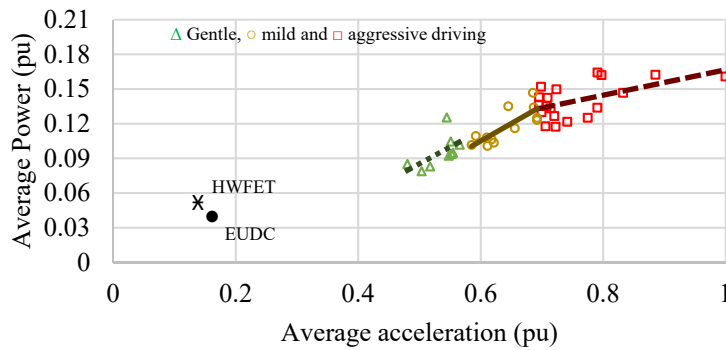
Fig. 3.7(a) and (b) shows the average battery power versus average acceleration for the standard cycles, the heavy and the light traffic cycles. Since the standard driving cycles have higher average velocity, their results are presented in light traffic cycles group. Considering this figure, standard cycles have lower average acceleration and therefore lower average power compared to the real driving cycles. In the studied heavy traffic cycles, the dominant driving style is mild driving with 57% of total. The aggressive and gentle driving styles are 18% and 25%, respectively. However, in the light traffic cycles, the dominant group is aggressive driving with 55%. The contribution of the mild and gentle driving styles is 25% and 20%, respectively.

Considering this data, it can be concluded that during the heavy traffic hours in the highway, driving style is heavily constrained by the traffic flow and a higher percentage of

drivers tend to drive less aggressive. But, in the light traffic hours, drivers are slightly (or not) constrained by the traffic flow and therefore more percentage of them can drive more aggressively, e.g. overtaking a slow lead vehicle. Also, considering Fig. 3.7, for the heavy traffic cycles, the drivers with higher acceleration (or aggressive drivers) demand 56.3% more power from the battery than the gentle drivers and about 23.9% more compared to the mild drivers, on average. In the light traffic cycles, the extra power demand percentage for the aggressive drivers is 46.6% and 16.6% compared to the gentle and mild drivers.



(a)



(b)

Fig. 3.7. Average battery power versus average acceleration: (a) heavy traffic cycles and (b) standard and light traffic cycles

Demanding more power from the battery in the aggressive driving causes a higher consumption of energy and higher *DOD*. Fig. 3.8 shows the *DOD* versus average acceleration for the standard and real-world driving cycles. The standard cycles have lower *DOD* due to the lower power demand from the battery. For the real-world driving cycles,

as the road stretch for all vehicles in this work is the same, it can be concluded that more acceleration (or pushing the gas and brake pedal more frequently) in driving leads to higher energy consumption on the battery.

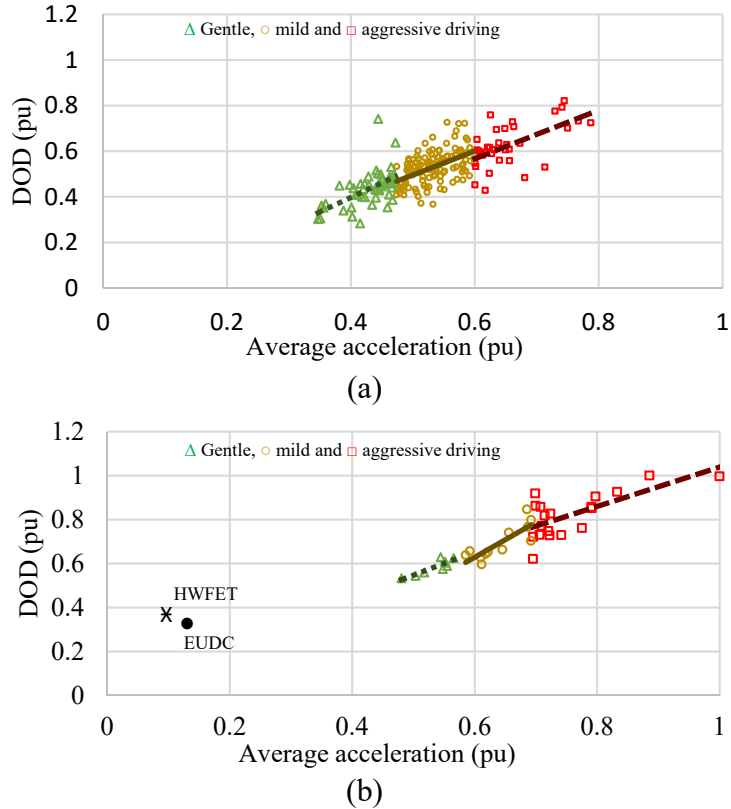


Fig. 3.8. *DOD* versus average acceleration: (a) heavy traffic cycles and (b) standard and light traffic cycles

To have a better insight on the energy consumption of the EV in the different driving styles, the kWh/100miles is used as an index and calculated for all vehicles in this test. The kWh/100miles index in the electric vehicles is similar to the L/100km index in the conventional gas vehicles. Fig. 3.9 presents the maximum and average kWh/100miles for heavy and light traffic cycles. Based on this figure's data, aggressive drivers extract 43% more energy from the battery compared to the gentle drivers in heavy traffic hours of the highway, on average. Also, in light traffic cycles, the extra energy consumption is 41.5% for the aggressive driving style.

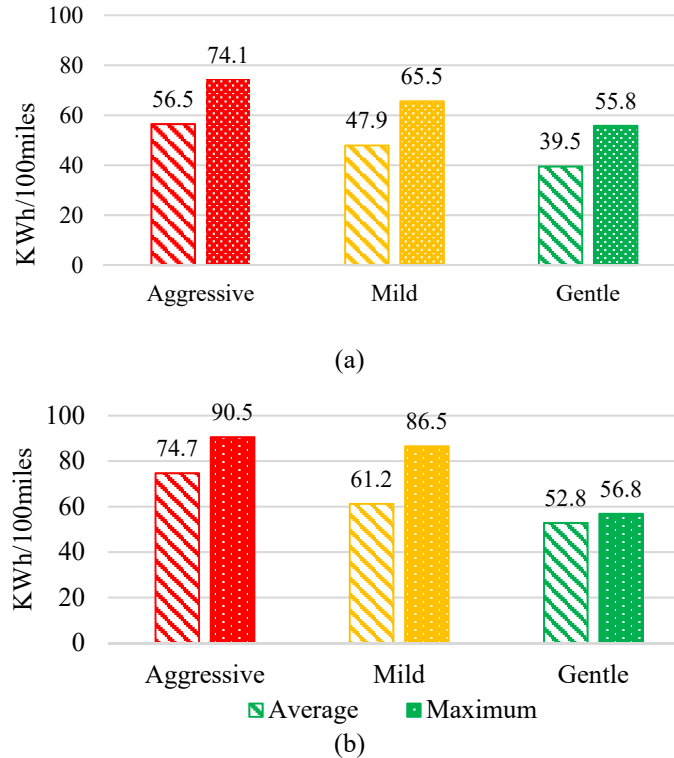


Fig. 3.9. Average and maximum kWh/100miles of 240 cycles: (a) heavy traffic cycles (b) light traffic cycles

The average gradient of SOC versus average acceleration for the standard cycles and heavy and light traffic cycles are depicted in Fig. 3.10(a) and (b). The gradient of SOC shows the energy transfer rate of the battery. These figures indicate that energy transfer rate in the battery for the standard cycles is lower than real driving cycles. Also, between different driving styles, it is higher for the aggressive driving in both the heavy and light traffic cycles.

From the battery aging point of view, the higher power and current demand from the battery reduces its life time and expedites the aging process. The capacity fade of the battery is dependent to the time, temperature, C_{rate} and DOD [12-13]. To illustrate the effect of different driving styles on the degradation of the battery with quantitative results, a capacity loss model is simulated in the developed tool.

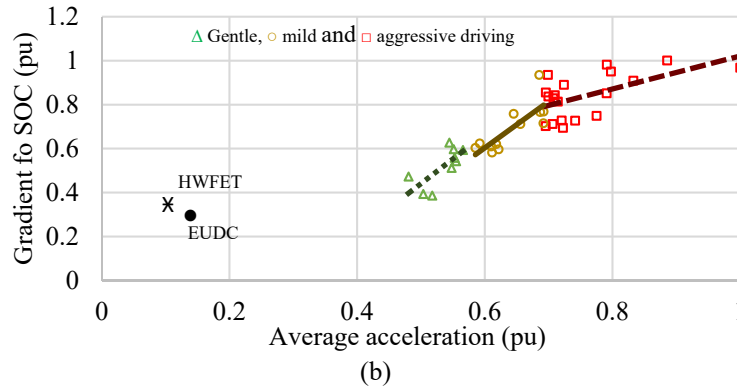
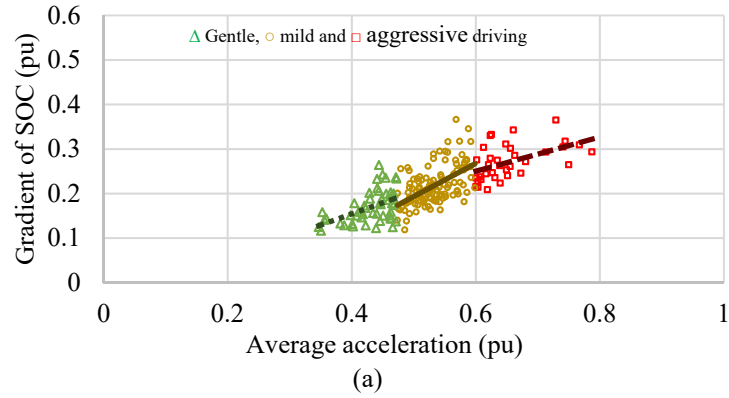


Fig. 3.10. The average gradient of SOC: (a) heavy traffic cycles and (b) standard and light traffic cycles

Based on the model used, the capacity fade can be expressed as follow [13-14]:

$$C_{loss} = B e^{(-E_a/RT)} A_h^z \quad (3-1)$$

where, C_{loss} is the percentage of capacity fade in the battery, B the pre-exponential factor, E_a the activation energy, R the gas constant and T the temperature. A_h in (3-1) is dependent to the number of cycles N , the DOD and the rated capacity of the battery C which can be calculated as (3-2).

$$A_h = N \cdot DOD \cdot C \quad (3-2)$$

The power law factor z relates the capacity loss to the square root of the time. To calculate the B and E_a , (3-3) and (3-4) can be used, respectively [15].

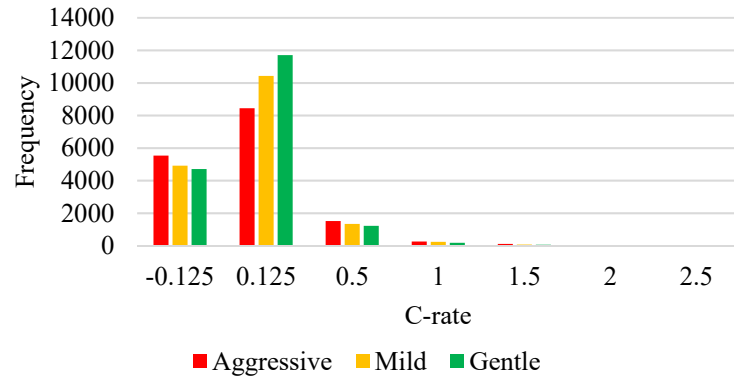
$$\ln(B) = 9.263 + e^{(-0.2797 C_{rate})} \quad (3-3)$$

$$E_a = 31500 - 370.5 C_{rate} \quad (3-4)$$

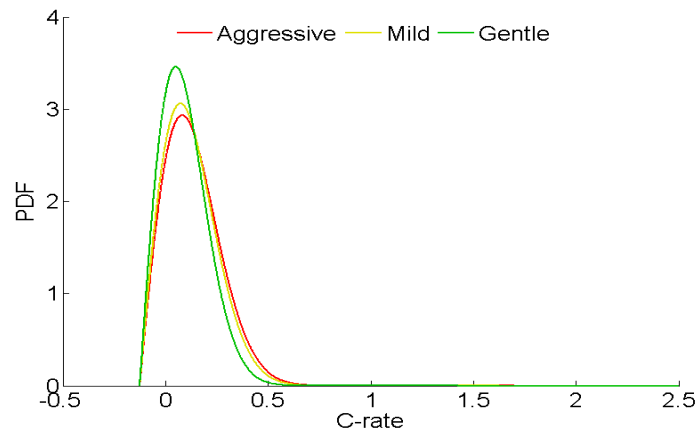
Considering that the current profile of the battery in the EV is not a uniform profile, the current data for each driving cycle is sampled every second, the C_{rate} and DOD are calculated for each sample and the frequency of each C_{rate} is counted. Then, the capacity fade for all driving cycles in each driving style is calculated. The results are in good agreement with the experimental tests performed on the battery [14-15].

Fig. 3.11(a) and (b) shows the frequency of different values of C_{rate} and the Rayleigh probability density function (PDF) of different driving styles in heavy traffic cycles. Considering these figures, C_{rate} is more concentrated around lower values for the gentle driving style, while it is more distributed on higher values for the aggressive driving style. Also, this result can be noticed from the PDF of gentle, mild and aggressive driving groups. Similar results are obtained for the light traffic cycles as depicted in Fig. 3.12(a) and (b). Fig. 3.12 also includes the results for the standard driving cycles. As shown in this figure, concentration of C_{rate} around lower values is higher for the standard cycles compared to both heavy and light traffic cycles.

Comparing the heavy and light traffic cycles, the distribution of C_{rate} for the heavy traffic cycles is heavily concentrated around lower values than the light traffic cycles, because of the traffic density in the heavy traffic hours. In addition, considering the PDF of C_{rate} (Figs. 3.11(b) and 3.12(b)) for two driving groups, in both heavy and light traffic cycles, the aggressive driving group has higher average value than the mild and gentle driving groups.



(a)



(b)

Fig. 3.11. (a) Frequency and (b) the Rayleigh probability density function of C_{rate} distribution for the heavy traffic cycles

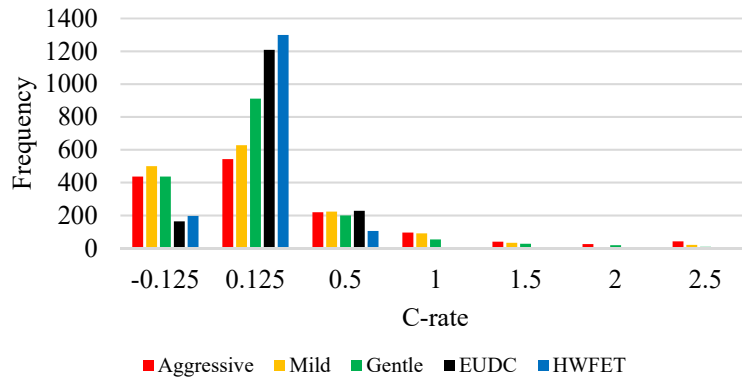
The Rayleigh probability density function for the C_{rate} distribution can be written as

(3-5).

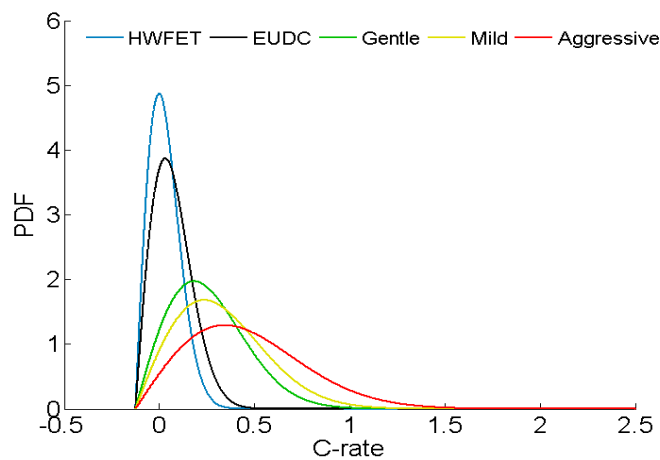
$$f(C_{rate}) = \frac{(C_{rate}+0.125)}{b^2} e^{-\frac{(C_{rate}+0.125)^2}{2b^2}} \quad (3-5)$$

where, b is the scale factor of the C_{rate} data. The average value and variance for the C_{rate} distribution can be expressed as (3-6).

$$Average = b \sqrt{\frac{\pi}{2}} \quad Variance = \frac{4-\pi}{2} b^2 \quad (3-6)$$



(a)



(b)

Fig. 3.12. (a) Frequency and (b) Rayleigh probability density function of C_{rate} distribution for the standard cycles and light traffic cycles

The scale factor, average and variance for PDF of C_{rate} data are presented in Table 3-1 for the standard cycles and different driving styles in both heavy and light traffic cycles. Based on these results, standard driving cycles have lower C_{rate} values which was concluded from Fig. 3.12.

The variance for the aggressive driving group is higher and it shows the distribution of C_{rate} in higher values. Also, as shown in the PDF of C_{rate} , the aggressive driving style tend to have higher positive C_{rate} values which can be numerically noticed from the average values depicted in the table.

Table 3-1. Rayleigh Distribution Parameters of C_{rate} Data

		Scale factor	Average	Variance
Heavy Traffic Cycles	Aggressive	0.206576	0.258901	0.018318
	Mild	0.197932	0.248067	0.016817
	Gentle	0.175201	0.219579	0.013176
Light Traffic Cycles	Aggressive	0.46963	0.588585	0.094672
	Mild	0.36084	0.452239	0.055891
	Gentle	0.30763	0.385551	0.040623
HWFET		0.124491	0.156024	0.006653
EUDC		0.156562	0.196218	0.010522

Based on the C_{rate} distribution in the tested driving cycles and using the model of (3-1), capacity fade for each driving group is calculated and displayed in Fig. 3.13. Considering the figure’s data, the capacity fade caused by the standard driving cycles is lower than real driving cases. So, they cannot accurately reflect the battery real aging process. Also, in the tested real-world driving cycles, the aggressive driving groups have higher battery degradation than the mild and gentle driving groups in both heavy and light traffic cycles.

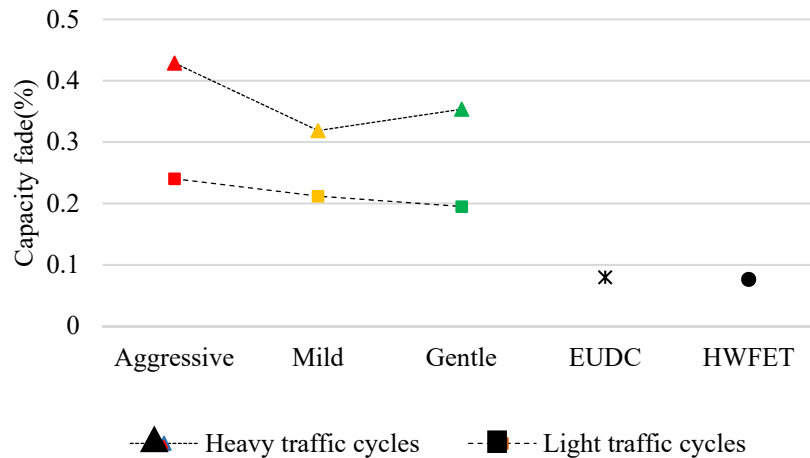


Fig. 3.13. Capacity loss in different driving styles

However, the capacity loss for the mild driving group is less than the gentle driving group for the heavy traffic cycles. The possible reason for this result can be the non-linearity of the capacity fade model, especially in the very low C_{rate} values. Note that this model is obtained from the real behavior of the battery in the experiments [12].

To illustrate the standard cycles and real-world driving patterns, Table 3-2 presents the summary of results for all analyzed cycles. Based on the presented data, the standard driving cycles have lower average acceleration than the real driving cases, so they are less dynamic and demand lower current and power from the battery and as a result they offer less capacity fade to the battery. Therefore, they do not reflect the real driving patterns effect on the EV battery.

Considering the results for the real driving cycles, the gentle drivers with less average acceleration demand less average power from the battery, in the both heavy and light traffic cycles, as noticed in Fig. 3.7. However, the maximum acceleration and power do not follow the average value's pace. For instance, the maximum acceleration and power for the mild driver in the heavy traffic cycles is more than these values for aggressive drivers. This can be noticed in maximum current, too.

The *DOD* and kWh/100 miles for the different driving styles in the both heavy and light traffic cycles follow the pattern of the average acceleration, i.e. the higher average acceleration, the more energy consumed during the driving period. Also, results show that driving with higher velocities consumes more kWh/100 miles; however, the velocity is a matter of road condition and traffic flow. In addition, the aggressive drivers cause more capacity loss compared to the mild and gentle drivers.

Table 3-2. Statistical Results of All Simulated Cycles

		Heavy traffic cycles			Light traffic cycles			Standard Cycles	
		Aggressive	Mild	Gentle	Aggressive	Mild	Gentle	EUDC	HWFET
Acceleration (m/s²)	Max.	14.61	15.22	13.57	15.70	10.93	13.92	1.389	1.475
	Ave.	1.039	0.848	0.684	1.199	0.988	0.849	0.194	0.172
Power (kW)	Max.	178.4	189.6	175.3	185.7	184.3	181.5	35.32	31.46
	Ave.	6.716	5.434	4.296	18.81	15.86	12.89	7.701	8.225
DOD (%)	Max.	0.293	0.259	0.264	0.357	0.302	0.225	0.120	0.122
	Ave.	0.223	0.189	0.156	0.293	0.248	0.209		
kWh per 100miles	Max.	74.11	65.53	55.75	90.53	86.54	56.80	30.99	27.89
	Ave.	56.45	47.89	39.48	74.66	61.22	52.82		
Current	Max.	4.841	4.987	4.754	4.941	4.658	4.375	0.56	0.51
Capacity fade (%)		0.429	0.319	0.354	0.240	0.212	0.195	0.079	0.076

3.3 Conclusion

In this chapter, the large data analysis of the electric vehicle in real-world driving cycles is presented and the effect of different driving styles on the EV battery performance and capacity fade is studied. Also, two standard driving cycles, EUDC and HWFET, are tested in this study and results are compared with the real-world driving cycles. Based on the results, the standard driving cycles substantially differ from the real-world driving patterns and are therefore unable to reflect the real drivers' behavior. As a result, using real-world driving patterns provides a more realistic approach to EV modeling, especially in terms of battery performance analysis and aging. Also, considering the real-world driving cycles' results, the traffic condition affects the driving style and the driving style has significant influence on both the energy efficiency and the battery aging. From the 240 cycles studied, it was observed that mild driving style was dominant during heavy traffic, due to the traffic flow constraint. However, aggressive driving was observed to be dominant in light traffic conditions. In general, aggressive driving showed higher energy

consumption than mild or gentle driving. However, aggressive and mild styles were similar in kWh/100miles in the heavy traffic, whilst during the light traffic, it was mild and gentle driving styles the ones that showed similar energy consumption. The difference in the traffic flow and its impact on battery performance was also observed in the probability of C_{rate} for each driving style. During heavy traffic, the highest probability was for the battery to be between 0 and 0.5 C_{rate} . Also, differences between driving styles were reduced due to the constraint imposed by the traffic flow. However, for light traffic, differences between driving styles were more visible and the probability of higher C_{rate} values was higher too. Also, the probability distribution function for the C_{rate} for light traffic show higher average and variance value for aggressive driving, showing a dominance of acceleration over the rest of styles. Aging simulations point towards mild driving styles being less sensitive to traffic conditions, whilst aggressive driving styles show a significant difference in capacity fade depending on the traffic conditions.

Next chapter will focus on the battery capacity fade in combination of EV daily tasks, including driving, recharging and vehicle to grid. We will try to study different daily scenarios and include possible battery cycling events to have a realistic comparison of the battery capacity fade in different situations. Also, the effect of temperature change in different locations on the battery degradation will be explored.

References

- [1] Xuebing Han, Minggao Ouyang, Languang Lu, Jianqiu Li, "A comparative study of commercial lithium ion battery cycle life in electric vehicle: Capacity loss estimation," *Journal of Power Sources*, vol. 268 pp. 658-669, 2014.
- [2] Xuebing Han, Minggao Ouyang, Languang Lu, Jianqiu Li, Yuejiu Zheng, Zhe Li, "A comparative study of commercial lithium ion battery cycle life in electrical vehicle: Aging mechanism identification," *Journal of Power Sources*, vol. 251 pp. 38-54, 2014.

- [3] Bor Yann Liaw, Rudolph G. Jungst, Ganesan Nagasubramanian, Herbert L. Case, Daniel H. Doughty, "Modeling capacity fade in lithium-ion cells," *Journal of Power Sources*, vol. 140, pp. 157–161, 2005.
- [4] P. Ramadass, Bala Haran, Ralph White, Branko N. Popov, "Mathematical modeling of the capacity fade of Li-ion cells," *Journal of Power Sources*, vol. 123 pp. 230–240, 2003.
- [5] M Broussely, S Herreyre, P Biensan, P Kasztejna, K Nechev, R.J Staniewicz, "Aging mechanism in Li ion cells and calendar life predictions," *Journal of Power Sources*, vol. 97–98, pp. 13-21, July 2001.
- [6] Anthony Barré, Frédéric Suard, Mathias Gérard, Maxime Montaru, Delphine Riu, "Statistical analysis for understanding and predicting battery degradations in real-life electric vehicle use," *Journal of Power Sources*, vol. 245 pp. 846-856, 2014.
- [7] Jie Wu, Kun Li, Yifei Jiang, Qin Lv, Li Shang and Yihe Sun, "Large-Scale Battery System Development and User-Specific Driving Behavior Analysis for Emerging Electric-Drive Vehicles," *Energies*, vol. 4, pp. 758-779, 2011.
- [8] Caihao Weng, Yujia Cui, Jing Sun, Huei Peng, "On-board state of health monitoring of lithium-ion batteries using incremental capacity analysis with support vector regression," *Journal of Power Sources*, vol. 235 pp. 36-44, 2013.
- [9] Clemente Capasso 1, Ottorino Veneri, "Experimental analysis on the performance of lithium based batteries for road full electric and hybrid vehicles," *Applied Energy*, vol. 136, pp. 921–930, 2014.
- [10] Feng Ju, Junwen Wang, Jingshan Li, Guoxian Xiao, and Stephan Biller, "Virtual Battery: A Battery Simulation Framework for Electric Vehicles," *IEEE Trans. Automation Science and Engineering*, vol. 10, no. 1, pp. 5-15, Jan. 2013.
- [11] A. Gauchia, M. Jafari, K. Zhang, L. Gauchia, "REV-Cycle: A MATLAB-based Tool for Large-Data Analysis of Real-Life Driving Cycles for Electric Vehicles," *IEEE Transportation Electrification Conference and Expo (ITEC'15)*, Dearborne, MI, June 2015.
- [12] I. Bloom, B.W Cole, J.J Sohn, S.A Jones, E.G Polzin, V.S Battaglia, G.L Henriksen, C Motloch, R Richardson, T Unkelhaeuser, D Ingersoll, H.L Case, "An accelerated calendar and cycle life study of Li-ion cells," *Journal of Power Sources*, vol. 101, Issue 2, pp. 238-247, Oct. 2001.
- [13] J. Wang, P. Liu, J. Hicks-Garner, E. Sherman, S. Soukiazian, M. Verbrugge, H. Tataria, J. Musser, P. Finamore, "Cycle-life model for graphite-LiFePO₄ cells," *Journal of Power Sources*, vol. 196, Issue 8, pp. 3942-3948, Apr. 2011.
- [14] Junyi Shen; Dusmez, S.; Khaligh, A., "Optimization of Sizing and Battery Cycle Life in Battery/Ultracapacitor Hybrid Energy Storage Systems for Electric Vehicle Applications," *IEEE Trans. Industrial Informatics*, vol.10, no.4, pp.2112-2121, Nov. 2014
- [15] Y. Zhang, C. Wang, and X. Tang, "Cycling degradation of an automotive LiFePO₄ lithium-ion battery," *Journal of Power Sources*, vol. 196, no. 3, pp. 1513–1520, Feb. 2011.

Chapter 4

Deterministic Aging Evaluation: Real-World Daily Driving and Vehicle-to-Grid Services ¹

Abstract

In this chapter, battery lifetime estimation of an electric vehicle (EV) using different driving styles on arterial roads integrating recharging scenarios in the neighborhood of the vehicle-to-grid (V2G) integration is studied. The real-world driving cycles from a fleet of connected vehicles are evaluated in an EV model with different charging options. Daily utility services are added to the simulations to explore the whole day performance of the battery and its daily degradation. Fifty driving cycles from different drivers on arterial roads are classified into aggressive, mild and gentle drivers based on their driving acceleration behavior. The standard level 1 and 2 chargers are considered for recharging and the frequency regulation, peak shaving and solar energy storage are assumed for the daily ancillary services. Also, the effect of temperature change on the battery degradation is explored. Simulation of active vs. passive thermal management systems in three different climates shows the significant impact of the battery temperature on its capacity fade.

¹ The material contained in this chapter was previously published in IEEE Transactions on Transportation Electrification.

4.1 Introduction

When widening the focus from the battery itself to its dependence on the EV environment's conditions, the basic aspect is to explore the battery performance and capacity fade under varying driving dynamics [1]. The power that an EV demands from its battery is not constant and has harsh fluctuations. These fluctuations originate from varying mechanical forces, road conditions and traffic flow dynamics [2]. As an example, Li et al have modeled the EV battery voltage variations under the dynamic current profiles and validated their model using on-board driving test results [3]. Recharging strategies are another aspect of interest in EV batteries, as studies show that the recharging strategy has a considerable effect on the battery performance [4]. Also, recharging behavior affects the optimal storage sizing of the charging stations [5]. Lunz et al [6] have studied the effect of different recharging patterns on the battery aging and energy costs. Bashash et al [7] have tried to optimize the charging strategy to reduce the electricity cost and the battery degradation. Other effectual factor on the EV battery application and its aging studies is the possibility of vehicle-to-grid (V2G) integration, as explored in the recent literature [8-13]. Importance of V2G is because it affects not only the battery health, but also the distribution system [14]. In [8] an empirical and in [9], a semi-empirical aging models for the EV battery with daily V2G services are developed which shows the significant impact of V2G on the battery aging. In another study, Bishop et al. [10] have suggested that the most effectual factor on the battery aging is the energy throughput. However, these studies have relied on the standard NEDC driving cycle. Other authors such as Peterson et al [11] have performed a similar experimental study on the battery cell degradation in simulated daily driving and ancillary services using UDDS cycle. Authors in [12] have developed models for the battery performance and its aging using pulse current and validated them with scaled-down driving power in the lab to study the V2G effect. In [13], authors apply

an energy-based model for battery aging and simulation results illustrate the battery aging in different cases. In these studies, the V2G service is simplified to a constant discharge current simulating the power flow from the vehicle to the grid. Note that the standard driving cycles does not reflect the real-world driving styles [2] and omits the possibility of comparison among the different drivers.

Considering three main factors of the EV battery aging in the daily use as driving, recharging and V2G services, all these studies have focused on one or two of these aging factors, while a real battery is subjected to combination of all. To the best of authors' knowledge, there is no comprehensive study that estimates and compares the battery life considering different driving styles like gentle or aggressive driving, recharging equipment and scheduling and different utility services, all together.

The main purpose of this chapter is to conduct a comparative study on the EV battery performance and lifetime estimation under different daily patterns including driving, recharging and V2G activities using real-world driving and utility services' data. This is to answer the questions about the battery aging behavior due to the change in the daily pattern. Therefore, in this chapter, we extend REV-Cycle, where automatic daily schedules for vehicles can be assembled based on their driving, parking and recharging and V2G services to analyze the battery daily operation and aging by type of service. The daily driving patterns are generated using on-board collected real-world driving data. This allows classifying the driving style shown by the drivers into three groups: gentle, mild and aggressive drivers. Also, different charging options (standard level 1 and 2) and drivers' different recharging behaviors are simulated. In addition, the EV simulated daily tasks include utility services such as frequency regulation, peak shaving and solar energy storage.

4.2 Driving Data

To study the battery aging in daily patterns, we need longer driving cycles, while our driving data in previous chapters were in the order of 10 seconds. So, Dr. Zhang's research group provided new driving data and we used these data which were longer, including urban and highway driving sessions. This section explains the procedure used to obtain this driving data. In this chapter, we processed real-world high-resolution (i.e. 0.1 second) connected vehicle driving data from the Basic Safety Message (BSM) dataset in the Safety Pilot Model Deployment (SPMD) program in the State of Michigan. The SPMD dataset contains the connected vehicle records from volunteered drivers using their own vehicles in the southeast of Michigan in April and October 2012. We process 50 driving cycles of 50 drivers to evaluate EV driving and battery energy management in the proposed EV simulation model. The 50 driving cycles are selected on several arterial road and highway segments with speed limits of 35 and 65mph on the same day. The BSMs are expected to be transmitted as periodic broadcast at a frequency of 10 Hz to meet latency and accuracy requirements of vehicle safety applications as is defined in Dedicated Short-Range Communications (DSRC) Message Set Dictionary (SAE J2735) [15]. Fig. 4.1 presents the driving cycle departure/arrival pattern.

The raw BSM dataset contains timestamp and position information with positioning errors (typically within a range of 5-300 meters). To identify the vehicle trajectory from the raw dataset to a path in the real-world traffic network, the implementation of a map-matching algorithm was able to match the 0.1-second high-resolution GPS-based driving trajectory to the traffic network using geographic and topologic information [16]. Through the algorithm, the traveled road segments were identified for each location of the connected vehicle driving trajectories. Fifty connected vehicles' driving cycles of different drivers on arterial roads in the Ann Arbor area were selected for this study.

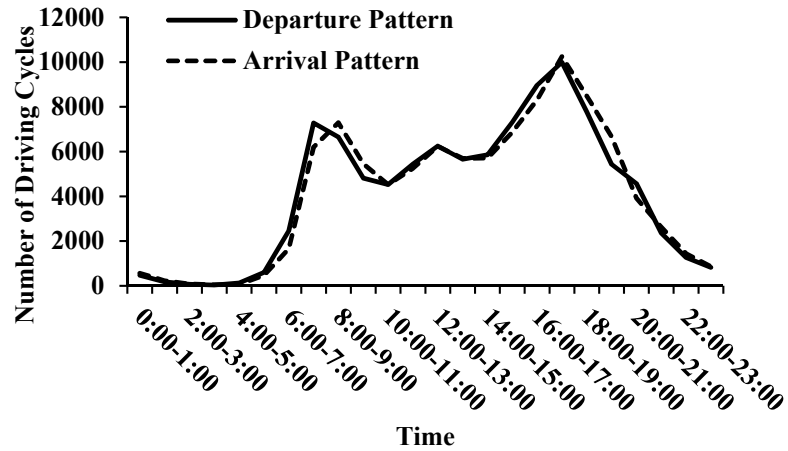


Fig. 4.1. Driving time patterns of SPMD connected vehicle dataset

To perform the simulation for daily task scenarios and to evaluate the EV performance and estimate the battery capacity fade, the basic feature of REV-Cycle is expanded to include driving, recharging and utility services. It is important to note that every single task's desired data (driving cycles, charging preference, etc.) should be provided as csv files and saved in the working folder. For the daily driving parts, simulation tool runs an EV model for the defined driving cycle, while for the battery charging or utility services, it only runs the battery model, as the rest of the EV model is not involved in these tasks. At the end of simulations, it saves all the required variables to estimate the battery aging associated with that day's tasks. The graphical explanation of simulation process is shown in Fig. 4.2.

4.3 Driving Cycles Analysis

To make a valid estimation on the battery aging which is close to a real EV battery performance, it is necessary to reproduce a generic and extensible daily driving pattern. Three main characteristics define the daily driving pattern: velocity profile, traveled distance and number and time of the trips in a day. We have obtained this information from

our recorded data. However, we have adjusted the simulated daily distance to the average distance of 29 miles to be able to make similar and comparable scenarios for the aging results. This daily travelled distance is in accordance with National Household Travel Survey (NHTS) [17].

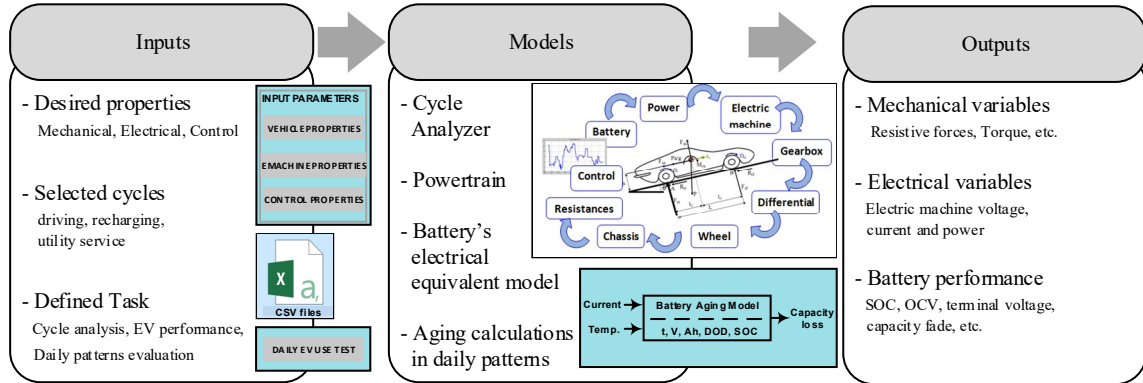


Fig. 4.2. EV battery performance and aging simulation process

To explore the driving cycles, a part of our recorded sample driver's velocity profile is shown in Fig. 4.3 (upper trace). It is worth noting that the duration of driving cycles varies among different drivers and this figure shows a part of sample driving which is 20 minutes long. A complete driving session is longer depending on the different driving styles. Running the electric vehicle model in such a driving cycle demands power from the battery as shown in Fig. 4.3 (lower trace) with the average value of 6.36 kW. We have also considered regenerative braking (RB) system in the simulations which is reported to be 8-13% for a conventional EV [18-19]. Note that the percentage of RB power can be different for HEVs, as their battery capacity and electric machine's power are smaller. The negative values in the power profile indicate the RB power back to the battery. Considering a fully charged battery at the beginning of the driving, the SOC profile for the mentioned driving cycle will be as Fig. 4.4 (upper trace). Considering this figure, 3.8% of the battery energy is consumed for 20 minutes of driving.

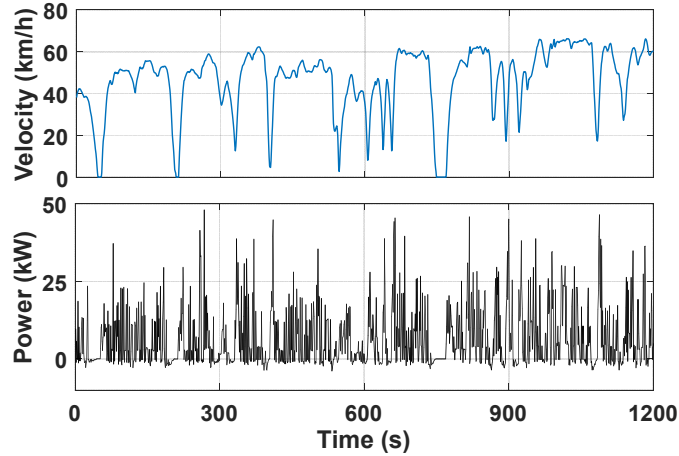


Fig. 4.3. Velocity profile and Battery power for a single driving

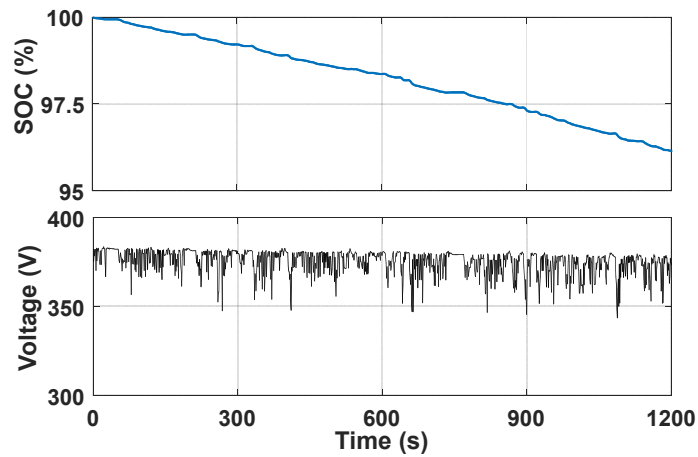


Fig. 4.4. Battery SOC and voltage profile for a single driving

Note that the positive slope of the SOC curve (increasing SOC) indicates the RB energy charging the battery. As the battery current in the driving period is not constant and it is time-variant, the voltage drop on the internal impedance of the battery is variable and therefore the battery terminal voltage has harsh fluctuations (Fig. 4.4 (lower trace)). In this figure, the maximum voltage drop on the internal impedance is 33.8V which is 8.9% of OCV at that instant in time. However, the overall trend of the battery voltage is descending, due to the battery being discharged during driving.

All drivers in this study are classified into three groups as *Gentle*, *Mild* and *Aggressive* drivers, as before. Based on this classification, among 50 drivers, 14 drive gently, 26 are mild drivers and 10 are aggressive. All drivers' single trip are simulated using the EV model and their current demand profiles from the battery are sampled with the resolution of 1 second and classified into 7 C-rates. There are two points that should be considered: First, the experimental driving cycles' resolution is 0.1 second whilst the simulated current profile is sampled by 1 second resolution to reduce the number of generated data and simplify the further calculations, Second, this classification adds some error to the calculations due to the difference in the real C-rate and the assigned C-rate in aging calculation which can be minimized by increasing the number of groups.

Fig. 4.5 (upper trace) shows the average frequencies of each C-rate for a single trip between three different driving styles. As expected, the aggressive drivers have larger number of C-rates compared to mild and gentle drivers for the same traveled distance. The average daily driving time is calculated for all drivers and are shown in Fig. 4.5 (lower trace). The driving distance was equal for all drivers, but the total driving time for aggressive drivers is slightly longer than for mild and gentle drivers. The conclusion of these results is that aggressive driving habits do not necessarily lead to faster arrival to the destination, as it reflects aggressive acceleration, but not sustained higher velocities.

4.4 Aging Evaluation Model

For the battery aging analysis throughout the cycles, we have used a general Arrhenius equation to model and calculate the battery capacity fade associated with the driving cycles. Bloom et al. [20] have used experimental data to present the battery capacity fade as a function of the time and the temperature.

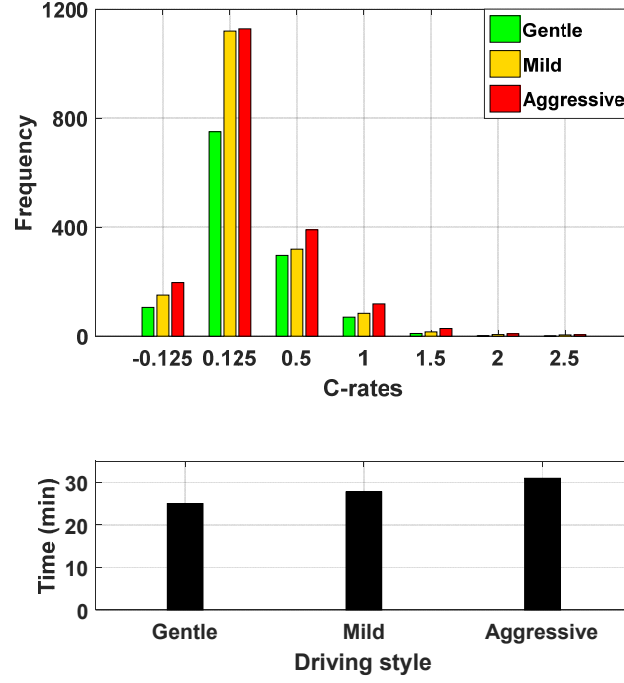


Fig. 4.5. C-rates' frequencies and daily driving duration for the different driving styles

Wang et al. [21] adopted and completed their results to develop an aging model relating the capacity fade to the C-rate, the total Ah and the temperature (4-1).

$$Q(\%) = B e^{-E_a/RT} Ah^z \quad (4-1)$$

where, Q is capacity fade and z is power factor. R is the gas constant and T is the temperature. E_a is activation energy and B is the pre-exponential factor. In this equation, Ah is the total ampere-hour throughput in a cycle and can be calculated as follow:

$$Ah = N \cdot DOD \cdot Ah_{rated} \quad (4-2)$$

where N is the number of cycles and DOD is depth of discharge for each cycle. Authors have related E_a and B to C-rate to show the effect of different C-rates on the aging. E_a is defined by (4-3) and B is expressed as an exponential equation by (4-4) in [22].

$$E_a = 31700 - 370.3Crate \quad (4-3)$$

$$\ln(B) = 1.226e^{-0.297Crate} + 9.263 \quad (4-4)$$

This model does not include the effect of SOC in the battery aging calculation. Suri et al. [23] have presented a similar model for the same battery cell including the effect of SOC as follows:

$$E_a = 31500 - 152.5Crate \quad (4-5)$$

$$B = \alpha.SOC + \beta \quad (4-6)$$

where, α and β can be defined for different ranges of average SOC:

$$\begin{cases} \alpha = 2896.6 & \beta = 7411.2 & \text{if } SOC < 0.45 \\ \alpha = 2694.5 & \beta = 6022.2 & \text{if } SOC \geq 0.45. \end{cases} \quad (4-7)$$

As this model uses average SOC of the cycle for aging evaluation and defines the parameters based on the SOC intervals smaller and greater than 0.45, it may result in error on deep cycling and/or middle SOC. To calculate the capacity fade for a driving cycle, the battery current and SOC are needed to calculate the C-rate and DOD. However, the battery current during the driving cycle is not constant and so it is not possible to put a single C-rate value for the whole cycle as the C-rate affects the battery aging behavior. Therefore, a numerical method is used after running the EV model for each driving cycle. The battery current data is sampled with 1 sec resolution and C-rates are calculated for each second and are grouped in different values as Fig. 4.5 (upper trace).

The DOD associated with each C-rate is calculated. So, the Ah and capacity fade caused by each C-rate in a single cycle is expressed as follows:

$$Ah(n) = DOD(n).Ah \quad (4-8)$$

$$Q_{Crate}(n) = B(n)e^{-E_a(n)/RT} Ah^z(n) \quad (4-9)$$

where, n indicates the variables value corresponding to each C-rate. The total capacity fade will be:

$$Q_{cycle} = \sum_n Q_{Crate}(n). \quad (4-10)$$

Eq. (4-10) calculates the capacity fade for a single cycle. To consider the repetition of cycles in daily pattern, for example in k^{th} cycle, the total Ah for each C-rate is summed up from 1^{st} cycle to k^{th} cycle, and the capacity fade is calculated by total Ah throughput for each C-rate. At the end of each cycle's simulation, the capacity is updated for the next cycling. This approximation method adds error to the calculation's result and its correctness needs to be validated. Therefore, it is simulated and compared with available experimental results and manufacturer data to test its mathematical consistency in different test conditions.

The cycle life of A123 Systems' 2.4 Ah 26650 LPF cell is presented in its datasheet [24]. Three different cycling tests for various temperatures and charge/discharge currents are simulated for two aging models [21, 23] with mentioned approximation (Fig. 4.6). As shown in upper trace of Fig. 4.6, the estimated battery capacity after 600 cycles in the model based on C-rates and SOC for three tests are 97.2%, 93.1% and 91.6% and for the model based on C-rates, the battery capacity are 93.8%, 85.2% and 82.7 % (Fig. 4.6, lower trace). Comparing these number to the manufacturer data which are about 98%, 95% and 92% indicates that the approximation method overestimates the capacity loss in the battery cycle life. This overestimation is about 1% for the model based on C-rates and SOC which is in acceptable error range. However, the model based on C-rates calculates the battery capacity loss 7.8% more, which is not negligible. Based on this comparison, we selected the model with less error and compared it with the rest of available experimental data. Fig. 4.7 shows the comparison of estimated battery cell capacity and experimental data from [25] which has tested different cells with cell level current profiles in real driving cycles at around 65% SOC and 45°C. The estimated capacity is very close to the experimental data

with a slight overestimation. Another set of experimental data are obtained from [21] with 2C charge/discharge currents in 10% DOD/60C, 50% DOD/45C and 90% DOD/60C and compared to the estimated cell capacity in Fig. 4.8. This figure indicate that the simulated results follow the experimental data and the presented estimation method is successful in evaluation of battery cycle aging. Also, it is expected to notice higher capacity loss in 10% DOD compared to 90% DOD for the same amount of Ah throughput in the same temperature, because the battery has higher SOC. The estimation results show this difference which is not reported in [21] as they have not considered the effect of SOC in their model, although the experimental data reflects that cycling in higher SOC leads to higher battery degradation.

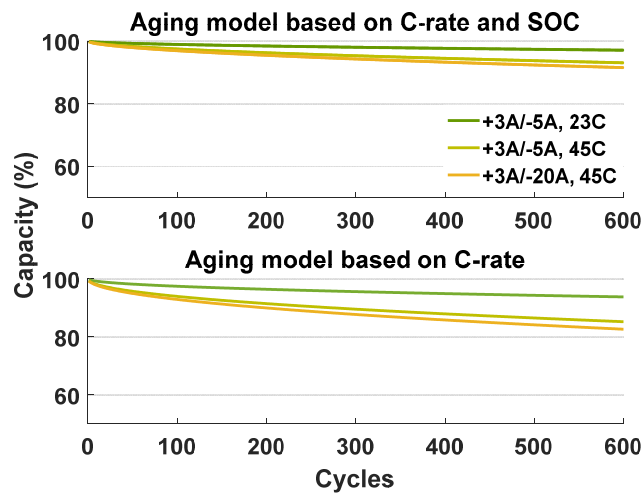


Fig. 4.6. Cycle aging estimation of 2.4 Ah 26650 LPF cell

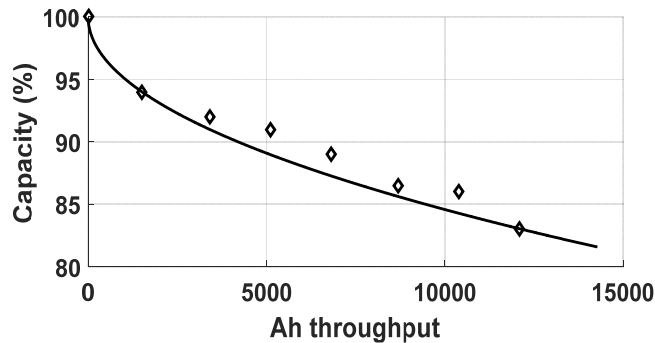


Fig. 4.7. Comparison of estimated cell capacity with experimental data of [21]

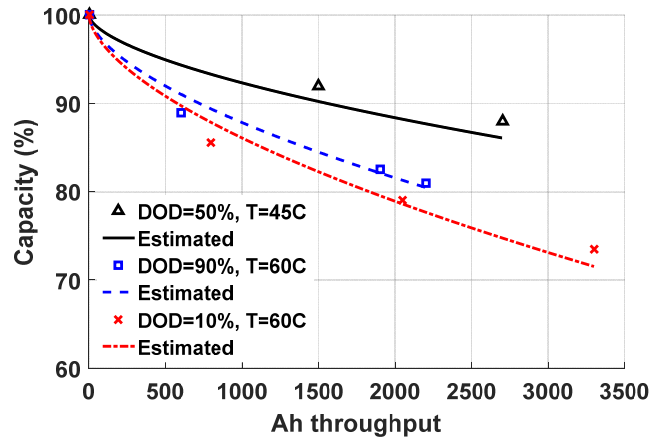


Fig. 4.8. Estimated cell capacity compared to experimental data from [23]

Considering the presented comparison between the capacity estimation simulations and the experimental data from [21, 24-25], the aging model has acceptable prediction of LFP cell aging and can be used for the EV battery's daily cycles aging evaluation. Note that this aging model estimates the cycle aging of the cell and it does not include the calendar aging.

Using the mentioned equations, the DOD and the capacity fade for all driving cycles are calculated and presented in Fig. 4.9 to evaluate single driving cycle aging difference among the drivers. The x-axis shows the 50 driving cycles which are sorted by their average acceleration from the smallest to the largest values. The upper trace and lower trace of the figure depict the DOD and capacity fade for single driving task, respectively.

Although there are some outlier points in this graph due to the different velocity profiles of the drivers for the same travelled distance, the total trend of DOD illustrates that the higher average acceleration (aggressive driving habits) leads to higher power demand from the battery. And in general, a higher average acceleration causes increased battery degradation due to the higher DOD and Crates, based on these driving data.

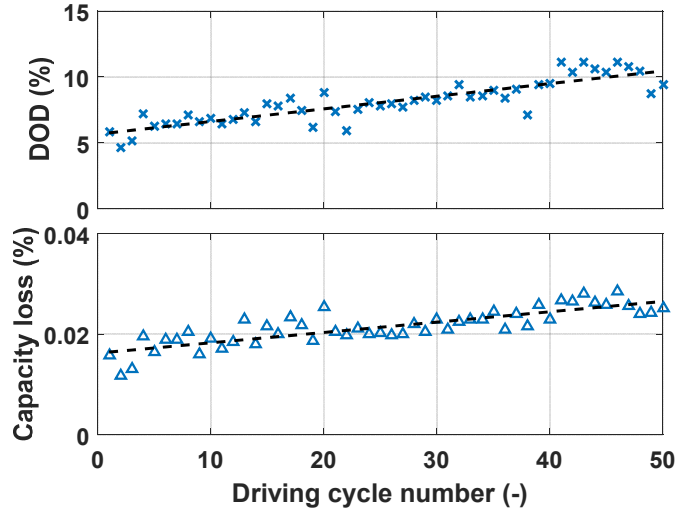


Fig. 4.9. Driving cycles' DOD and capacity loss trend (ordered in the x-axis by increasing average acceleration)

4.5 Daily Case Scenarios Study

The daily use pattern of an electric vehicle includes several driving periods followed by recharging and possible utility services. To estimate its battery's cycle life in a general daily task, this chapter assumes several case scenarios. To generate these scenarios, the possible daily tasks options are as driving styles (aggressive, mild and gentle), recharging facilities (level 1 (1.5kW) and level 2 (7.6kW)) chargers and ancillary services as frequency regulation, load peak shaving and storage for solar energy. It is worth noting that similar to the driving cycles that are real-world driving data, the real frequency regulation data is obtained from Pennsylvania-New Jersey-Maryland (PJM) Interconnection for August 2016 [26] and solar power data is collected in the Keweenaw Research Center at Michigan Tech. for August 2016 [27]. In addition, based on a report by Idaho National Lab. about the charging behavior of EV drivers in USA [28], 98% of the charging events happen at the home and work with mostly L-1 and L-2 chargers (99%) rather than with fast DC chargers. So, considering only L-1 and L-2 stations in the daily scenarios is a valid assumption. Table 4-1 presents detailed information about these scenarios. The simulated scenarios are

selected to reflect different tasks a vehicle can provide both to the driver and to the grid. These scenarios are presented in three groups as the aging due to (1) Driving styles, (2) Recharging options and (3) V2G services.

Table 4-1. Simulated case scenarios

Daily scenarios	Travelled distance (Miles)	Type and time of charging (1.5 or 7.6kW)	Utility service type 7.6 kW
<i>Driving</i>	29	L-1 overnight	-
<i>Driving with different recharging options</i>	29	L-2 overnight	-
	29	Uncontrolled vs. controlled L-2	-
	58	L-2 overnight (Every other day)	-
<i>Driving, recharging and V2G services</i>	29	L-2 overnight	Frequency regulation
	29	L-2 overnight	Freq. Reg. and peak shaving
	58	L-2 overnight (every other day)	Frequency regulation
	29	L-2 overnight	Solar energy storage and peak shaving

4.5.1 Aging of different driving styles: Scenario 1: Daily driving and overnight L-1 charging

In this scenario, the daily pattern consists of the daily 29 miles driving followed by the L-1 overnight recharging. This plan is simulated for all three driving groups (aggressive, mild and gentle). Fig. 4.10 shows the simulated 24-hour battery power and SOC for a sample driver in this scenario with three trips at 7:30am, 12:30pm and 4:30pm and L-1 recharging. For this driver, the whole day driving extracts 6.56 kWh energy from the battery and overnight charging takes about 4 hours and 25 minutes. Average charging time for three gentle, mild and aggressive driver groups are 4h29m, 5h29m and 6h53m, respectively. As a result, aggressive driving behavior leads to spending more time on

recharging. The trend of overnight L-1 charging time for all drivers is shown in Fig. 4.11. Based on this result, the aggressive driving behavior leads to longer recharging time overnight. It is important to note that the outlier points in the recharging time are originated from the different DODs for all drivers at the end of day.

This scenario is repeated until 100,000 miles of travelled distance in simulation and the battery cell capacity fade vs. its total Ah throughput is estimated and shown in Fig. 4.12. Two main differences among different driving groups are noticeable. First, for the same travelled distance, gentle drivers' group extract 3443Ah from a cell while the mild and aggressive groups have 4341Ah and 5566Ah, respectively, which are 26% and 61% higher than gentle group. Second, the average cell capacity for gentle, mild and aggressive driving groups are 92.6%, 91% and 89.4% in this scenario, which shows the effect of driving behavior on the battery's cycle aging. Aggressive drivers not only extract higher amount of Ah from the battery, but also, they demand higher C-rates which accelerate the cycling capacity loss even more.

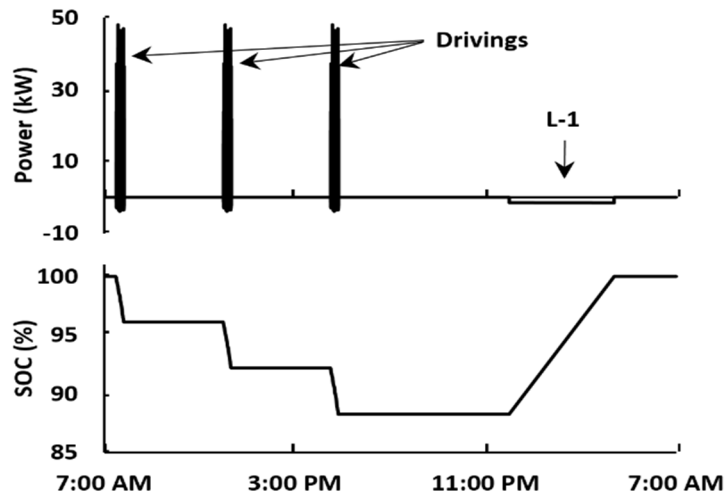


Fig. 4.10. Daily battery power and SOC for scenario 1

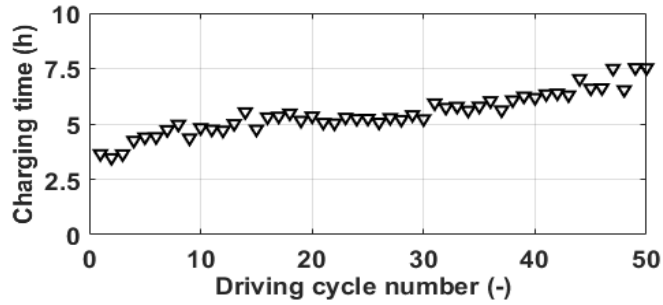


Fig. 4.11. All drivers' overnight charging time trend

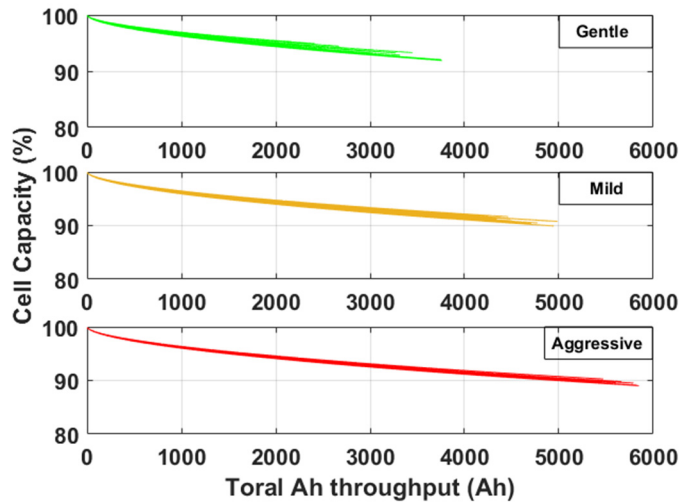


Fig. 4.12. Battery capacity for all drivers, comparison of driving styles

4.5.2 Aging of different recharging options

As the different recharging facilities and habits affect the battery aging, they are simulated as three case scenarios to compare the recharging options impact on the battery.

4.5.2.1 Scenario 2: Difference of charging facilities: L-1 vs L-2

This case scenario is similar to the previous one, with the only difference being that the overnight charging uses an L-2 charging station, to make a comparison between L-1 and L-2 charging. The overnight recharging with L-2 charger takes about 52 minutes, which is about five times less than L-1 charger for the same sample driver. No significant difference in the battery capacity fade results of L-1 and L-2 chargers was noticed in the

simulations (Fig. 4.13) due to the small C-rates of both chargers compared to the driving C-rates, although the capacity fade for L-2 charger is slightly higher in numbers.

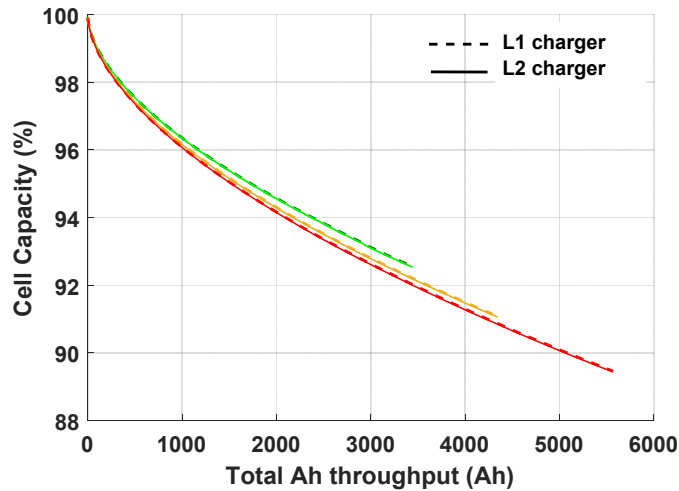


Fig. 4.13. Different charging facilities effect on the cell’s capacity fade: aggressive (red), mild (yellow) and gentle (green)

4.5.2.2 Scenario 3: Recharging behavior: uncontrolled vs. controlled charging

Uncontrolled charging stands for the charging without considering any specific time of day and charging happens whenever the vehicle is plugged in, while controlled charging delays the charging to a time of day in which the grid has extra power and the energy price is lower which mostly happens after midnight. Controlled charging helps the grid to perform load shifting with filling it valley during night and indirectly prevent higher peaks during day. So, the controlled charging can be considered as a utility service, too. In uncontrolled charging, after each driving session, the vehicle is considered to be plugged in and start charging. Therefore, three driving cycles are followed by three charging periods. This case is compared to the controlled overnight charging. Note that the total Ah throughput will not change in these two cases.

The comparative results of the battery capacity are depicted in Fig. 4.14. Although uncontrolled charging reduces the risk of running out of the battery for unexpected long

driving, it increases the battery degradation. Daily controlled charging increases the battery durability by 15.8% compared to uncontrolled charging, on average. This is because of higher SOC of the battery for uncontrolled charging during cycling.

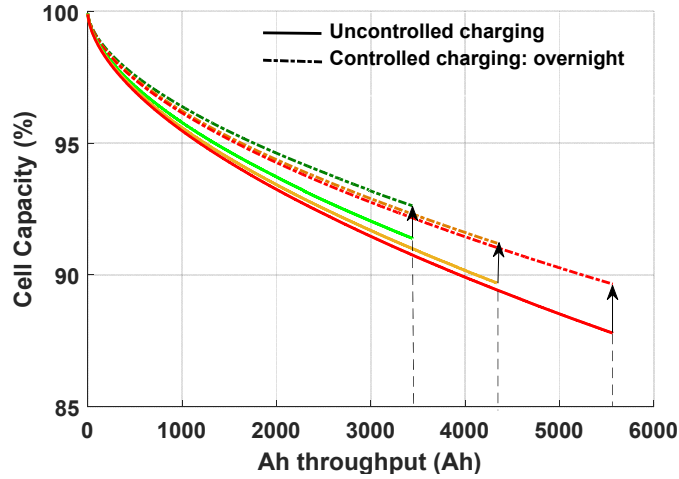


Fig. 4.14. Battery capacity comparison for uncontrolled and controlled charging: aggressive (red), mild (yellow) and gentle (green)

4.5.2.3 Scenario 4: Every-other-day L-2 charging

In this case, one day only has driving cycles and the other day has driving cycles in addition to overall recharging with L-2 charger. This scenario is applicable to most of city life daily patterns. The charging time for this scenario is 1 hour and 44 minutes. Fig. 4.15 indicates the battery capacity comparison for every day and every other day L-2 charging methods. The battery life increases by 26.3% for this scenario. This improvement in the battery capacity loss is higher for the aggressive driving group, due to higher cell Ah throughput for this group after similar travelled distance (Fig. 4.15).

4.5.3 Aging of daily utility service

In the advanced V2G integration environment, the utility services are included as one of the EV daily tasks, and in particular frequency regulation, peak shaving and solar energy integration. In this section, to emphasize on the aging effect of the utility services, the

results represent the average of all driving cycles, regardless of the driving style classification.

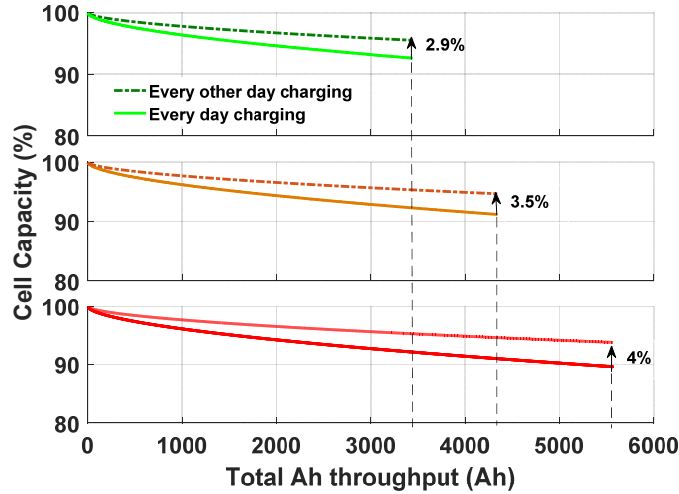


Fig. 4.15. Daily and every other day charging effect on the battery capacity

4.5.3.1 Scenario 5: Frequency regulations and peak shaving with L-2 charging

In this case, for the sample driver, after morning and noon driving, there are 2 hours of frequency regulation task as part of the EV daily pattern from 2-4pm. Then, the evening driving takes place, after which the EV can participate in grid tasks by load peak shaving at 7pm. After these, the L-2 overnight charging completes the daily pattern. It is important to note the peak shaving is performed by a bi-directional L-2 connection between the EV and the grid.

Fig. 4.16 depicts the battery power and SOC for this pattern. Aging model simulation results show that adding the daily frequency regulation increases the average battery capacity fade for all drivers by 14.3% (Fig. 4.17(a)). It also leads to 900Ah more Ah throughput from the cell which is equivalent to 187.5 full cycles. Adding 2 hours daily peak shaving to EV tasks has more aging effect on the cell with 22.8% higher capacity fade and 533 equivalent full cycles Ah throughput (Fig. 4.17(b)).

In addition, including the peak shaving in daily pattern along with the frequency regulations leads to 35.6% more decreased capacity and 3460Ah more total Ah throughput, on average. Note that the aging model is not linear and therefore, the aging due to both services together is not equal to the sum of aging caused by individual services.

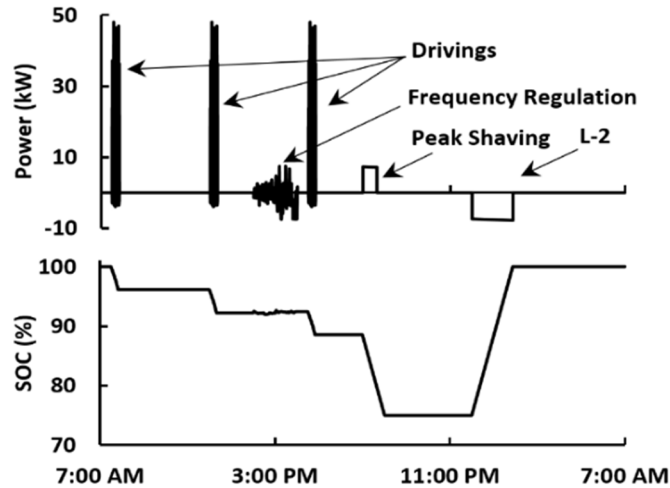
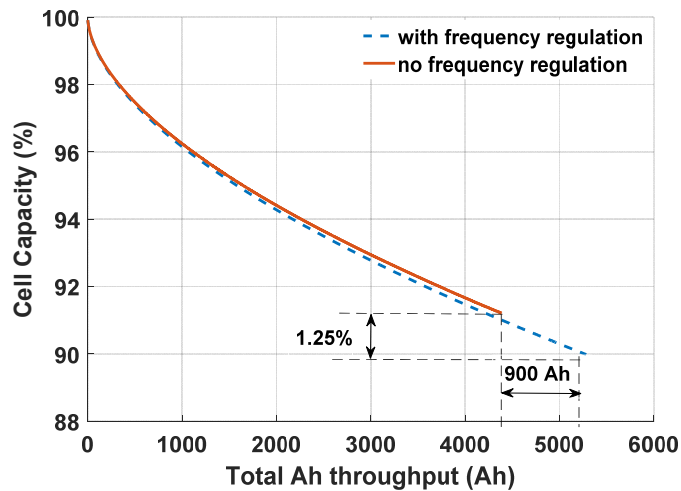
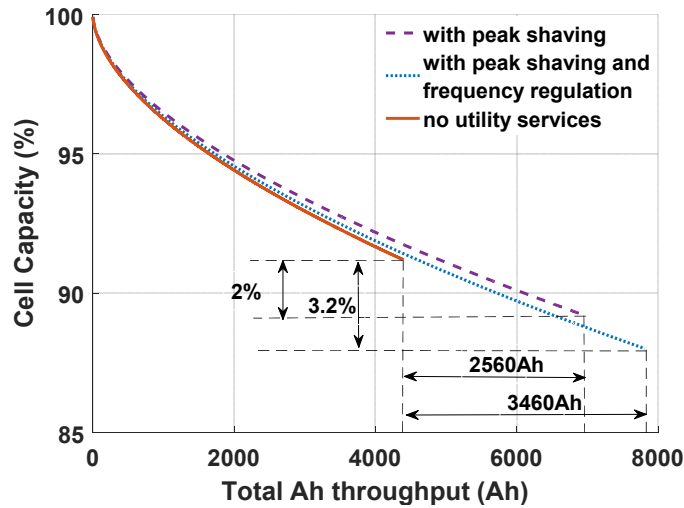


Fig. 4.16. Daily battery power and SOC for scenario 5



(a)



(b)

Fig. 4.17. Comparison of frequency regulation and peak shaving impact on the cell capacity

4.5.3.2 Scenario 6: Every other day L-2 charging with frequency regulations

As noticed from scenario 5 results, performing utility services by the EV causes a notable change in the battery life. However, users can gain the V2G incentives provided by the utility. As noticed before in the scenario 4 results, every other day charging helps to decrease the battery capacity loss due to cycling in lower SOC. It seems that reducing the charging frequency to every other day and performing the utility services in lower SOC can prevent the severe battery aging under V2G scenarios, and potentially add economic benefits.

Fig. 4.18 shows and compares the battery capacity results for daily L-2 charging and every other day L-2 charging with frequency regulations. This figure indicates that there is very small difference in capacity fade between these two cases, although the total Ah throughput is increased by adding frequency regulation. Therefore, every other day recharging allows performing frequency regulations and gaining profit from the utility for almost the same battery life of every day recharging. Note that the peak shaving is not

possible in this case, as it requires higher DODs and every other day charging provides the driving energy requirements.

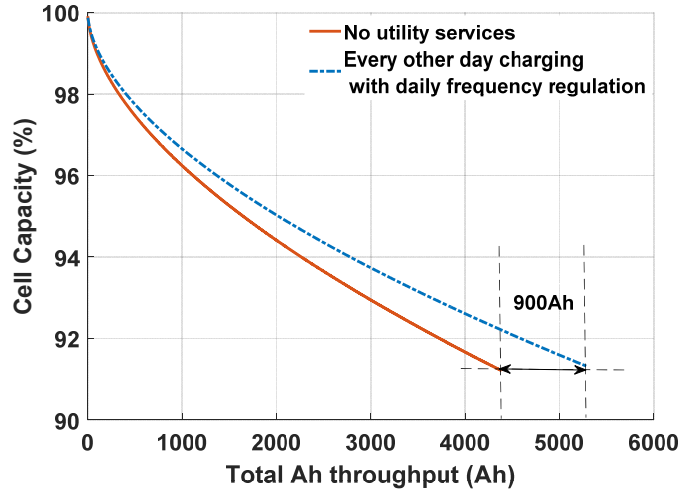


Fig. 4.18. Cell capacity for Scenario 6

4.5.3.3 Scenario 7: Morning solar energy storage for evening peak shaving

It is assumed that the vehicle’s battery is used as storage for the output power of PV panels before noon and it provides power for the peak shaving during high load peaks of evening. For this scenario, after morning driving, the vehicle is plugged in and absorbs the PV panels’ power from 8 AM to 12 PM.

The PV panels’ provided current is shown in Fig. 4.19. Note that the duration of this mode depends on each driver’s SOC when the vehicle is plugged at the morning. Following this daily scenario leads to 37.2% more capacity fade after similar travelled distance to the case with no utility services (Fig. 4.20) which is due to the higher SOC, similar to frequency regulation service. However, this scenario has significant benefit for the grid in its daily load management. The added total Ah throughput in this case is same as the scenario with peak shaving service.

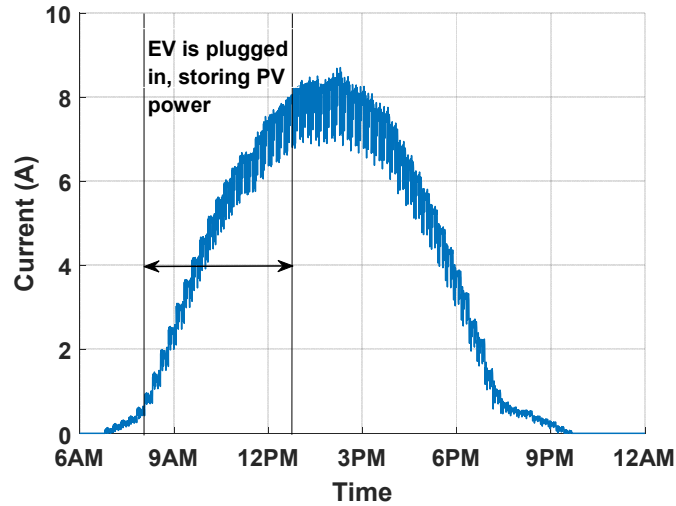


Fig. 4.19. PV panels generated current for storage in the EV battery

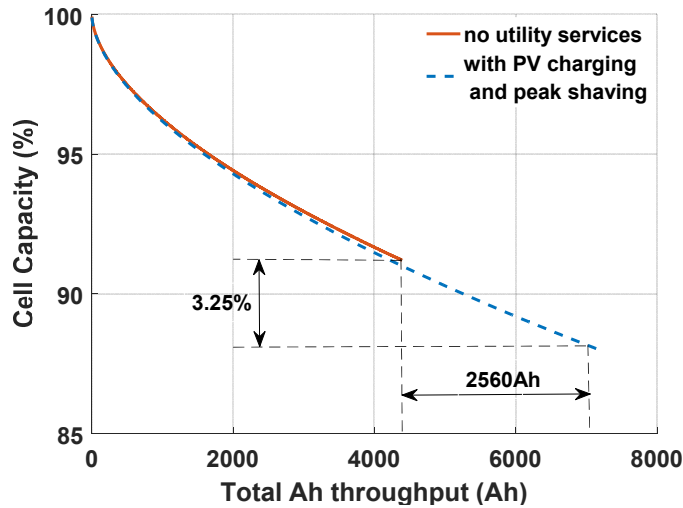


Fig. 4.20. Effect of morning solar energy storage and evening peak shaving on the cell capacity

4.6 Different Climates' Impact on Battery Aging

Temperature is one of the key factors on the battery capacity fade [29], as both high and low temperatures adversely affect the battery life. Active thermal management systems on the EV battery pack unifies the thermal distribution inside the pack and keeps the temperature in pre-defined value with acceptable tolerance, while passive thermal management systems use cabin/ambient air for battery's heat dissipation [30]. In the

previous section, active thermal management is considered for the simulations. To investigate the impact of temperature changes on the battery capacity fade, we assume a second thermal scenario in which the battery has passive thermal management system. The daily average temperature data of year 2016 for Ann Arbor, Michigan (the city that the driving data are collected) [31] is used to compare the capacity fade difference between active and passive thermal management systems.

The capacity fade results of two thermal management systems for scenario 1 is shown in Fig. 4.21. As noticed, changes in the battery temperature cause higher capacity fade for the same daily scenario. Cyclic fluctuations in the capacity fade is resulted from the cyclic temperature change. To compare the effect of different climates, the daily average temperature data of the same year for two other cities in US (Miami, Florida and Phoenix, Arizona) are used to evaluate the battery capacity fade (Fig. 4.22). The daily scenario for these three climates is same and only the temperature profile is changed. Based on these results, for the same daily scenario, the battery capacity fade in Phoenix and Miami is higher than Ann Arbor, due to the higher temperatures.

In addition, it is noticed that the capacity fade curve for Phoenix and Ann Arbor has higher cyclic fluctuations than Miami. The answer for this difference can be found in the annual temperature distribution of these cities. If the temperature data of these cities is fitted to a normal distribution as seen in Fig. 4.23, it is clear that the temperature data of Ann Arbor and Phoenix are more dispersed around their average value, which means that the temperature difference in hot and cold seasons is larger. This fluctuation in the temperature leads to different capacity fade rates during the entire year.

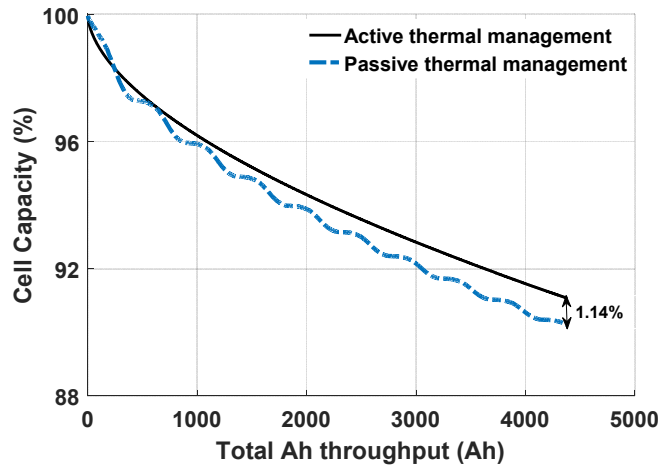


Fig. 4.21. Capacity fade for active vs. passive thermal management systems

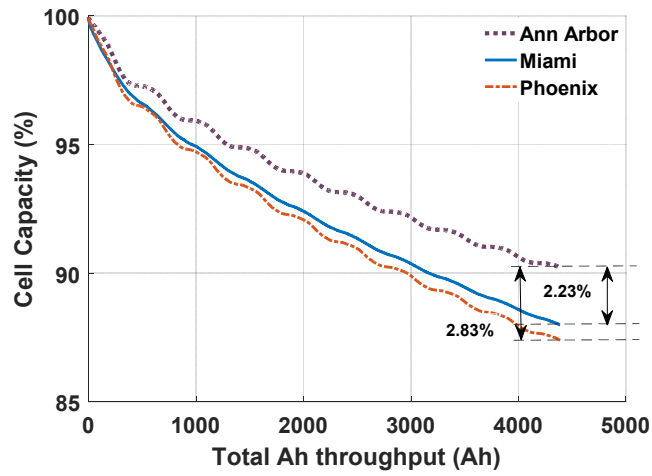


Fig. 4.22. Capacity fade in different climates

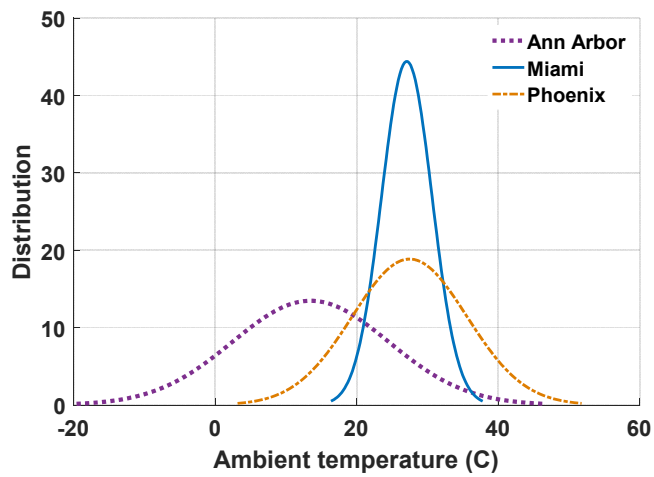


Fig. 4.23. Normal distribution of temperature data

4.7 Discussion

The presented results are summarized in Table 4-2 to make a quantitative comparison between the different daily scenarios. All the provided data in this table are average values. It is important to note that the presented quantitative results are based on the data pool used for this study and reflect the statistical analysis of these data. Although the data used in this study are real-world recorded data, it can vary for different locations and weathers. The statistical results for the driving data shows that the higher accelerations in driving lead to larger power demand from the battery and therefore larger DOD. The aggressive driving group demands 9% and 18% more power from the battery compared to the mild and gentle drivers, respectively. Considering different driving time duration, the aggressive group consumes about 28.9% and 45.7% more energy than the mild and the gentle groups, respectively.

Difference in the energy consumption of different driving groups is originated from different acceleration/deceleration profiles and daily driving duration. Aggressive driving group's average acceleration is about two times the gentle drivers' average acceleration. Higher acceleration/deceleration rates significantly increase the power demand from the battery. Although the vehicle is equipped with regenerative braking, it only collects up to a 10% of the braking/deceleration power and the rest of it is wasted by mechanical brake. In addition, aggressive driving group spend more time for their daily commute compared to gentle drivers. Also, the capacity fade for higher accelerations is faster.

For a single driving cycle, the battery degradation for the gentle driving group is 30% and 14% less than the aggressive and mild driving groups. Hence, in general, aggressive driving behavior causes higher energy consumption and faster battery degradation, which raises both short-term and long-term costs. The charging time for the different charger

options and their battery life estimation results indicate that using the L-2 charger is time efficient (about 5 times less) and has no considerable difference on the battery aging.

The capacity loss percentage after 100,000 miles of driving for different daily scenarios are estimated and presented in Table 4-2, too. It is noticed that uncontrolled charging behavior accelerates the battery capacity loss, while controlled every day or every other day charging not only decrease the battery aging, but also helps the grid in daily load shifting for overnight valley filling.

After similar driving distance, the lowest capacity fade is for the scenario 4 which is for three driving events a day and every other day L-2 charging. The daily 2-hour frequency regulation can reduce the battery life about 14% and peak shaving can decrease the life by 23% although it has a positive benefit from the grid's perspective.

The impact of peak shaving service on the cycle aging is more than frequency regulation (8.5%) after equal days of service due to higher Ah throughput. However, for a similar Ah throughput, the aging slope is higher for the frequency regulation service and it leads to more capacity fade compared to peak shaving. This is because the peak shaving has higher DOD and therefore the Ah related to peak shaving happens in lower SOC, while the frequency regulation has very small DOD due to its fluctuating power and it keeps the SOC higher which increases aging slope. The maximum capacity loss among scenarios is in the case of solar energy storage and peak shaving as V2G services.

Comparing the cell total Ah throughput in different scenarios indicates that daily 29 miles of driving results in about 926.5 full cycle equivalent Ah throughput at the end of 100,000 miles travelled distance. Including daily frequency regulation leads to 1114 full cycle equivalent in total and peak shaving increases it to 1460. Solar energy storage does not increase the total Ah throughput, as it just compensates a part of required recharging.

Results of the different thermal management systems show that passive thermal management increases the capacity fade by 9.8%. The reason for this difference is the excessive capacity fade due to the harsh weather condition which is eliminated in the active thermal management. It is also noticed that the capacity fade for the same daily scenario in Ann Arbor is 18.6% and 21.8% less than Phoenix and Miami weather conditions.

Table 4-2. Statistical results of simulations

		Drivers		
		Aggressive	Mild	Gentle
<i>Driving cycles</i>	Ave. Acc. (m/s ²)	0.981	0.713	0.514
	Ave. P (kW)	6.571	6.012	5.567
	Ave. daily DOD (%)	31.78	24.838	19.87
	Daily energy (kWh)	10.48	8.126	7.192
	Cycle capacity fade	0.027	0.022	0.019
<i>Recharging duration</i>	L-1 charging	6h 53m	5h29m	4h29m
	L-2 charging	1h20m	1h4m	52m
<i>Daily scenarios'</i>	L-1 overnight	10.35	8.80	7.38
	L-2 overnight	10.54	8.92	7.45
	Uncontrolled L-2	12.2	10.4	8.62
	Every other day L-2	6.20	5.32	4.48
<i>Capacity</i>	L-2 and Freq. Reg.	11.6	10.0	8.60
<i>loss %</i>	L-2 and peak shaving	12.2	10.8	9.50
	L-2, Freq. Reg. and peak shaving	13.4	12.0	10.7
	Every other day L-2, Freq. Reg.	10.1	8.7	7.53
	Solar energy storage, peak shaving	13.6	12.1	10.9
<i>Different Climates Capacity</i>	Ann Arbor, Michigan	11.6	9.78	8.18
	Miami, Florida	14.2	12.1	10.0
	Phoenix, Arizona	14.9	12.6	10.5
<i>loss % (Passive Cooling)</i>				

4.8 Conclusions

Considering the ongoing interest of both the vehicle owners and manufacturers on the electric vehicles, and different charging options and possibilities of V2G services, we have quantified the effect of different daily patterns on the EV battery performance and lifetime estimation. For this purpose, a set of real-world connected vehicle driving data were used to develop daily scenarios that included driving, charging and utility services. Note that the capacity fade model estimates the cycle aging only and it does not include the calendar aging. Also, effect of temperature on the battery life is explored for three different US cities based on their annual temperature data. These are the highlighted findings and observations from the results:

- In the driving cycles' analysis, we observed that variations among driving styles are responsible for an 18% power demand and a 45% energy consumption difference between gentle and aggressive drivers. Also, the driving style has considerable impact on the battery aging, as the aggressive drivers' battery life is 23.5% and 38.9% less than the mild and gentle drivers, respectively.
- Uncontrolled recharging leads to increased battery degradation due to the higher SOCs. Scheduling the recharging to after midnight times not only reduces the electricity costs and helps the grid to perform load shifting, but also leads to a 15.8% more battery life than uncontrolled charging during the day. There is no significant difference in the aging results of using different charging facilities (L-1 or L-2), although the charging time is significantly less for L-2 charger.
- Daily V2G tasks decreases the battery capacity with different rates. Based on the results, the negative effect of the peak shaving service on the battery aging is more pronounced than for frequency regulation for similar number of days because of higher

DODs of peak shaving. However, for equal Ah throughput, capacity fade slope is higher for frequency regulations due to higher SOC. Using EV battery as storage for PV panels' output power for evening peak shaving does not change the total Ah throughput the cell, however it leads to about 37% battery degradation.

- Active thermal management reduces the battery aging rate by controlling the battery temperature, while the passive thermal management can increase the capacity fade due to the harsh thermal conditions in the cold and hot seasons. This increase depends on the different climates and their annual temperature distribution, e.g. it is 9.8% for Ann Arbor, 25.9% for Miami and 29.2% for Phoenix. Therefore, the EV battery's health condition should be evaluated based on its thermal management system and climate.

After exploring the battery capacity fade in different conditions, it is observed that all the effectual factors of the battery capacity fade are subjected to change due to the difference in time, location, vehicle's owner, availability of chargers, and utility services possibility. It is not possible to simulate and study all the possible scenarios. All these variations make the aging phenomena more probabilistic than deterministic. Therefore, the perspective is changed and the battery capacity fade is modeled considering all uncertainties in its effective variables. With this analysis method, it is possible to consider the variations in the daily task, change in temperature, and all other factors that may not be known. Next chapter is going to present such a probabilistic method of capacity fade modeling based on Bayesian Networks.

References

- [1] Caihao Weng, Yujia Cui, Jing Sun, Hwei Peng, "On-board state of health monitoring of lithium-ion batteries using incremental capacity analysis with support vector regression," *Journal of Power Sources*, Volume 235, 1 August 2013, Pages 36-44.

- [2] M. Jafari, A. Gauchia, K. Zhang and L. Gauchia, "Simulation and Analysis of the Effect of Real-World Driving Styles in an EV Battery Performance and Aging," in *IEEE Transactions on Transportation Electrification*, vol. 1, no. 4, pp. 391-401, Dec. 2015.
- [3] Jianwei Li, Michael S. Mazzola, "Accurate battery pack modeling for automotive applications," *Journal of Power Sources*, Volume 237, 1 September 2013, Pages 215-228.
- [4] Changfu Zou, Xiaosong Hu, Zhongbao Wei, Xiaolin Tang, "Electrothermal dynamics-conscious lithium-ion battery cell-level charging management via state-monitored predictive control," *Energy*, vol. 141, pp. 250-259, 2017.
- [5] S. Negarestani, M. Fotuhi-Firuzabad, M. Rastegar and A. Rajabi-Ghahnavieh, "Optimal Sizing of Storage System in a Fast Charging Station for Plug-in Hybrid Electric Vehicles," in *IEEE Transactions on Transportation Electrification*, vol. 2, no. 4, pp. 443-453, Dec. 2016.
- [6] Benedikt Lunz, Zexiong Yan, Jochen Bernhard Gerschler, Dirk Uwe Sauer, "Influence of plug-in hybrid electric vehicle charging strategies on charging and battery degradation costs," *Energy Policy*, Volume 46, July 2012, Pages 511-519.
- [7] Saeid Bashash, Scott J. Moura, Joel C. Forman, Hosam K. Fathy, "Plug-in hybrid electric vehicle charge pattern optimization for energy cost and battery longevity," *Journal of Power Sources*, Volume 196, Issue 1, 1 January 2011, Pages 541-549.
- [8] Martin Petit, Eric Prada, Valérie Sauvant-Moynot, "Development of an empirical aging model for Li-ion batteries and application to assess the impact of Vehicle-to-Grid strategies on battery lifetime," *Applied Energy*, Volume 172, 15 June 2016, Pages 398-407.
- [9] E. Sarasketa-Zabala, E. Martinez-Laserna, M. Bercibar, I. Gandiaga, L.M. Rodriguez-Martinez, I. Villarreal, "Realistic lifetime prediction approach for Li-ion batteries," *Applied Energy*, Volume 162, 15 January 2016, Pages 839-852.
- [10] Justin D.K. Bishop, Colin J. Axon, David Bonilla, Martino Tran, David Banister, Malcolm D. McCulloch, "Evaluating the impact of V2G services on the degradation of batteries in PHEV and EV," *Applied Energy*, Volume 111, November 2013, Pages 206-218.
- [11] Scott B. Peterson, Jay Apt, J.F. Whitacre, "Lithium-ion battery cell degradation resulting from realistic vehicle and vehicle-to-grid utilization," *Journal of Power Sources*, Volume 195, Issue 8, 15 April 2010, Pages 2385-2392.
- [12] Andrea Marongiu, Marco Roscher, Dirk Uwe Sauer, "Influence of the vehicle-to-grid strategy on the aging behavior of lithium battery electric vehicles," *Applied Energy*, Volume 137, 1 January 2015, Pages 899-912.

- [13] Clemens Guenther, Benjamin Schott, Wilfried Hennings, Paul Waldowski, Michael A. Danzer, "Model-based investigation of electric vehicle battery aging by means of vehicle-to-grid scenario simulations," *Journal of Power Sources*, Volume 239, 1 October 2013, Pages 604-610.
- [14] J. Hu, C. Si, M. Lind and R. Yu, "Preventing Distribution Grid Congestion by Integrating Indirect Control in a Hierarchical Electric Vehicles' Management System," in *IEEE Transactions on Transportation Electrification*, vol. 2, no. 3, pp. 290-299, Sept. 2016.
- [15] Booz, Allen, Hamilton, "Its Technical Support Services Data Capture and Management Program: Safety Pilot Model Deployment – One Day Sample Data Environment Data Handbook," US Department of Transportation, Research and Technology Innovation Administration Intelligent Transportation Systems --Joint Program Office, July 1, 2014.
- [16] Zhao, S., Zhang, K., 2016. A data-driven optimization model to observe individual dynamic choices of activity-travel-path using connected vehicles as mobile sensors. Accepted to present at the *96th Annual Meeting of Transportation Research Board*, Washington D.C., 2017.
- [17] A. Santos, N. McGuckin, H.Y. Nakamoto, D. Gray, and S. Liss, "Summary of Travel Trends: 2009 National Household Travel Survey," *US Department of Transportation*, June 2011.
- [18] Chen Lv, Junzhi Zhang, Yutong Li, Ye Yuan, Mechanism analysis and evaluation methodology of regenerative braking contribution to energy efficiency improvement of electrified vehicles, *Energy Conversion and Management*, Volume 92, 1 March 2015, pp 469-482.
- [19] X. Nian, F. Peng and H. Zhang, "Regenerative Braking System of Electric Vehicle Driven by Brushless DC Motor," in *IEEE Transactions on Industrial Electronics*, vol. 61, no. 10, pp. 5798-5808, Oct. 2014.
- [20] I Bloom, B.W Cole, J.J Sohn, S.A Jones, E.G Polzin, V.S Battaglia, G.L Henriksen, C Motloch, R Richardson, T Unkelhaeuser, D Ingersoll, H.L Case, "An accelerated calendar and cycle life study of Li-ion cells," *Journal of Power Sources*, Volume 101, Issue 2, 15 October 2001, Pages 238-247.
- [21] John Wang, Ping Liu, Jocelyn Hicks-Garner, Elena Sherman, Souren Soukiazian, Mark Verbrugge, Harshad Tataria, James Musser, Peter Finamore, "Cycle-life model for graphite-LiFePO₄ cells," *Journal of Power Sources*, Volume 196, Issue 8, 15 April 2011, Pages 3942-3948.
- [22] J. Shen, S. Dusmez and A. Khaligh, "Optimization of Sizing and Battery Cycle Life in Battery/Ultracapacitor Hybrid Energy Storage Systems for Electric Vehicle Applications," in *IEEE Transactions on Industrial Informatics*, vol. 10, no. 4, pp. 2112-2121, Nov. 2014.
- [23] Girish Suri, Simona Onori, A control-oriented cycle-life model for hybrid electric vehicle lithium-ion batteries, *Energy*, Vol. 96, pp. 644-653, 2016.
- [24] A123 Systems, Inc., "Technical datasheet of nano-phosphate high power lithium ion cell ANR 26650m1b battery," 2011.

- [25] Pierfrancesco Spagnol, Simona Onori, Nullo Madella, Yann Guezennec, John Neal, Aging and Characterization of Li-Ion Batteries in a HEV Application for Lifetime Estimation, *IFAC Proceedings Volumes*, Vol. 43, Issue 7, 2010, Pages 186-191.
- [26] Pennsylvania-New Jersey-Maryland (PJM) Interconnection, Ancillary Services, 2016, Available online: <http://www.pjm.com/markets-and-operations/ancillary-services.aspx>.
- [27] Keweenaw Research Center/Michigan Technological University, Houghton, Michigan, Available online: <http://mtukrc.org/about.htm>.
- [28] American Recovery and Reinvestment Act (ARRA), “Plugged in: How Americans Charge their Electric Vehicles,” Sept. 2015. Available Online: <https://avt.inl.gov/content/pubs-az>
- [29] Anthony Barré, Benjamin Deguilhem, Sébastien Grolleau, Mathias Gérard, Frédéric Suard, Delphine Riu, “A review on lithium-ion battery ageing mechanisms and estimations for automotive applications,” in *Journal of Power Sources*, Vol. 241, pp. 680-689, 2013.
- [30] Jiling Li, Ahen Zhu, “Battery Thermal Management Systems of Electric Vehicles,” *Master’s Thesis*, Department of Applied Mechanics, Chalmers University of Technology, Sweden, 2014.
- [31] U.S. Climate Data, 2016, Available online: <https://www.usclimatedata.com/>

Chapter 5

Probabilistic Aging Evaluation: Hierarchical Bayesian Network Model¹

Abstract

This Chapter proposes a probabilistic estimation of the electric vehicle (EV) battery capacity fade in Bayesian framework. Since the battery aging factors such as temperature, current, and SOC are not fixed and they change in different times, locations and by the different users, the deterministic models cannot accurately evaluate the battery capacity fade. Therefore, a probabilistic presentation of the capacity fade including all uncertainties of the measurements/observations of the variables can be a proper solution. We have developed a hierarchical Bayesian Network (BN) model for the EV battery capacity fade considering all the possible effectual variable. The mathematical expression of the model is extracted based on Bayes' theorem, the probability distributions for all variables and their dependencies are carefully chosen and Metropolis-Hastings Markov Chain Monte Carlo (MCMC) sampling method is applied to generate the posterior distributions. The model is trained with a subset of experimental data (85%) to obtain its unseen parameters and tested with other 15% of data to prove its accuracy. Also, three case studies for different drivers, different grid services' frequencies and different climates are explored with the developed model to show its flexibility with different input data.

¹ The material contained in this chapter is in preparation for submission to a journal.

5.1 Introduction

The battery degradation is evaluated by two main approaches: data-driven prognostics and model-based methods [1]. The data-driven methods are mostly used for real-time applications and after training through a set of data, they use present measurements data from the battery to predict the battery SOH. Different types of Kalman filters (KF) [2], relevance vector machine (RVM) [3] and functional principal component analyses (FPCA) [4] are some of these methods. These methods need expert knowledge to relate the available data to the battery health condition and superior programming skills. However, they are less complicated in calculations and easy to implement in online applications.

The model-based approach, on the other hand, is based on the historical data of the battery performance and relies on the mathematical expression for the battery capacity fade evaluation. Electrochemical models, equivalent circuit models (ECMs), and empirical aging models are different groups of this approach. Electrochemical models evaluate the battery degradation with chemical properties of the battery components such as solid electrolyte interface (SEI) layer growth, cycleable lithium loss or lithium concentration decrease [5], [6]. ECMs simulate the battery aging with change in the value of the circuit components with cycling and mainly use the electrochemical impedance spectroscopy (EIS) test results to estimate the circuit elements' value [7], [8]. The empirical aging models [9]–[11] are fitting mathematical equation to extensive experimental results obtained from accelerated aging tests on the battery. These models mostly use different forms of Arrhenius equation to include the effect of different aging factors such as SOC, C-rate and temperature.

The shortcoming of the model-based aging studies is that they rely on deterministic mathematical equations and consider the aging effectual factors as fixed values during cycling. However, neither the aging phenomena is deterministic, nor its effecting factors stay constant during the life of the battery. In electric vehicle (EV) application, the capacity fade of the battery during cycling is directly affected by the driver's behavior, charging facilities availability, grid services presence and the temperature/weather condition [12]. None of these factors can be defined by fixed values and they carry significant uncertainties. Therefore, deterministic models are not reliable in evaluating the battery capacity fade for different usage conditions and probabilistic methods including the uncertainties of the measurements and process such as Bayesian models can present more informative and accurate evaluation of the battery capacity fade [13].

Different Bayesian models are applied to estimate the battery SOH which are mostly proposed for online applications. He et al. [14] proposed the online SOH estimation with the Dynamic Bayesian networks (BN). In this study, the terminal voltage measurements in the constant current charging cycle is used to estimate the SOC of the battery in different time interval. Their model uses the charging voltage profile as input and gives the probability of the battery being in different capacity classes. Similarly, Jin et al. have estimated the spacecraft secondary life battery's capacity fade using online charge/discharge measurements [15]. In [16], Electrochemical Impedance Spectroscopy (EIS) test results are used to estimate the battery internal impedance as a battery health index. Simplified Bayesian model known as "naive" Bayes is proposed in [17] to predict the battery SOH. Naive Bayes assumes that unobserved variables are independent and therefore it simplifies the Bayes theorem. This method of modeling eliminates the hierarchical parts of Bayesian network which present the intermediate hidden states. Mishra et. al. [18] have maintained the hierarchical properties of BN in their model,

however, they use simple ECM model and estimate the end of life of the battery based on discharge measurements and do not consider the effect of temperature and dynamics of the cycling current. Refs. [19], [20] have used the capacity measurements to make prediction of the remaining useful life (RUL) of the battery.

In these previous Bayesian approaches there is a more focused effort on using it as a classifier or estimator without considering the external factors and their variations. We propose that there is a better quality to BNs that can be used for battery degradation modeling, and that is the fact that it surfaces dependency and causality. Causality is of utmost importance for batteries as their aging is affected by a high number of hierarchical variables that depend upon external factors to the battery, which is the strength of BN models [21], [22].

Acknowledging the advantage of Bayesian models in considering the uncertainties of the variables and estimating the hidden states of the process and providing probability distributions instead of point value estimations, we proposed a hierarchical Bayesian model for the probabilistic battery capacity fade evaluation in the EV application. This model does not target online application and is focused around proposing a Bayesian framework that can relate external factors to battery aging evaluation. The Bayesian network for this problem is developed including all observed and unobserved variables and mathematical presentation of the model is extracted. The probability distributions for the variables are defined and Markov Chain Monte Carlo (MCMC) sampling is employed to obtain the posterior distributions. The model training, test and case study are presented to show its performance. This model reflects the uncertainties of measurements and process, it precisely evaluates the capacity fade and provides more informative results, and it is applicable for any type of input data with proper training.

5.2 Bayesian Models and EV Battery Aging Factors

Contrary to deterministic models that use direct mathematical equations to present the relationship between variables, BN models are probabilistic presentation of variables conditional to observed data. Graphical representation of the BN includes “nodes” and ‘edges” in which each node is a random variable connected to its parent nodes through edges. The relationship between parents and child nodes is defined by Bayes’ theorem. The key point of BN is that it classifies the variables into two groups: “Observations” and “Unobserved variable” and treats all unobserved quantities as random variables. Based on the Bayes’ theorem, the unobserved variables including unmeasured/unseen quantities and model parameters (\mathbf{x}) are conditional to observations/measurements (\mathbf{y}) as follow:

$$P(\mathbf{x}|\mathbf{y}) = \frac{P(\mathbf{y}|\mathbf{x})P(\mathbf{x})}{P(\mathbf{y})} \quad (5-1)$$

where, $P(\mathbf{x}|\mathbf{y})$ is the posterior distribution, $P(\mathbf{y}|\mathbf{x})$ is the likelihood of observations, $P(\mathbf{x})$ is the prior distribution of unobserved variables, and $P(\mathbf{y})$ is the marginal distribution of vector of observations and can be calculated by (5-2). The bold style denotes “vector” of variables.

$$P(\mathbf{y}) = \int P(\mathbf{y}|\mathbf{x})P(\mathbf{x})d\mathbf{x}. \quad (5-2)$$

This presentation of a problem is capable to include all uncertainties of the measurements, sampling, parameters, and modeling. However, analytically solving of (2) is not possible for large number of the unobserved variables \mathbf{x} . Therefore, it should be solved by numerical approximation methods like Markov Chain Monte Carlo (MCMC) sampling.

The main capacity fade factors of the electric vehicle battery are temperature, SOC, cycling C-rate, and total Ah throughput (5-3) [9], [23]. Among these factors, temperature

is independent, and all other factors are dependent to the frequency of daily tasks (driving, recharging, utility services) and human factors (driving styles and recharging habits).

$$Q_{loss} = f(T, SOC, I_c, Ah) \quad (5-3)$$

None of these factors are fully determined and there are uncertainties in each. Temperature pattern cannot be fully predicted, the driving distance and style are dependent to the needs of the vehicle owner and his/her personality, and recharging and possibility of the utility services are upon access to the power grid. Therefore, it is not possible to accurately estimate the battery capacity fade using a deterministic mathematical model while its variables are stochastic, and BN probabilistic approach can be a proper solution for the battery capacity fade modeling.

5.3 BN Modeling Process

5.3.1 Network Development

In the first step to develop the BN for EV battery capacity fade, observations and unobserved quantities are defined. The battery cell's capacity fade percentage is measurable (q), however it has measurement uncertainty and it should be estimated to consider the measurement error (λ). The estimated capacity fade percentage is affected by the total Ampere-hour throughput (Ah), state of charge (SOC), temperature distribution (\bar{T}), and C-rates (I_c). The temperature distribution can be obtained from its measurements (T) including the measurement and sampling uncertainties. SOC and Ah can be obtained from C-rates and C-rates is dependent to the battery voltage (u) and battery power (P_b). The battery voltage has a distribution between its fully charged and fully discharged voltage values. P_b , on the other hand, is dependent to the wheel power (P_w), auxiliary power (P_{aux}), EV mechanical and electrical parts' efficiencies index (δ), the charging/grid services power

(P_g) and all these factors' contribution coefficients (k_n , $n=1,2,\dots,7$). The contribution coefficients are considered for probabilities of driving, standard L1, L2, and L3 chargers, frequency regulations, peak shaving and solar power integration. The powers for charging and grid services (P_{L1-3} : L1, L2 and L3 chargers powers, P_s , P_f , P_{ps} : solar panel, frequency regulations and peak shaving powers) are considered to be perfectly observed and therefore they do not reflect any uncertainties. Also, P_{aux} is considered to have distribution between 5-15% of the driving power. The charging power is assumed to be known and the grid services is performed by the standard L2 charging station.

The wheel power can be calculated from the vehicle velocity distribution (\bar{v}) and the acceleration distribution (\bar{a}) using the governing mechanical equations. \bar{v} and \bar{a} are obtained from the velocity and acceleration measurements (v and a) considering their measurement and sampling errors. Also, parameters are defined to relate all these variables dependencies as aging parameters, α , β , E_a , η , ζ , ε , and vehicle mechanical parameters, γ , ω , and φ .

In our problem, there are $i=1 \dots N$ observations and in each observation, we have K , M , and J measurements for v and a , T , and q , respectively. Our expert domain knowledge was used to create the network structure based on the observations and unobserved variables as shown in Fig. 5.1. Note that other such models may be differently developed but statistically indistinguishable based on the independencies/dependencies entailed by the model. The network has three main parts: "data" shows the observations/measurements, "process model" includes the aging and EV variables and 'parameters' define the model variables' dependencies. Solid edges refer to the probabilistic relationship, while the dashed edges show deterministic dependencies and the nodes at the beginning of these arrows are not random variables.

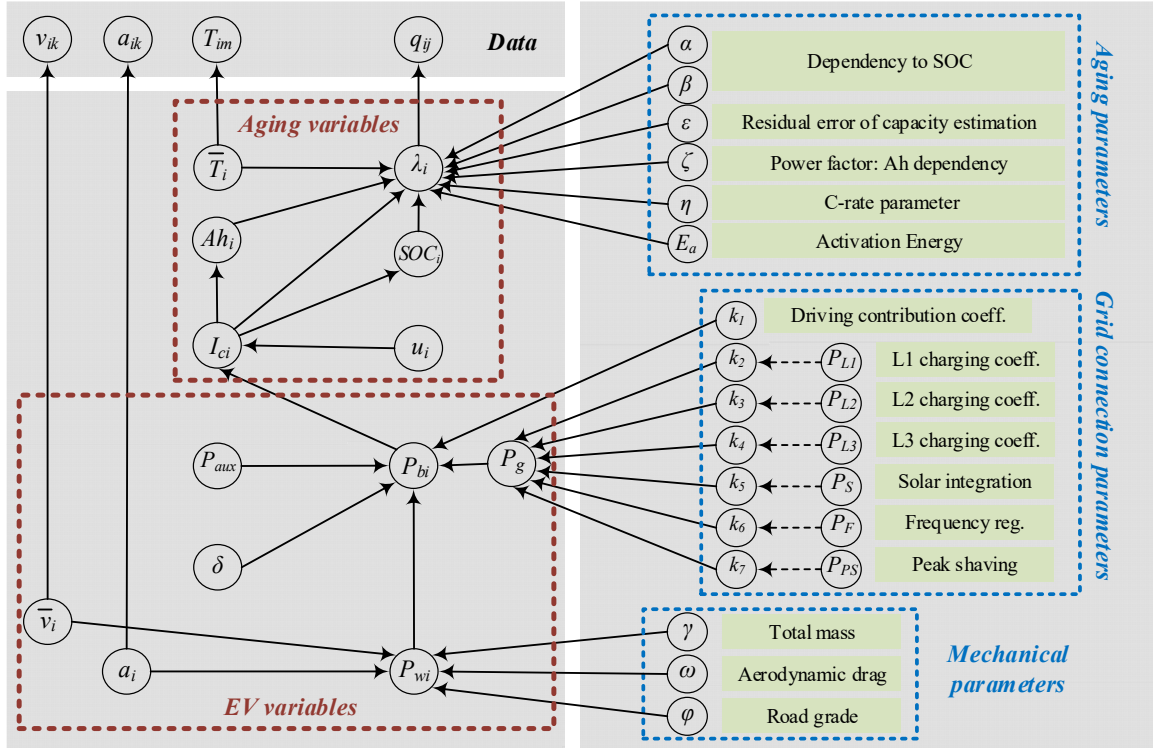


Fig. 5.1. Graphical view of the developed BN

5.3.2 Mathematical Expression

Considering the nodes and edges of the network in Fig. 5.1, the mathematical expression of the model considering all variables' uncertainties can be written as (5-4) to (5-8). In (5-4), “[]” denotes the “probability of” the variable inside the brackets. Note that the sign between left and right side of the equation is not “=” and it is “ \propto ”, because the marginal distributions of the observations (refer to the denominator of (5-1)) are not included in this equation. Therefore, the MCMC sampling method is used to draw large number of samples from the posterior distributions and estimate them with distribution fitting. To apply MCMC, the probability distribution function (PDF) of all variables should be defined based on their properties and full conditionals for all variables should be written.

$$[\lambda, \bar{T}, I_c, Ah, SOC, u, P_b, P_w, \bar{a}, \bar{v}, P_{aux}, \delta, \alpha, \beta, E_a, \eta, \zeta, \varepsilon, \mathbf{k}_n, \gamma, \omega, \varphi | \mathbf{a}, \mathbf{v}, \mathbf{T}, \mathbf{q}] \propto$$

$$\prod_{i=1}^N \prod_{j=1}^J [q_{ij} | \lambda_i] \times [\lambda_i | f_i] \times \prod_{m=1}^M [T_{im} | \bar{T}_i] \times [\bar{T}_i] \times \prod_{k=1}^K [a_{ik} | \bar{a}_i] \times [\bar{a}_i] \times [v_{ik} | \bar{v}_i] \quad (5-4)$$

$$\times [\bar{v}_i] \times [Ah_i | I_{ci}] \times [SOC_i | I_{ci}] \times [I_{ci} | y_i] \times [u_i] \times [P_{bi} | g_i] \times [P_{aux}] \times [\delta]$$

$$\times [P_{wi} | h_i] \times [\alpha] \times [\beta] \times [E_a] \times [\eta] \times [\zeta] \times [\varepsilon] \times [\mathbf{k}_n] \times [\gamma] \times [\omega] \times [\varphi]$$

$$f_i = (\alpha SOC_i + \beta) \exp\left(\frac{-(E_a - \eta I_{ci})}{R \bar{T}_i}\right) Ah_i^\zeta + \varepsilon \quad (5-5)$$

$$y_i = \frac{P_{bi}}{u_i} \quad (5-6)$$

$$g_i = k_1 \left(\frac{1}{\delta} P_{wi} + P_{aux}\right) + k_n P_{gn} \quad n = 2, \dots, 7 \quad (5-7)$$

$$h_i = \gamma \bar{a}_i \bar{v}_i + \omega \bar{v}_i^3 + \varphi \bar{v}_i \quad (5-8)$$

Referring to the model's variables and exploring their properties, it is possible to define a proper distribution function for them. Among variables, λ , Ah , u , and \bar{v} are definitely equal to or greater than zero. Therefore, gamma PDF is used to define their distribution. For the same reason, the gamma PDF is used to define the parameters, too. The SOC and δ values vary in [0-1] interval, so a Beta PDF is more appropriate for these variables. C-rates are mostly concentrated on positive small values and it has a tail toward larger numbers. Therefore, a Rayleigh PDF defines its properties better. The rest of variables including powers, acceleration and temperature are defined with the normal PDF as they are centered around a value with possibility of both positive and negative tails. Using the defined PDFs, we have derived the full conditionals for all variables to apply the MCMC. An example of full conditionals for λ , I_c , \bar{v} , and δ are presented in (5-9) to (5-12).

$$[\lambda | \cdot] \propto \prod_{i=1}^N \prod_{j=1}^J N(q_{ij} | \lambda_i) \times G(\lambda_i | f_i) \quad (5-9)$$

$$[I_c | \cdot] \propto \prod_{i=1}^N G(\lambda_i | f_i) \times G(Ah_i | I_{ci}) \quad (5-10)$$

$$\times B(SOC_i | I_{ci}) \times R(I_{ci} | y_i)$$

$$[\bar{v} | \cdot] \propto \prod_{i=1}^N N(P_{wi} | h_i) \prod_{k=1}^K G(v_{ik} | \bar{v}_i) \times G(\bar{v}_i) \quad (5-11)$$

$$[\delta | \cdot] \propto \prod_{i=1}^N N(P_{bi} | g_i) B(\delta) \quad (5-12)$$

where, $[\lambda | \cdot]$ stands for the λ conditional to all the variables related to it and it should include all the terms that have λ from (5-4). Also, N, G, B, and R refer to normal, gamma, beta, and Rayleigh PDFs, respectively. It is important to note that all these PDFs require values for their standard deviation (SD) to calculate the probabilities, which are defined based on the properties of each variable. For example, we have considered 10% of the capacity fade measurements as their distribution's SD.

5.3.3 MCMC Sampling Implementation

The model requires the initial values for all variables to initiate the MCMC. For the unseen variables such as *SOC*, *Ah* and powers, calculations from the input data are used to define the initial guess. However, for the parameters which are more important to be initiated properly, different sources of information are used. ε is the residual of (5-5) and therefore, its initial value is considered to be zero. E_a and ζ are activation energy and power factor respectively, and based on the reports from literature [24], their initial guess is 31000

and 0.5, respectively. Initial values for α , β , and η are selected based on the engineering judgment. Considering the governing mechanical equations of the vehicle, γ reflects the total vehicle mass which is the mass of vehicle in addition to the mass of passengers. Initial value of ω is calculated from (5-13) to reflect the effect of aerodynamic drag of the vehicle and for φ , the initial value is calculated by (5-14) to include the impact of rolling resistance and road grade.

$$\omega^{(1)} = 0.5\rho C_x A_f \quad (5-13)$$

$$\varphi^{(1)} = mgf_r \cos\theta + mg\sin\theta \quad (5-14)$$

where, ρ is the air density, C_x is the aerodynamic coefficient, A_f is the vehicle frontal area, m is the vehicle mass, f_r is the rolling coefficient and θ is the road grade. k_n ($n=1,2,..7$) are initiated based on the different daily tasks probability and their contribution on the total Ah throughput of the battery. Initial value for k_1 is the driving task contribution on the Ah. This value for k_2 , k_3 , and k_4 which are related to the portion of each charging facility (L1, L2 and L3, respectively) is obtained based on a report from Idaho National Lab about the charging patterns of EVs in USA [25]. For k_5 to k_7 , contribution of the solar integration, frequency regulation and peak shaving in the daily tasks' Ah is considered as the first guess.

The MCMC sampling starts with the defined initial values for all variables ($x^{(1)}$). In iteration r , a random proposal value ($x^{(P)}$) is offered based on the current value of the variable ($x^{(r)}$), for the next value of x as:

$$x^{(*)} \sim N(x^{(r)}, \sigma_T) \quad (5-15)$$

where, σ_T is tuning SD. Then, the full conditional is calculated for both the proposal and current values and Metropolis-Hastings sampling criteria is used to accept or reject the proposal value as (5-16).

$$R = \min\left(1, \frac{[x^{(P)}|\cdot]}{[x^{(r)}|\cdot]} \times \frac{[x^{(r)}|x^{(P)}]}{[x^{(P)}|x^{(r)}]}\right) \quad (5-16)$$

The proposal value is accepted as the next value of the variable in the chain ($x^{(r+1)}$) with probability R and it is rejected and the current value is kept by probability $1-R$. Applying this method to all variables and repeating it generates draws from the posteriors which can be used to estimate their distributions.

The last challenge in MCMC implementation is when the number of measurements in an observation is high (e.g. the acceleration data with resolution of 1 second in 30 minutes of driving). In that case, the multiplication of probabilities leads to a significantly small quantity that prevents the sampling criteria from accepting the proposal values. To solve this issue, we have reduced the number of data by taking their average value. However, to define the number samples that are correlated and can be averaged, the autocorrelation of the data are calculated and the data points with an autocorrelation smaller than 0.2 are considered to be uncorrelated. The autocorrelation for observation data y can be calculated as (5-17).

$$A(lag) = \frac{\mathbf{E}[(y_t - \mu)(y_{t+lag} - \mu)]}{\sigma^2} \quad (5-17)$$

where, \mathbf{E} is expected value operator, μ and σ are the average and SD of the data. As shown in Fig. 5.2 for a sample acceleration data, for the samples with index difference of 7 or greater, the autocorrelation is less than 0.2 (uncorrelated) and therefore, every 7 data points are used for averaging and reducing the number of data. This method is used for other input data, too.

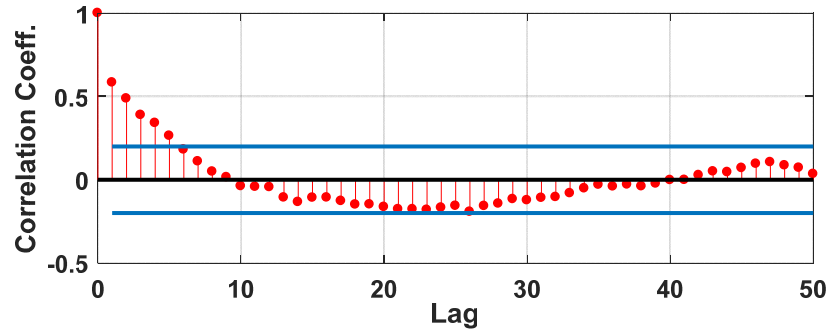


Fig. 5.2. Sample autocorrelation for acceleration data

5.4 Training Data

To train the model and obtain the parameters, we have used three sets of experimental results on A123 ANR26650, 2.3 Ah LFP cells' capacity fade in different cycling conditions [26]. These data are shown in Fig. 5.3 which relates the capacity fade percentage to the total Ah throughput. The tests are performed different in temperature, SOC and C-rates.

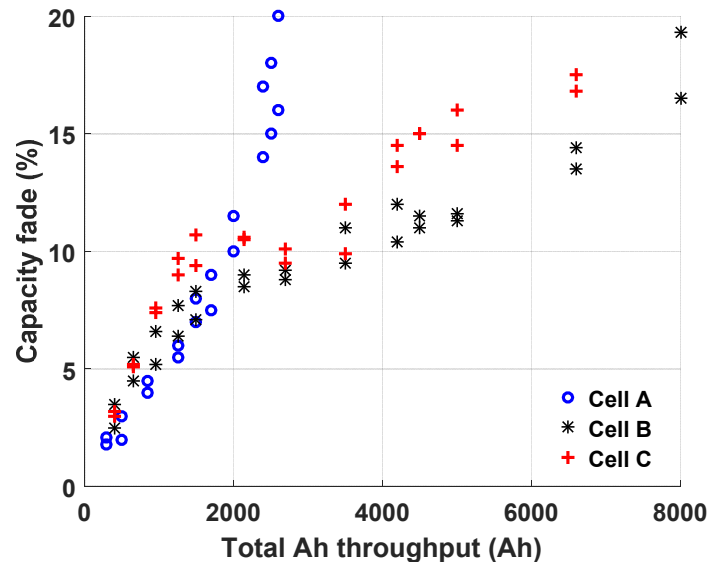


Fig. 5.3. Capacity fade data for three different test conditions [26]

From these data, 70 data points are randomly selected to be used in training. The remaining 12 data points are kept for testing the model. The model obtains the

measurements and initial values for the intermediate variables and generates chains of 10000 samples for each variable using the mentioned MCMC sampling method. Fig. 5.4(a) shows the MCMC samples for one of the capacity fade data points which is draws from posterior distribution. Based on this figure, the model is consistent in sampling and it does not wander around different values. These samples are used to fit distributions to the variables. Histogram and fitted gamma distribution of the samples in Fig. 5.4(a) are depicted in Fig. 5.4(b). Variation of fitted distribution's mean and SD for this data chain with 95% confidence interval are ± 0.8 and ± 0.03 , respectively.

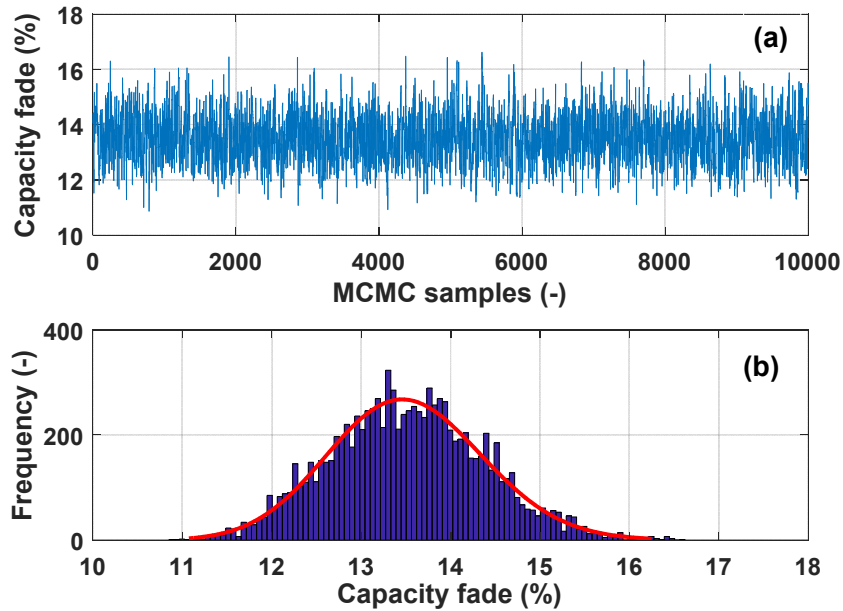


Fig. 5.4. (a) Chain of samples for a capacity fade data point and (b) Histogram and gamma distribution of the sample chain

The procedure is applied for all the variables and their fitted PDFs are obtained. The model's capacity fade estimation gamma distributions based on the measurements are depicted in Fig. 5.5(a). Each of these PDFs reveals the fact that the capacity fade percentage is not a fixed value and it varies between values with different probabilities to include the uncertainties of the measurements and the modeling process. For instance, the bold black

plotted PDF in Fig. 5.5(a) shows variation between 11-17% capacity fade with average of 13.51% for two measurements of 13.6% and 14.5% and other uncertainties in the temperature, C-rate, and all other measurements.

To show that the results of the model's training are reliable, we have compared the mean value of PDFs in Fig. 5.5(a) to the mean of experimental measurements of the capacity fade (Fig. 5.5(b)). This figure also indicates the estimation dispersion in two SD interval ($\pm 2\sigma$). These results indicate that the model's training and parameters' tuning are successful.

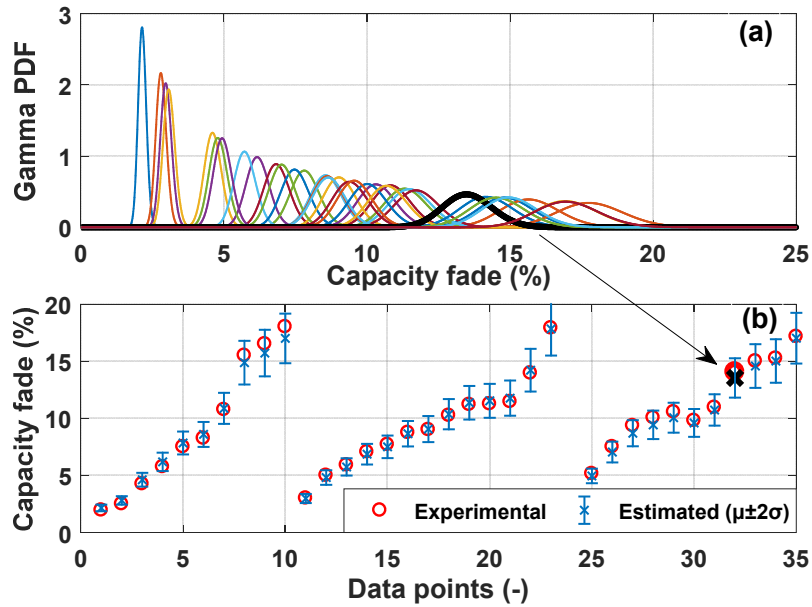


Fig. 5.5. Training set: (a) Capacity fade percentage gamma PDFs and (b) mean of PDFs compared to experimental data

Using the results of the training set, we have obtained the model parameters' distribution. The PDFs for α , β , ζ , and ε are plotted in Fig. 5.6 where, α , β , and ζ have gamma distribution and ε has normal distribution.

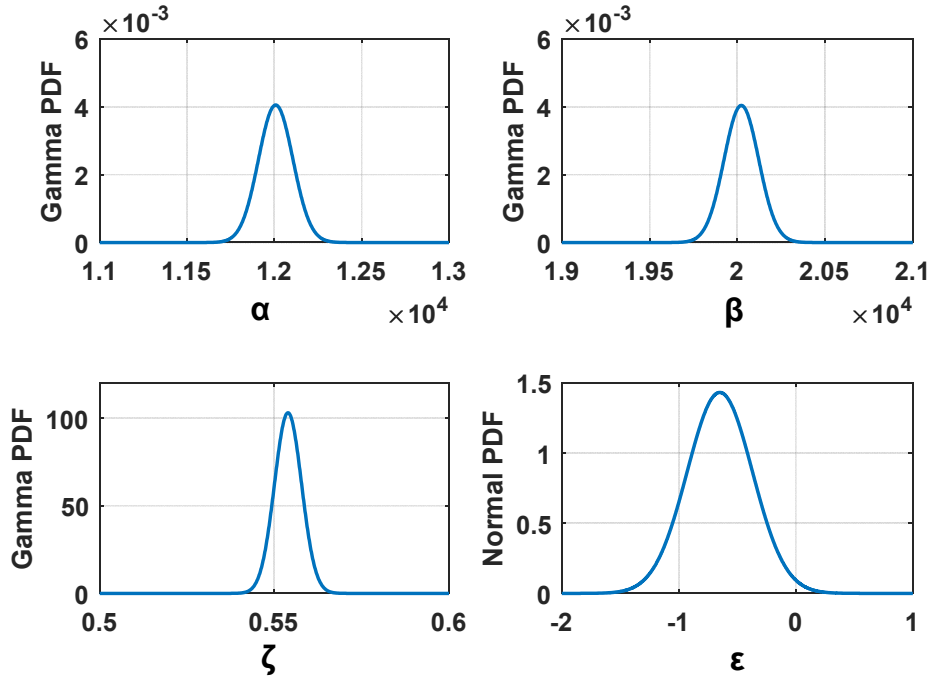


Fig. 5.6. Model parameters' PDF

5.5 Model Evaluation with Test Set

From the data, 12 data points (different from the training set) are used to test the model's estimation precision. Note that these data points are for six observations with two measurements in each observation. The gamma distribution of the estimated capacity fade percentage for these observations are shown in Fig. 5.7(a) and the mean of these distributions are compared to the measurements in Fig. 5.7(b). Considering these figures, in most cases the estimated average is between two measured values and the model is successful in estimating the capacity fade percentage. The R^2 for this comparison is 0.95 which indicates acceptable precision of the model estimation. The merit of this model is that it can be applied to any set of experimental data and after tuning the parameters, it can estimate the battery capacity fade with high accuracy.

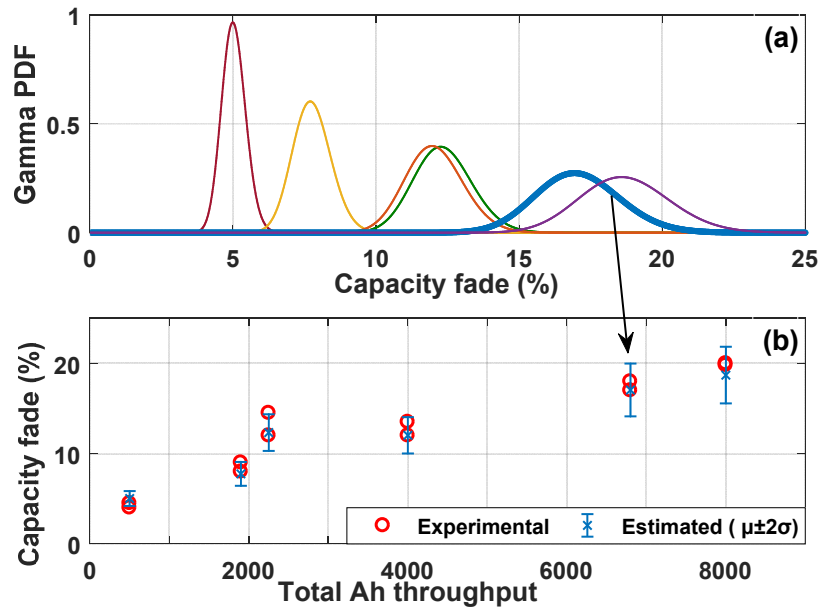


Fig. 5.7. Test set: (a) capacity fade estimation distributions and (b) comparison of estimated and measured capacity fade

5.6 Case Study: BN Model Performance

In this section, we show how the developed BN model can estimate the battery capacity fade in different cases with different provided data to indicate its flexibility. Three cases are studied here. First, the effect of different drivers is explored by the model. The variables that are directly affected in this case are shown in Fig. 5.8 network with green color. The second case explores the impact of the frequency of grid services which directly changes contribution coefficients and the grid power (red section in Fig. 5.8). Last, the battery capacity fade in four different states of USA depending on their weather condition is simulated using their daily temperature data (blue variables in Fig. 5.8).

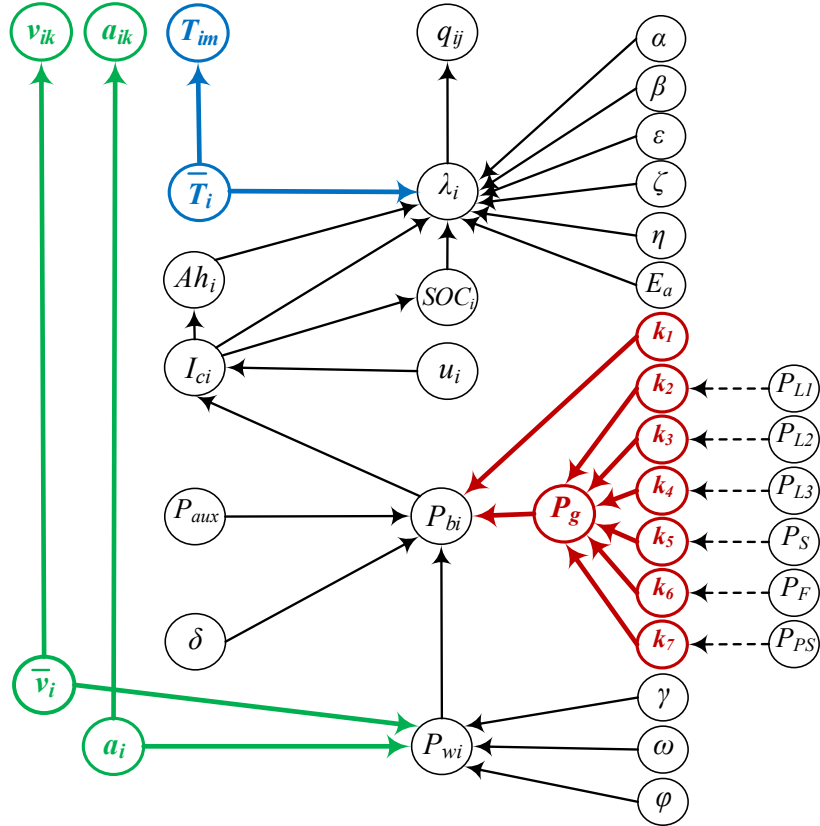


Fig. 5.8. Directly affected parts of BN network in driving data (green), grid services frequency (red) and different locations/weather (blue)

5.6.1 EV Daily Driving and Grid Services

In this case, it is considered that the EV is going to have its driving sessions in addition to grid services such as solar integration, frequency regulations and peak shaving, provided by it. Therefore, its battery cycling will include the driving, recharging and utility services. To simulate different drivers impact, recorded driving data of 45 drivers in Ann Arbor, MI [27] is used to simulate the daily driving pattern. For the recharging, based on an INL report [25], it is assumed that 38%, 55%, and 7% of all recharging events are performed by L1, L2, and L3 chargers, respectively. Grid services are simulated by using recorded solar power data and PJM frequency regulations and peak shaving data. Note that

this information is used to calculate the initial values of the contribution coefficients. The model is run for the capacity fade estimation after about 100000 miles of driving.

The model output for the driving cycles includes 45 independent distributions, with their kernel plotted in Fig. 5.9(a) to present the whole driving data distribution. This figure shows that the velocity data varies between 15 and 45 mph. Fig. 5.9(b) shows the acceleration PDFs for these driving cycles. The color code in this figure is based on the average absolute acceleration, (red to green color change refers to high to low values). We assume that the drivers with higher average acceleration (red curves) which means more frequent accelerations/decelerations during driving period are more aggressive drivers, while the gentle drivers have lower average acceleration (green curves). More information on how this was concluded can be found in [27].

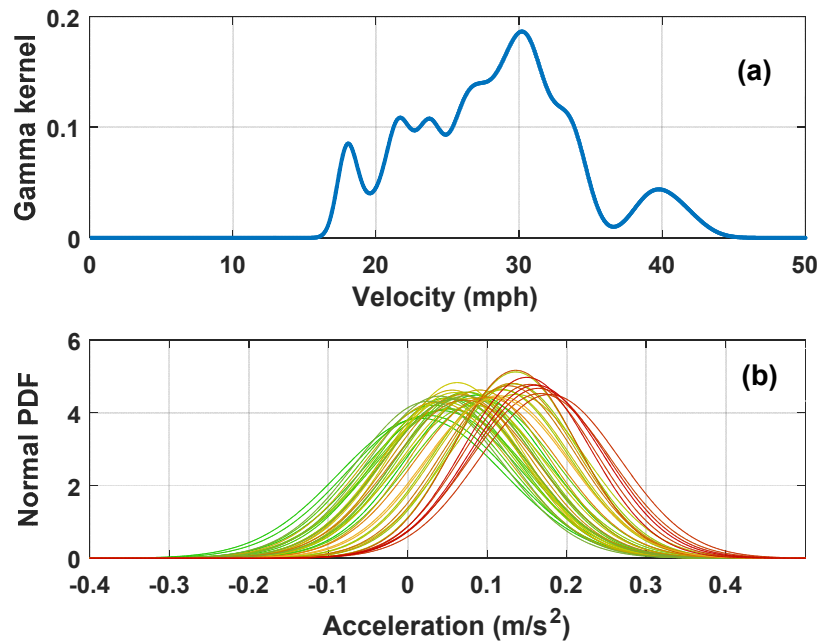


Fig. 5.9. (a) Velocity kernel and (b) acceleration PDFs

The model's estimation for the efficiencies and the auxiliary power are shown in Fig. 5.10 (a) and (b). The battery power includes the effect of the charging events and grid services, as well. Therefore, the contribution of the driving and each of the recharging facilities in addition to grid services' contributions are estimated by the model and shown in Fig. 5.10(c). Reminding that k_1 refers to driving contribution, k_2 to k_3 stands for recharging facilities and k_5 to k_7 shows the grid services contribution coefficients, the driving's contribution is centered at 0.286 with higher values accounting for the regenerative braking and lower values referring to the auxiliary power. The L1, L2 and L3 chargers have contribution distributions, centered at 0.123, 0.18, and 0.021, respectively. Also, the contribution of solar integration, frequency regulation and peak shaving are 0.096, 0.093, and 0.151, respectively.

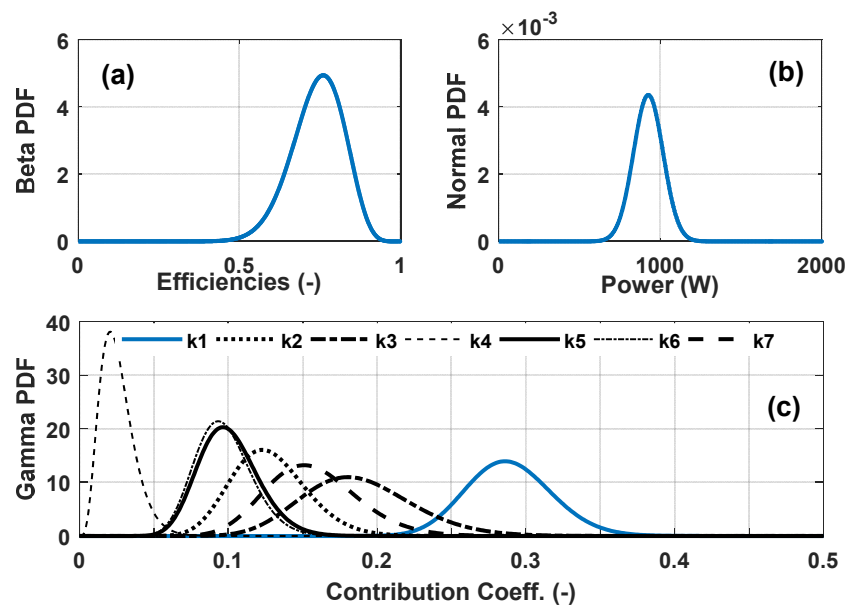


Fig. 5.10. PDFs of (a) EV power train efficiencies, (b) Auxiliary power and (c) contribution coefficients of driving and recharging events

The model output for the SOC and Ah distributions are depicted in Fig. 5.11(a) and (b). These distributions show the effect of all EV tasks, including grid services. Also, it

indicates that the gentle drivers SOC distributions have higher mean values, while there is no significant difference on the distributions' variance. However, they have lower total Ah throughput mean values with lower variances which shows that the model estimates the higher Ah distributions with more uncertainties. It is important to note that the SOC and Ah have direct relationship with capacity fade and therefore, based on the trend of these distributions, these two factors are in race.

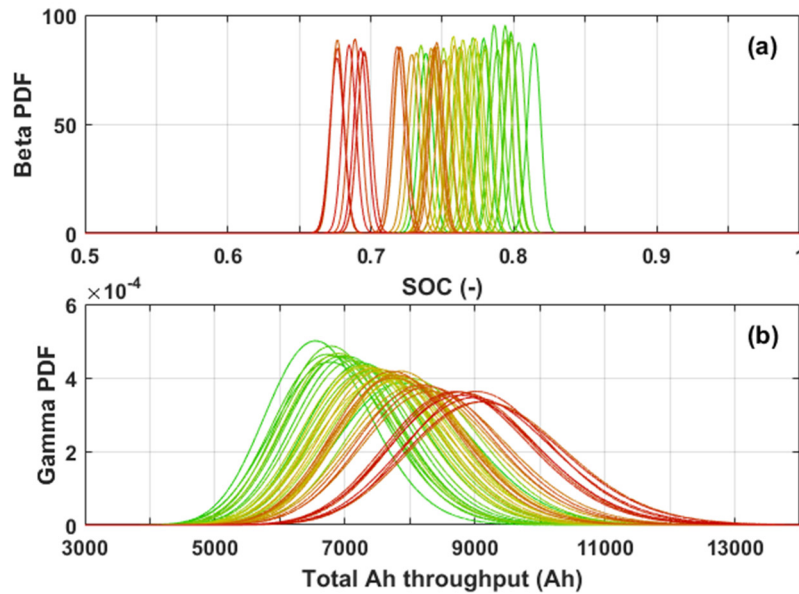
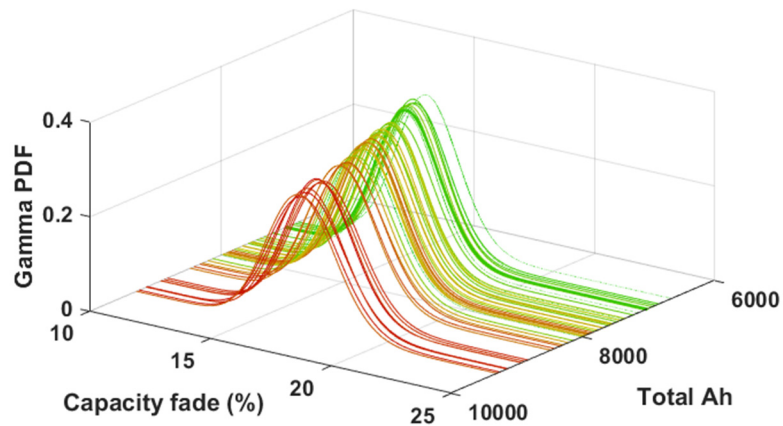


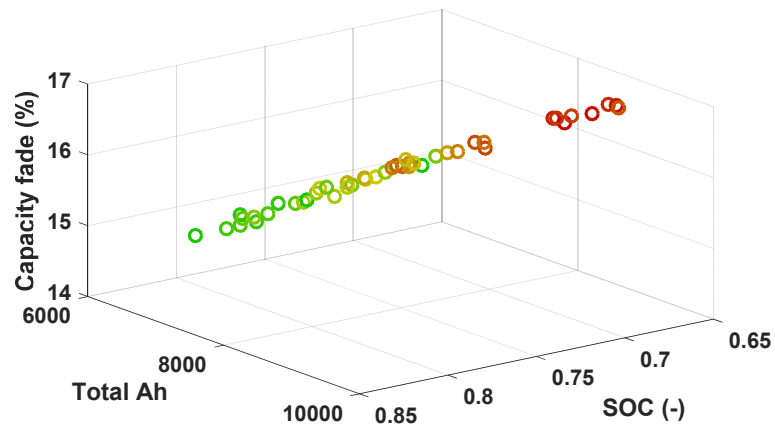
Fig. 5.11. (a) Beta PDFs of SOC and (b) gamma PDFs of Ah for all drivers

The most important result of the model is capacity fade percentage estimation which is shown in Fig. 5.12. Considering Fig. 5.12(a), the capacity fade PDFs have higher mean value for the aggressive drivers. The SD of distributions are similar, varying between 1.2 and 1.4. From red to green, the SD is decreasing, which can be the effect of Ah distributions' SD. Comparing the effects of Ah and SOC in Fig. 5.12(b) indicates that the Ah is more dominant factor in capacity fade, as the drivers with higher Ah have higher capacity fade at the end of driving period, although their SOC is lower. Considering the

color change (refers to average acceleration) in these figures' data, there are outlier points which indicates that the capacity fade has no linear relationship with the acceleration profile. However, the general trend shows strong relationship between aging and driving aggressiveness.



(a)



(b)

Fig. 5.12. (a) Capacity fade PDFs and (b) mean of capacity fade PDFs respect to Ah and SOC means

5.6.2 Effect of grid services' contributions

As there is no defined pattern for the grid services and availability of the service, the infrastructures and the willingness of the vehicle owner changes its significantly, we have

simulated 5 patterns for the frequency of three mentioned grid services as never, once a month, every week, every other day, and daily. Running the model for these patterns changes the contribution coefficient's estimation as shown in Fig. 5.13. In this figure, k_1 (driving) is shown in trace (a), k_2 to k_3 (charging) and k_5 to k_7 (grid services) are aggregated and shown in trace (b) and (c), respectively. It is obvious that if the frequency of grid services events increases, the portion of driving and recharging in the total battery Ah decreases, although the total Ah increases significantly by adding more grid services events (Fig. 5.14 (a)). This increase in Ah increases the capacity fade percentage accordingly, as indicated in Fig. 5.14(b). Note that adding different number of these events changes the battery power, C-rate and SOC distributions, as well.

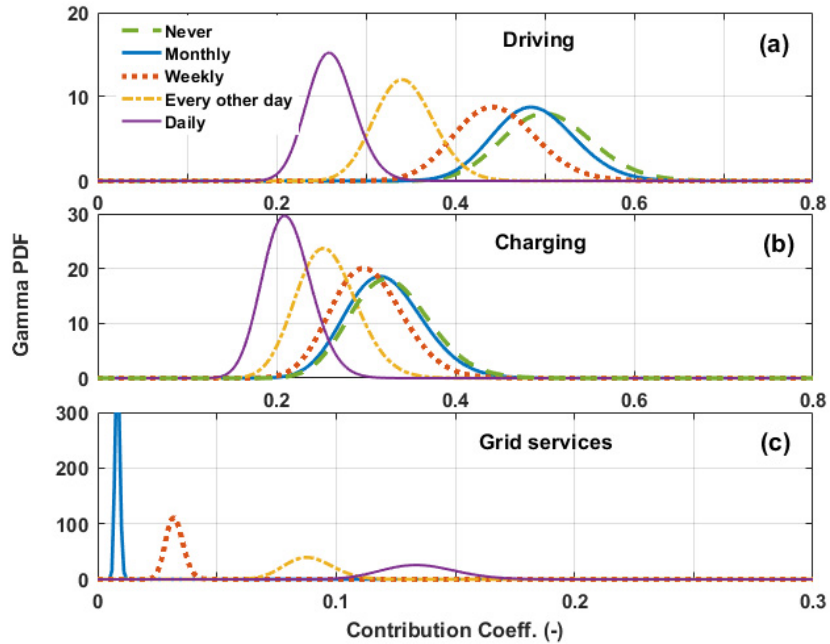


Fig. 5.13. Contribution Coefficients PDFs in different frequency of grid services events

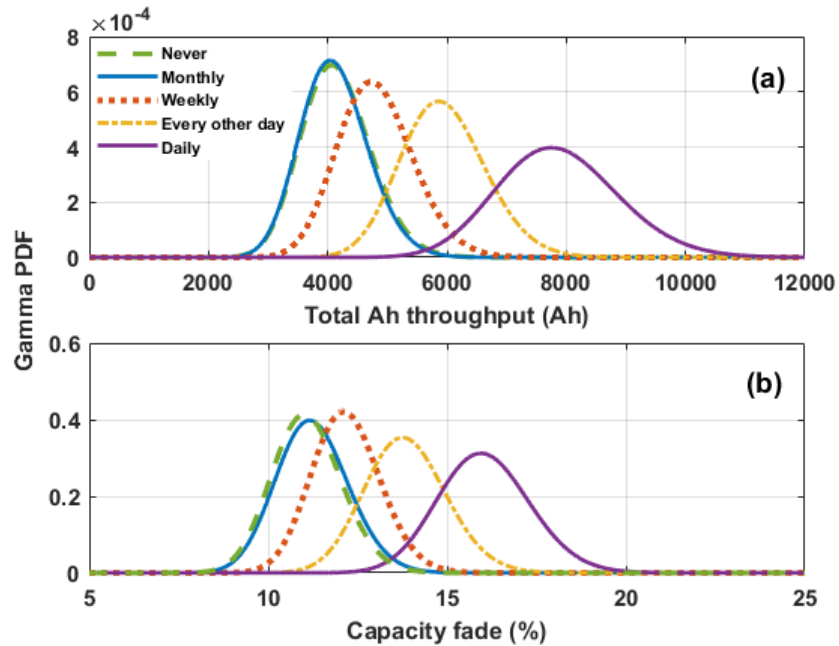


Fig. 5.14. (a) Total Ah and (b) capacity fade PDFs for different frequency of grid services events

5.6.3 Impact of location/weather change

If the EV is driven in different climates, the capacity fade will change based on the temperature pattern. To explore the effect of temperature change, we have extracted the daily temperature data for four US cities with different climates (Phoenix, Ann Arbor, Miami, and Portland) in 2017 and run the model for these temperature observations. The normal distribution of the annual temperature in these cities are shown in Fig. 5.15 (a). These temperature patterns lead to different capacity fade estimations as plotted in Fig. 5.15 (b). From the figure, there is no significant difference between Phoenix and Miami, as their average temperature is similar, however the small difference can be caused by the higher range of temperature change in Phoenix and making more harsh temperature condition for the battery. Ann Arbor has a very wide annual temperature range because of its cold winters, while Oregon's temperature distribution has smaller SD. Lowest capacity fade happens in Oregon and highest is in Phoenix.

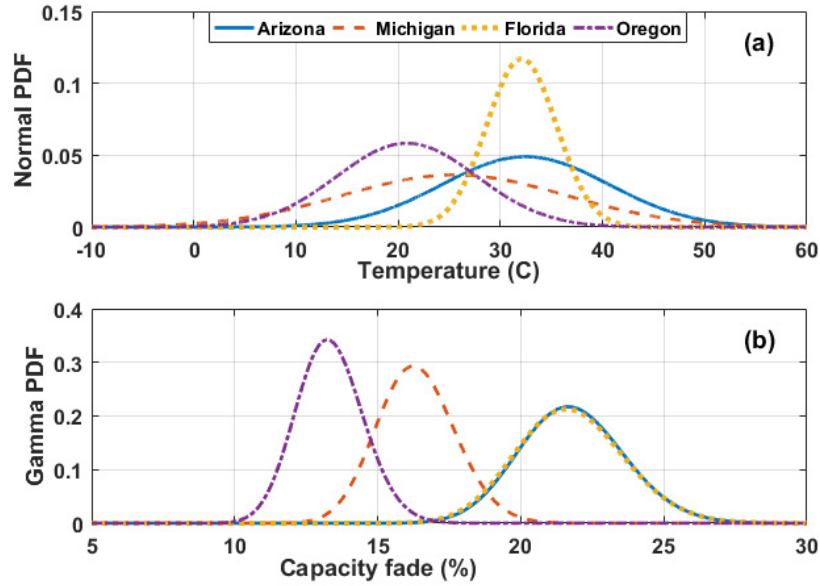


Fig. 5.15. (a) Temperature and (b) capacity fade distributions for different climates

5.7 Conclusion

The battery capacity fade modeling and estimation has uncertainties due the probabilistic nature of its effectual factors such as current and temperature. Therefore, deterministic models cannot completely explain the capacity fade process. Bayesian models are proved to successfully map the causality in probabilistic processes and the battery aging phenomena has similar process. Therefore, in this chapter, we proposed a probabilistic model using a hierarchical Bayesian model for the EV battery capacity fade estimation to include the uncertainties in the variables' measurements and modeling process. The Bayesian network for this purpose is developed, the mathematical expression of the model including all random variables are extracted and Metropolis-Hastings MCMC sampling method is used to calculate the posterior distributions. The model is trained and tested by a set of experimental data. Test results show that the model is successful in estimating the capacity fade percentage with 95% accuracy. Also, three case studies are

explored by the model to show its performance in different input data. The effect of different driving styles, different grid services tasks, and different temperature profiles are examined to estimate the capacity fade and result are presented. The outputs of model for all the variables are probability distributions which reflect their inherited uncertainties. Overall results prove that the probabilistic modeling of the capacity fade through Bayesian networks is a promising solution for the battery degradation estimation in different cycling conditions. The merit of this method is that it is applicable for any kind of experimental/measured inputs, if it is trained by the prior data.

References

- [1] W. He, N. Williard, M. Osterman, and M. Pecht, "Prognostics of lithium-ion batteries based on Dempster-Shafer theory and the Bayesian Monte Carlo method," *J. Power Sources*, vol. 196, no. 23, pp. 10314–10321, 2011.
- [2] R. Xiong, F. Sun, Z. Chen, and H. He, "A data-driven multi-scale extended Kalman filtering based parameter and state estimation approach of lithium-ion polymer battery in electric vehicles," *Appl. Energy*, vol. 113, pp. 463–476, 2014.
- [3] X. Qin, Q. Zhao, H. Zhao, W. Feng, and X. Guan, "Prognostics of remaining useful life for lithium-ion batteries based on a feature vector selection and relevance vector machine approach," *2017 IEEE Int. Conf. Progn. Heal. Manag.*, pp. 2–7, 2017.
- [4] Y. Cheng, C. Lu, T. Li, and L. Tao, "Residual lifetime prediction for lithium-ion battery based on functional principal component analysis and Bayesian approach," *Energy*, vol. 90, pp. 1983–1993, 2015.
- [5] K.-C. Chiu, C.-H. Lin, S.-F. Yeh, Y.-H. Lin, C.-S. Huang, and K.-C. Chen, "Cycle life analysis of series connected lithium-ion batteries with temperature difference," *J. Power Sources*, vol. 263, pp. 75–84, 2014.
- [6] M. Safari, M. Morcrette, a. Teysot, and C. Delacourt, "Multimodal Physics-Based Aging Model for Life Prediction of Li-Ion Batteries," *J. Electrochem. Soc.*, vol. 156, no. 3, p. A145, 2009.
- [7] J. Remmlinger, M. Buchholz, T. Soczka-Guth, and K. Dietmayer, "On-board state-of-health monitoring of lithium-ion batteries using linear parameter-varying models," *J. Power Sources*, vol. 239, pp. 689–695, 2013.

- [8] T. Bruen and J. Marco, "Modelling and experimental evaluation of parallel connected lithium ion cells for an electric vehicle battery system," *J. Power Sources*, vol. 310, pp. 91–101, 2016.
- [9] Y. Zhang, C. Y. Wang, and X. Tang, "Cycling degradation of an automotive LiFePO₄ lithium-ion battery," *J. Power Sources*, vol. 196, no. 3, pp. 1513–1520, 2011.
- [10] L. Lam and P. Bauer, "Practical capacity fading model for Li-ion battery cells in electric vehicles," *IEEE Trans. Power Electron.*, vol. 28, no. 12, pp. 5910–5918, 2013.
- [11] N. Omar *et al.*, "Lithium iron phosphate based battery - Assessment of the aging parameters and development of cycle life model," *Appl. Energy*, vol. 113, pp. 1575–1585, 2014.
- [12] M. Jafari, A. Gauchia, S. Zhao, K. Zhang, and L. Gauchia, "Electric Vehicle Battery Cycle Aging Evaluation in Real-World Daily Driving and Vehicle-to-Grid Services," *IEEE Trans. Transp. Electrifi.*, vol. 7782, no. c, pp. 1–1, 2017.
- [13] C. Hu, G. Jain, C. Schmidt, C. Strief, and M. Sullivan, "Online estimation of lithium-ion battery capacity using sparse Bayesian learning," *J. Power Sources*, vol. 289, pp. 105–113, 2015.
- [14] Z. He, M. Gao, G. Ma, Y. Liu, and S. Chen, "Online state-of-health estimation of lithium-ion batteries using Dynamic Bayesian Networks," *J. Power Sources*, vol. 267, pp. 576–583, 2014.
- [15] G. Jin, D. E. Matthews, and Z. Zhou, "A Bayesian framework for on-line degradation assessment and residual life prediction of secondary batteries in spacecraft," *Reliab. Eng. Syst. Saf.*, vol. 113, no. 1, pp. 7–20, 2013.
- [16] B. Saha, K. Goebel, S. Poll, and J. Christophersen, "Prognostics Methods for Battery Health Monitoring Using a Bayesian Framework," *Instrum. Meas. IEEE Trans.*, vol. 58, no. 2, pp. 291–296, 2009.
- [17] S. S. Y. Ng, Y. Xing, and K. L. Tsui, "A naive bayes model for robust remaining useful life prediction of lithium-ion battery," *Appl. Energy*, vol. 118, pp. 114–123, 2014.
- [18] M. Mishra, J. Martinsson, M. Rantatalo, and K. Goebel, "Bayesian hierarchical model-based prognostics for lithium-ion batteries," *Reliab. Eng. Syst. Saf.*, vol. 172, no. December 2017, pp. 25–35, 2018.
- [19] E. Cripps and M. Pecht, "A Bayesian nonlinear random effects model for identification of defective batteries from lot samples," *J. Power Sources*, vol. 342, pp. 342–350, 2017.
- [20] J. Guo, Z. Li, and M. Pecht, "A Bayesian approach for Li-Ion battery capacity fade modeling and cycles to failure prognostics," *J. Power Sources*, vol. 281, pp. 173–184, 2015.
- [21] M. B. Hooten, N. T. Hobbs, and A. M. Ellison, "A guide to Bayesian model selection for ecologists," *Ecol. Monogr.*, vol. 85, no. 1, pp. 3–28, 2015.

- [22] N. Trifonova, A. Kenny, D. Maxwell, D. Duplisea, J. Fernandes, and A. Tucker, “Spatio-temporal Bayesian network models with latent variables for revealing trophic dynamics and functional networks in fisheries ecology,” *Ecol. Inform.*, vol. 30, pp. 142–158, 2015.
- [23] G. Suri and S. Onori, “A control-oriented cycle-life model for hybrid electric vehicle lithium-ion batteries,” *Energy*, vol. 96, pp. 644–653, 2016.
- [24] J. Shen, S. Dusmez, and a Khaligh, “Optimization of Sizing and Battery Cycle Life in Battery/UC Hybrid Energy Storage System for Electric Vehicle Applications,” *Ind. Informatics, IEEE Trans.*, vol. PP, no. 99, p. 1, 2014.
- [25] Idaho National Laboratory, “Plugged In: How Americans Charge Their Electric Vehicles,” pp. 1–24, 2015.
- [26] J. Groot, “State-of-health estimation of Li-ion batteries: cycle life test methods,” *PhD, CHALMERS Univ. Technol.*, p. 138, 2012.
- [27] M. Jafari, A. Gauchia, K. Zhang, and L. Gauchia, “Simulation and Analysis of the Effect of Real-World Driving Styles in an EV Battery Performance and Aging,” *Ieee Trans. Transp. Electrifi.*, vol. 1, no. 4, pp. 391–401, 2015.

Conclusions

This dissertation presents four stages of my research about evaluation of the electric vehicle's battery aging and proposes a Bayesian Network approach for probabilistic modeling of the capacity fade estimation. In first step, REV-Cycle, the simulation tool for the EV battery performance and aging evaluation is developed. Second step explores the effect of different driving styles and aggressiveness on the battery energy consumption and capacity fade. Third step includes the charging equipment and utility services to the EV daily tasks and examines the capacity fade in different daily scenarios. In addition, the effect of temperature change is studied in this step. Last step of this research proposes a Hierarchical Bayesian Network model for estimation of the battery capacity fade considering all uncertainties of the variables, measurements and modeling process. The model is developed with full conditionals and Markov Chain Monte Carlo algorithm employed to generate the posterior distributions and Metropolis-Hastings sampling criteria is used to accept the proposal values of the chain. The distributions for the variables are selected based on their properties using the expert domain knowledge. The results of model are presented and discussed in detail. Here are highlighted findings of different phases of work:

- **Phase 1:** Comparing the battery performance in the standard driving cycles and real-world driving data indicates that the power and current demand from the battery in standard cycles are very smooth, while these profiles have very harsh fluctuations in real driving cases. Note that the current profile has significant effect on the battery aging. Therefore, standard driving cycles are not a reliable source for aging evaluation and real driving data should be used for this purpose.

- **Phase 2:** Study of 240 driving cycles in a recorded section of highway shows that the traffic flow significantly affects the driving style, as light traffics encourages more aggressive behaviors. On average, aggressive drivers consume 43% more kWh compared to the gentle drivers. Also, they demand higher current peaks from the battery due to their accelerations and their C-rate distribution is averaged in higher values. The higher current demand and consequently higher Ah in aggressive driving style leads to higher driving capacity fade percentage compared to the mild and gentle drivers. The results show significant relationship of acceleration profile and energy consumption and battery degradation, regardless of the driving distance.
- **Phase 3:** Including the different recharging facilities and behaviors in addition to the grid services to the daily EV tasks and evaluating the battery capacity fade in different daily scenarios illustrates that: First, there is not significant difference in capacity fade results between L1 and L2 chargers, however, the controlled overnight charging causes less capacity fade compared to uncontrolled charging. Second, in different utility services, peak shaving has higher impact on the battery aging than the frequency regulations due to the higher extracted Ah. Solar integration does not change the total Ah throughput, but it increases the capacity fade due to the higher SOCs. Third, thermal management system has significant impact on the battery health, as passive cooling cannot maintain the battery temperature in the optimum point and ambient temperature causes higher capacity fade in harsh weather conditions. In general, external factors of the battery capacity fade are not constant and vary in different ways. Therefore, it is not possible to study all of the scenarios one by one and this problem should be studied considering the effectual factors' probabilities and uncertainties.

- **Phase 4:** The Bayesian models have proven success upon modeling the probabilistic processes, considering the all uncertainties of the measurements, parameters, process. It can include the causality of battery aging factors from the vehicle owner's behavior in driving, recharging and willingness to the grid services to the temperature and climate conditions in a hierarchical modeling approach. It is adoptable to different input data and all unseen variables can be estimated based on their natural properties by defining proper distribution functions. Our developed model have shown successful estimation of the battery capacity fade on experimental data and therefore it can be used for estimation of different EV battery usage case studies. The model considers the contribution of different cycling events (driving, recharging and grid services) in battery capacity fade, however, due to the lack of data, it does not includes the probability of the frequency of different grid services. The advantage of this model is that it is flexible to be expanded to include other unseen factors and it can be combined with other Bayesian models, e.g. residential battery storage BN model. In addition, it is flexible in being used for different technologies and applications of the batteries, if it is trained with proper prior data. In a nutshell, Bayesian modeling approach is demonstrated to be more informative and flexible tool in estimating the EV battery capacity fade compared to the deterministic point value estimating approaches.

Contributions

After analyzing different aging evaluation methods and models and realizing that the deterministic aging models fail to completely and accurately evaluate the battery degradation behavior considering its varying external factors, a probabilistic aging model is proposed based on the Hierarchical Bayesian Networks. So, the main contribution of this dissertation is developing HBN model and estimation of the EV battery capacity fade considering all uncertainties of the measurements, process and modeling. Since the developed model is a hierarchical model, it can represent the dependency of the battery aging to the very far external factors, such as driver aggressiveness or solar panel output. And because it is based on the probability distributions for all of the variables, it successfully maps the changes in the EV battery tasks such as driving distance or charging frequency. These changes cannot be tracked by deterministic models. Combination of HBN and MCMC algorithm provides a strong tool which helps to evaluate the EV battery capacity fade more accurate (due to lower sensitivity to input data and its uncertainty such as measurement error) and complete (due to including unseen variables and their uncertainty). The proposed method of battery aging evaluation is not limited to EV application and it can be easily adopted and used in other application and cycling conditions which opens a new path in the battery degradation modeling.

Future work

This dissertation proposed a Bayesian Network approach for probabilistic estimation of the EV battery capacity fade considering uncertainties of driving behavior, recharging facilities and availability, and grid services. However, there are some shortcomings that can be studied in future researches of this topic as follows:

- The proposed model does not include the calendar aging of the battery which plays significant role in the overall health condition of the battery. Another BN can be developed for the calendar aging and connected to the presented model to completely predict the remaining useful life of the EV battery.
- This model focuses on the capacity fade of the battery which directly affects the EV's range. However, another important aging factor is power fade which decreases by the battery internal impedance rise. Future studies can focus on the power fade of the EV battery as another index of the battery state of health.
- The last but not least suggestion is to study the probabilistic optimization of the mentioned entities. This optimization can be performed in two ways: first, to develop the cost function based on the interested variable of the target entity and consider other entities' constraints such as EV battery aging constraint, second, to bring all variables in the cost function, instead of limiting their contribution.

A Copyright documentation

Chapter 2:



The screenshot shows the Copyright Clearance Center RightsLink interface. At the top left is the Copyright Clearance Center logo. To its right is the RightsLink logo. Further right are navigation buttons for Home, Create Account, and Help, along with a chat bubble icon. On the left side, there is a blue box with the IEEE logo and the text: "Requesting permission to reuse content from an IEEE publication". In the center, there is a list of metadata for a document: Title: REV-cycle: A MATLAB-based tool for large-data analysis of real-life driving cycles for electric vehicles; Conference Proceedings: Transportation Electrification Conference and Expo (ITEC), 2015 IEEE; Author: A. Gauchia; Publisher: IEEE; Date: June 2015; Copyright © 2015, IEEE. On the right side, there is a LOGIN box with the text: "If you're a copyright.com user, you can login to RightsLink using your copyright.com credentials. Already a RightsLink user or want to [learn more?](#)".

Thesis / Dissertation Reuse

The IEEE does not require individuals working on a thesis to obtain a formal reuse license, however, you may print out this statement to be used as a permission grant:

Requirements to be followed when using any portion (e.g., figure, graph, table, or textual material) of an IEEE copyrighted paper in a thesis:

- 1) In the case of textual material (e.g., using short quotes or referring to the work within these papers) users must give full credit to the original source (author, paper, publication) followed by the IEEE copyright line © 2011 IEEE.
- 2) In the case of illustrations or tabular material, we require that the copyright line © [Year of original publication] IEEE appear prominently with each reprinted figure and/or table.
- 3) If a substantial portion of the original paper is to be used, and if you are not the senior author, also obtain the senior author's approval.

Requirements to be followed when using an entire IEEE copyrighted paper in a thesis:

- 1) The following IEEE copyright/ credit notice should be placed prominently in the references: © [year of original publication] IEEE. Reprinted, with permission, from [author names, paper title, IEEE publication title, and month/year of publication]
- 2) Only the accepted version of an IEEE copyrighted paper can be used when posting the paper or your thesis on-line.
- 3) In placing the thesis on the author's university website, please display the following message in a prominent place on the website: In reference to IEEE copyrighted material which is used with permission in this thesis, the IEEE does not endorse any of [university/educational entity's name goes here]'s products or services. Internal or personal use of this material is permitted. If interested in reprinting/republishing IEEE copyrighted material for advertising or promotional purposes or for creating new collective works for resale or redistribution, please go to http://www.ieee.org/publications_standards/publications/rights/rights_link.html to learn how to obtain a License from RightsLink.

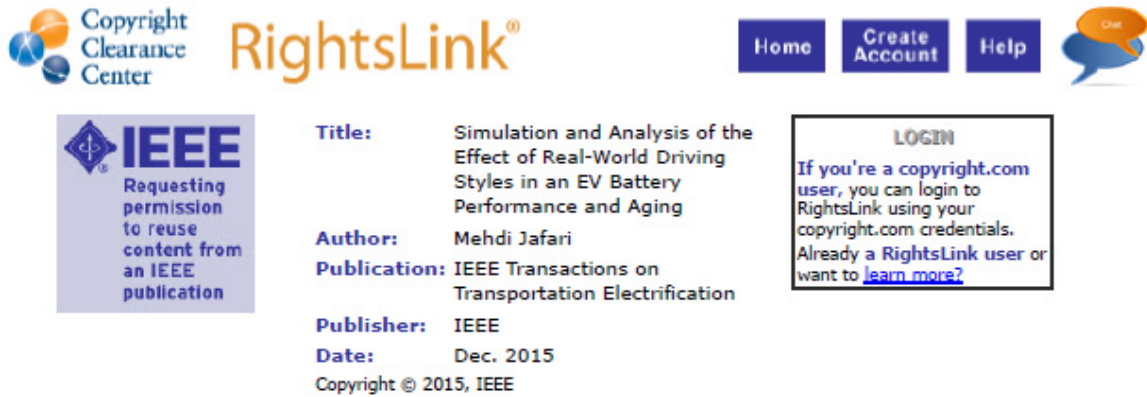
If applicable, University Microfilms and/or ProQuest Library, or the Archives of Canada may supply single copies of the dissertation.

BACK

CLOSE WINDOW

Copyright © 2018 Copyright Clearance Center, Inc. All Rights Reserved. [Privacy statement](#). [Terms and Conditions](#). Comments? We would like to hear from you. E-mail us at customer@copyright.com

Chapter 3:



The screenshot shows the RightsLink website interface. At the top left is the Copyright Clearance Center logo. To its right is the RightsLink logo. Further right are navigation buttons for Home, Create Account, and Help, along with a chat icon. Below the navigation is a large blue box with the IEEE logo and the text: "Requesting permission to reuse content from an IEEE publication". To the right of this box, the following information is displayed:

Title: Simulation and Analysis of the Effect of Real-World Driving Styles in an EV Battery Performance and Aging
Author: Mehdi Jafari
Publication: IEEE Transactions on Transportation Electrification
Publisher: IEEE
Date: Dec. 2015
Copyright © 2015, IEEE

To the right of this information is a "LOGIN" box with the text: "If you're a copyright.com user, you can login to RightsLink using your copyright.com credentials. Already a RightsLink user or want to [learn more?](#)"

Thesis / Dissertation Reuse

The IEEE does not require individuals working on a thesis to obtain a formal reuse license, however, you may print out this statement to be used as a permission grant:

Requirements to be followed when using any portion (e.g., figure, graph, table, or textual material) of an IEEE copyrighted paper in a thesis:

- 1) In the case of textual material (e.g., using short quotes or referring to the work within these papers) users must give full credit to the original source (author, paper, publication) followed by the IEEE copyright line © 2011 IEEE.
- 2) In the case of illustrations or tabular material, we require that the copyright line © [Year of original publication] IEEE appear prominently with each reprinted figure and/or table.
- 3) If a substantial portion of the original paper is to be used, and if you are not the senior author, also obtain the senior author's approval.

Requirements to be followed when using an entire IEEE copyrighted paper in a thesis:

- 1) The following IEEE copyright/ credit notice should be placed prominently in the references: © [year of original publication] IEEE. Reprinted, with permission, from [author names, paper title, IEEE publication title, and month/year of publication]
- 2) Only the accepted version of an IEEE copyrighted paper can be used when posting the paper or your thesis on-line.
- 3) In placing the thesis on the author's university website, please display the following message in a prominent place on the website: In reference to IEEE copyrighted material which is used with permission in this thesis, the IEEE does not endorse any of [university/educational entity's name goes here]'s products or services. Internal or personal use of this material is permitted. If interested in reprinting/republishing IEEE copyrighted material for advertising or promotional purposes or for creating new collective works for resale or redistribution, please go to http://www.ieee.org/publications_standards/publications/rights/rights_link.html to learn how to obtain a License from RightsLink.

If applicable, University Microfilms and/or ProQuest Library, or the Archives of Canada may supply single copies of the dissertation.

BACK

CLOSE WINDOW

Copyright © 2018 Copyright Clearance Center, Inc. All Rights Reserved. [Privacy statement](#). [Terms and Conditions](#).
Comments? We would like to hear from you. E-mail us at customer@copyright.com

Chapter 4:



RightsLink®

Home

Create Account

Help



Title: Electric Vehicle Battery Cycle Aging Evaluation in Real-World Daily Driving and Vehicle-to-Grid Services
Author: Mehdi Jafari
Publication: IEEE Transactions on Transportation Electrification
Publisher: IEEE
Date: March 2018
Copyright © 2018, IEEE

LOGIN
If you're a [copyright.com](#) user, you can login to RightsLink using your [copyright.com](#) credentials.
Already a [RightsLink user](#) or want to [learn more?](#)

Thesis / Dissertation Reuse

The IEEE does not require individuals working on a thesis to obtain a formal reuse license, however, you may print out this statement to be used as a permission grant:

Requirements to be followed when using any portion (e.g., figure, graph, table, or textual material) of an IEEE copyrighted paper in a thesis:

- 1) In the case of textual material (e.g., using short quotes or referring to the work within these papers) users must give full credit to the original source (author, paper, publication) followed by the IEEE copyright line © 2011 IEEE.
- 2) In the case of illustrations or tabular material, we require that the copyright line © [Year of original publication] IEEE appear prominently with each reprinted figure and/or table.
- 3) If a substantial portion of the original paper is to be used, and if you are not the senior author, also obtain the senior author's approval.

Requirements to be followed when using an entire IEEE copyrighted paper in a thesis:

- 1) The following IEEE copyright/ credit notice should be placed prominently in the references: © [year of original publication] IEEE. Reprinted, with permission, from [author names, paper title, IEEE publication title, and month/year of publication]
- 2) Only the accepted version of an IEEE copyrighted paper can be used when posting the paper or your thesis on-line.
- 3) In placing the thesis on the author's university website, please display the following message in a prominent place on the website: In reference to IEEE copyrighted material which is used with permission in this thesis, the IEEE does not endorse any of [university/educational entity's name goes here]'s products or services. Internal or personal use of this material is permitted. If interested in reprinting/republishing IEEE copyrighted material for advertising or promotional purposes or for creating new collective works for resale or redistribution, please go to http://www.ieee.org/publications_standards/publications/rights/rights_link.html to learn how to obtain a License from RightsLink.

If applicable, University Microfilms and/or ProQuest Library, or the Archives of Canada may supply single copies of the dissertation.

BACK

CLOSE WINDOW

Copyright © 2018 [Copyright Clearance Center, Inc.](#) All Rights Reserved. [Privacy statement](#), [Terms and Conditions](#).
Comments? We would like to hear from you. E-mail us at customercare@copyright.com